2018

Transcription factor MEF2A fine-tunes gene expression in the atrial and ventricular chambers of the adult mouse heart

BOSTON UNIVERSITY

GRADUATE SCHOOL OF ARTS AND SCIENCES

Dissertation

TRANSCRIPTION FACTOR MEF2A FINE-TUNES GENE EXPRESSION IN THE ATRIAL AND VENTRICULAR CHAMBERS OF THE ADULT MOUSE HEART

by

JOSE LUIS MEDRANO

B.S., Massachusetts Institute of Technology, 2007

Submitted in partial fulfillment of the

requirements for the degree of

Doctor of Philosophy

2018

Approved by

First Reader _____

Francisco J. Naya, Ph.D.
Associate Professor of Biology

Second Reader _____

Thomas Gilmore, Ph.D.
Professor of Biology

DEDICATION

To my brother Oscar and my sister Janelle,

always follow your dreams

To my mother and my father,

thank you for believing in me

ACKNOWLEDGMENTS

I would like to thank many individuals who have helped me tremendously during my graduate studies at Boston University.

First and foremost, I would like to thank my thesis advisor, Dr. Francisco Naya. Thank you for letting me join your lab, supporting my efforts over many years, and being an amazing mentor. I have faced numerous challenges during my graduate studies, and your continued guidance has allowed me to successfully begin the next chapter in my career. I would also like to thank my thesis committee members, Dr. Thomas Gilmore, Dr. Ulla Hansen, Dr. John Tullai, and Dr. Horacio Frydman. Thank you for all of your input and ideas from my numerous committee meetings, as well as thesis editing suggestions.

I would like to thank the many members of the Naya Lab, both past and present, who have made a positive impact during my time at Boston University. Thank you to Dr. Christine Synder-Weaver, Dr. Cody Desjardins, Tiffany Dill, Heather Hook, Christopher Petty, Tarik Zahr, Jessica Pondish, Yi Feng, Akuah Kontor, Colleen Drapek, and Nicole Mason.

I would also like to thank graduate students in the CM and MCBB program who have been a great support network during my time at Boston University. Thank you to Quinn Ho, Szilvia Kiriakov, Patrick Stoiber, Maggie O'Connor, Albert Mondragon, Zach Gardner, Jenny Lei, and Ndidi Obi. I would also like to thank Dr. Trevor Grant, Dr. Shasha Ji, Kyle Berry, Aviva Gonzalez, Ally & Charlie Carlton-Smith, Janani Ramachandran, Michael Lin, and the rest of my friends in Boston who have supported

and encouraged me over the last few years, especially nearing the end of my thesis. A big thank you to my roommates Ashley Penvose and Dan Zuch for being the most amazing housemates a guy like me could ever ask for.

Finally, I would like to thank my parents, Jose and Maria Medrano, and my two siblings, Oscar and Janelle. Thank you for all of your continued support and unconditional love.

TRANSCRIPTION FACTOR MEF2A FINE-TUNES GENE EXPRESSION IN THE ATRIAL AND VENTRICULAR CHAMBERS OF THE ADULT MOUSE HEART

JOSE LUIS MEDRANO JR

Boston University Graduate School of Arts and Sciences, 2018

Major Professor: Francisco J. Naya, Associate Professor of Biology

ABSTRACT

The distinct morphological and functional properties of mammalian heart chambers arise from an elaborate developmental program involving cell lineage determination, morphogenesis, and dynamic spatiotemporal gene expression patterns. While a number of transcription factors have been identified for proper gene regulation in the chambers, the complete transcriptional network that controls these patterns remains poorly defined. Previous studies have implicated MEF2 transcription factors in the regulation of chamber-restricted enhancers. To better understand the mechanisms of MEF2-mediated regional gene regulation in the heart, MEF2A knockout (KO) mice, a model that displays a predominantly ventricular chamber phenotype, are used herein. Transcriptomic analysis of atrial and ventricular tissue from adult MEF2A KO hearts revealed extensive differences in chamber gene expression across the heart, with a larger proportion of dysregulated genes in atrial chambers. Thus, it is hypothesized that MEF2A differentially regulates expression of target genes and cellular pathways in cardiac

chambers. Functional pathway analysis of genes preferentially dysregulated in the atria and ventricles supported this hypothesis and revealed distinct MEF2A-dependent cellular processes in each cardiac chamber. In atria, MEF2A regulated the expression of genes involved in fibrosis and adhesion, whereas in ventricles, it controlled genes involved in inflammation and endocytosis. Additional studies uncovered preferential dysregulation of molecular components of these pathways in MEF2A KO hearts. Phosphorylated focal adhesion kinase (FAK) levels, relating to cell adhesion, were preferentially downregulated in KO atria, and TRAF6 proteins levels, relating to inflammation, were preferentially downregulated in KO ventricles. Finally, analysis of transcription factor binding site motifs of differentially dysregulated genes uncovered distinct MEF2A coregulators for the atrial and ventricular gene sets. A subset of these transcriptional coregulators were found to cooperate with MEF2A to activate MEF2-dependent reporters *in vitro*. In conclusion, these results suggest a mechanism in which MEF2 transcriptional activity is differentially recruited to fine-tune gene expression levels in each cardiac chamber. This regulatory mechanism ensures the optimal output of gene products for proper physiological function of the atrial and ventricular chambers. Lastly, one of the preferentially dysregulated genes, *Bex1*, was further characterized. Future studies will focus on the role of MEF2A-regulated *Bex1* in the adult heart.

TABLE OF CONTENTS

LIST OF TABLES

LIST OF FIGURES

LIST OF ABBREVIATIONS AND ACRONYMS

°C	degrees Celsius
18s	18S ribosomal RNA
A (DNA)	adenine
α	alpha
A (cardiac)	atria
β	beta
Bex1	brain expressed X-linked 1
bHLH	basic Helix-Loop-Helix
Bmp2	bone morphogenetic protein 2
bp	base pair(s)
BLAST	basic local alignment search tool
BSA	bovine serum albumin
C	cytosine
$CaCl_2$	calcium chloride
CArG box	cytosine adenine-rich guanine box
cDNA	complementary DNA
ChIP	chromatin immunoprecipitation
CKII	creatine kinase II
CT	threshold cycle
C-terminal	carboxyl terminal
DAPI	4',6-diamidino-2-phenylindole

Δ	delta; change
DMEM	Dulbecco's Modified Eagle Medium
DNA	deoxyribonucleic acid
DTT	dithiothreitol
E-	embryonic day
EDTA	Ethylenediaminetetraacetic acid
EGR1	early growth response protein 1
EGTA	ethylene glycol-bis(β-aminoethyl ether)-N,N,N',N'-tetraacetic acid
EMSA	electrophoretic mobility shift assay
ENCODE	Encyclopedia of DNA Elements
ER	estrogen receptor
EREF	estrogen response element family
FAK	focal adhesion kinase
FC	fold change
G	guanine
g	gram
g	gravities
GAPDH	glyceraldehyde-3-phosphate dehydrogenase
GST	glutathione S-transferase
h	hour(s)
HAT	histone acetyl transferase
HBSS	Hank’s Balanced Salt Solution

HCl	hydrochloric acid
HDAC	histone deacetylase
HEPES	4-(2-hydroxyethyl)-1-piperazineethanesulfonic acid
HRP	horseradish peroxidase
IACUC	Institutional Animal Care and Use Committee
IPA	Ingenuity Pathway Analysis
Itga7	integrin subunit alpha 7
KD	knockdown
KO	knockout
L	liter
LB	lysogeny broth
lncRNA	long non-coding RNA
m	meter
μ-	micro
m-	milli-
M	molar
MADS	MCM1, Agamous, Deficiens, and SRF
Mef2a	myocyte-specific enhancer factor-2
MHC	myosin heavy chain
min	minute(s)
mRNA	messenger ribonucleic acid
MSP-RON	Macrophage stimulating protein – Recepteur d'Origine Nantais

n-	nano-
N-terminal	amino terminal
Na_2CO_3	sodium carbonate
NaCl	sodium chloride
NaOH	sodium hydroxide
NCBI	National Center of Biotechnology Information
ncRNA	non-coding RNA
NEB	New England Biolabs
Nkx2.5	NK2 homeobox 5
NKXH	NKX homeodomain factors
NRVM	neonatal rat ventricular myocytes
NTR	neurotrophin receptor
p	p-value; probability value (statistical measurement of significance)
p-	pico-
PAGE	polyacrylamide gel electrophoresis
PBS	phosphate-buffered saline
PCR	polymerase chain reaction
PEI	polyethylamine
PECAM	platelet endothelial cell adhesion molecule; cluster of differentiation 31 (CD31)
PMSF	phenylmethane sulfonyl fluoride
qRT	quantitative reverse transcriptase

R	purine (adenine or guanine)
RNA	ribonucleic acid
RNase	ribonuclease
rpm	revolutions per minute
RT	reverse transcriptase
SD	standard deviation
SDS	sodium dodecyl sulfate
sec	second(s)
seq	sequencing
SRF	serum response factor
T	thymine
TBS	Tris-buffered saline
TF	transcription factor
TFBS	transcription factor binding site
Tg	transgenic
TRAF6	TNF receptor associated factor 6
Tris	tris(hydroxymethyl)aminomethane
TSS	transcription start site
UTR	untranslated region
UV	ultraviolet
-V	volts
V	ventricles

W	weak nucleic acids (adenine or thymine)
WT	wild-type
WT1	Wilms tumor 1
Xirp2	Xin Actin Binding Repeat Containing 2
Y	pyrimidine (thymine or cytosine)

CHAPTER ONE: Introduction

1.1 Introduction

The genetic program of the developing heart involves a network of signaling molecules and transcription factors to properly form this complex organ. Given the complexity of the heart, even subtle perturbations in the regulation of these pathways, or in the formation of a specific cardiac structure can ultimately lead to heart disease and death. The overall goal of this research is to understand the transcriptional regulation behind the gene programs and cellular pathways involved in cardiac muscle. Many key transcription factors involved in cardiogenesis and cardiac homeostasis have been identified and only a few are known to be evolutionarily conserved and important for muscle development. One of these factors is MEF2.

This thesis focuses on the role of the MEF2A transcription factor in atrial and ventricular chambers in the adult mouse heart. Previous findings have established MEF2 proteins as key regulators essential in differentiation and developmental gene programs in mammalian cardiac muscle. The purpose of this research is to gain a better understanding of the cellular pathways and gene programs that MEF2A differentially regulates throughout the chambers of the adult heart.

1.2 Myocyte enhancer factor-2

1.2.1 Discovery and structure of MEF2 proteins

Myocyte enhancer factor-2 (MEF2) proteins are an evolutionarily conserved family of transcription factors that are present in organisms from yeast to humans. In

mice and humans, there are four MEF2 family members designated MEF2A, –B, –C, and –D, each encoded by a separate *Mef2* gene. MEF2 factors are a subfamily of proteins belonging to the evolutionarily ancient MADS-box family of transcription factors that bind to A/T-rich sequences. Named after the four founding members in the family (MCM1 from *Saccharomyces cerevisiae*, AGAMOUS from *Arabidopsis thaliana*, DEFICIENS from *Antirrhinum majus*, and SRF from *Homo sapiens*), MADS-box proteins also bind to A/T-rich sequences (Shore & Sharrocks 1995).

All four mammalian MEF2 factors contain an N-terminal MADS-box, a MEF2 domain, and a C-terminal transcriptional activation domain (Figure 1.1) (Black & Olson 1998, McKinsey *et al.* 2002, Potthoff & Olson 2007). The MADS-box is 57 amino acids in length, located at the beginning of the amino terminus and serves as the minimal domain required for DNA binding. Adjacent to the MADS-box is a 29 amino acid motif known as the MEF2 domain. This sequence is required for high affinity DNA binding, dimerization, and transcriptional co-factor recruitment (Molkentin *et al.* 1996). Unlike other MADS-box transcription factors, only MEF2 proteins possess a MEF2 domain. MEF2 factors are capable of homo– and heterodimerization, but they are unable to dimerize with other MADS-box family members (Black & Olson 1998, Desjardins & Naya 2016). This observation suggests that specific residues within the MADS-box motif of MEF2 proteins confer the specificity for heterodimerization onto the MEF2 family (Black & Olson 1998). Lastly, the C-terminal region of MEF2 factors functions as the transcriptional activation domain.

Due to the high similarity of *Mef2* exon-intron organization between mammals and invertebrates, it is likely that these genes evolved from a common ancestral *Mef2* gene (Black & Olson 1998). While mammals possess four distinct *Mef2* genes, invertebrates have a single *Mef2* gene and vertebrates possess three or more (Desjardins & Naya 2016). Indeed, MEF2 is expressed from yeast to humans (Black & Olson 1998, Dodou & Treisman 1997, Gaspera *et al.* 2009, Hinits *et al.* 2012, Lilly *et al.* 1994).

1.2.2 Tissue distribution of MEF2 proteins

In mammalian species, *Mef2* genes display overlapping but distinct temporal and spatial expression patterns in embryonic and adult tissues (Edmondson *et al.* 1994). Throughout development, *Mef2* expression is high in developing muscle cell lineages. In flies, *D-mef2* is expressed throughout the unspecified mesoderm after gastrulation, and later expression is restricted to the cardiac, skeletal, and smooth muscle lineages (Lilly *et al.* 1994, Nguyen *et al.* 1994, Taylor *et al.* 1995).

It has been documented in vertebrate studies that *Mef2* transcripts are ubiquitous, however, somatic, cardiac, and visceral muscle show an enrichment for this family of proteins (Potthoff & Olson 2007). In mice, *Mef2c* and *Mef2b* are the first two *Mef2* genes to be expressed in mesodermal precursor cells at around embryonic day 7.5 (E7.5), with *Mef2a* and *Mef2d* genes expressed about a day later in the myocardium of the developing heart (Edmondson *et al.* 1994, Naya *et al.* 1999). *Mef2* gene expression is also detected in developing skeletal and smooth muscle cell lineages. These observations demonstrate that the *Mef2* promoters are responsive to various transcription factors, and that *Mef2*

expression levels can differ within a specific tissue type, dependent on the spatial expression profile of activating and repressing factors.

Mice carrying a *lacZ* reporter under the control of either the *desmin* MEF2 enhancer (*des-MEF2-lacZ*) or *c-jun* MEF2 enhancer (*jun-MEF2-lacZ*) have been generated to study the expression pattern of MEF2 proteins during mouse embryogenesis (Naya *et al.* 1999). Expression of the *lacZ* transgene in these mice was detected as early as E7.5 in cardiac progenitor cells. Ultimately, *MEF2-lacZ* transgenic mice showed *lacZ* expression in somites, skeletal muscle, cardiac mesoderm, and the heart tube during embryogenesis. *LacZ* expression was also detected in specific regions of the brain in adult mice (Naya *et al.* 1999).

It is interesting to note that recent studies have shown an enrichment of MEF2A in atrial chambers of the mouse heart (Zhao *et al.* 2002). This spatially differential expression pattern of MEF2A throughout the heart suggests that MEF2A has a role in atrial chambers. However, these experiments demonstrating atrial enrichment of MEF2A lack controls and require a more thorough investigation with proper quantification analysis (Zhao *et al.* 2002).

1.2.3 Regulation of MEF2 expression and activity

1.2.3.1 Transcriptional regulation

The promoters of each *Mef2* gene are activated by different factors in a tissue-dependent manner. In skeletal muscle development the *Mef2c* gene is a direct target of the basic helix-loop-helix (bHLH) protein MyoD, whereas in the anterior heart field ISL1

and GATA transcription factors activate the expression of *Mef2c* in the developing heart (Dodou *et al.* 2004, 2003). It has been shown that *Mef2a* is transcriptionally autoregulated in the heart. Depending on different signaling activities, *Mef2a* splice variants are expressed, and transcription of the *Mef2a* gene is subject to positive or negative regulation by its own protein products (Ramachandran *et al.* 2008). These results demonstrate that the promoters of each *Mef2* gene respond to different regulatory factors in a tissue-dependent manner.

1.2.3.2 Post-transcriptional regulation

The 3'-untranslated region (3'-UTR) of *Mef2a* transcripts is subject to an additional level of regulation. It has been observed that the 3'-UTR of the *Mef2a* transcript functions as a cis-acting translational repressor (Black *et al.* 1997). While the molecular mechanism of this observed post-transcriptional regulation was unknown at the time, it was later discovered that microRNA (miRNA) 155 (miR-155) significantly represses MEF2A expression and subsequently impairs myoblast differentiation (Seok *et al.* 2011). Additionally, expression of miR-1 is restricted to striated muscle, and miR-1 negatively regulates the expression of *Mef2a* in cardiomyocytes (Ikeda *et al.* 2009). Recently, studies have shown the 3'-UTR of *Mef2d* is targeted by miR-218. The targeting of *Mef2d* by miR-218 suppresses cardiac myxoma, the most common type of human heart tumor (Cao *et al.* 2015). Regulation via the 3'-UTR of *Mef2* transcripts can explain the differences between mRNA and protein levels among different tissues types.

1.2.3.3 Post-translational modification

Post-translational modifications of MEF2 proteins play an important role in DNA-binding activity and protein stability. The MADS-box domain in all MEF2 proteins contains a conserved casein kinase II (CKII) phosphorylation site (Black & Olson 1998). Phosphorylation of this site enhances the DNA-binding activity of MEF2C (Molkentin *et al.* 1996). Separate phosphorylation motifs in MEF2 factors have also been found to regulate their stability *in vitro* (Cox *et al.* 2003). Specifically, a KSPPP amino acid sequence is conserved in MEF2 isoforms across many species. The phosphorylation of the serine residue in the KSPPP motif is mediated by p38 MAPK and promotes the degradation of MEF2A (Cox *et al.* 2003). Both MEF2 and p38 MAPK are known regulators of cardiac development. Recent studies provide evidence for a functional role of a p38 MAPK/MEF2 signal transduction cascade in cardiomyocyte biology (Han & Molkentin 2000)

In addition to phosphorylation-associated covalent modifications, MEF2 factors have been shown to be post-translationally acetylated and SUMOylated (Small Ubiquitin-like Modifier). Acetylation of MEF2C in skeletal muscle cells results in the enhancement of MEF2C DNA- and chromatin-binding activity (Angelelli *et al.* 2008). Mutating these acetylation sites affects the synergistic effect of MEF2C with bHLH factor Myogenin, and non-acetylatable MEF2C inhibits differentiation in C2C12 cells (Ma *et al.* 2005). MEF2A undergoes SUMOylation both *in vitro* and *in vivo*, and interestingly, mutating the SUMOylation site (K395) of MEF2A enhances its DNA-binding activity compared to wild-type MEF2A (Riquelme *et al.* 2006). Altogether, these studies demonstrate that

post-translational modifications of MEF2 proteins play an important role in the regulation of their transcriptional activity.

1.2.4 MEF2 target genes

Many target genes of MEF2 signaling have been discovered. The first MEF2 target gene was *Mck* (Gossett *et al.* 1989). This gene contained an upstream enhancer site harboring the MEF2 consensus sequence. Since then, researchers have continued to characterize direct targets of MEF2, ultimately linking MEF2 protein to a variety of cellular and molecular pathways in various tissues. These MEF2 gene targets have been discovered through detailed studies combining microarray technologies and promoter analysis of candidate target genes. MEF2 proteins have been shown to directly target numerous genes involved in different cellular processes, including myogenic factors (*MyoD* and *MRF4*), enzymes (*aldolase A*), structural proteins (*desmin*), and glucose transport proteins (*GLUT4*) (Black *et al.* 1995, Black & Olson 1998, Dechesne *et al.* 1994, Hidaka *et al.* 1993, Kuisk *et al.* 1996, Liu *et al.* 1994). The transcription factor BOP is a regulator of the anterior heart field, and MEF2C can transcriptionally regulate *Bop* expression through a MEF2-responsive element in the *Bop* promoter (Phan *et al.* 2005). ChIP-exo techniques have been used in both cardiomyocytes and skeletal muscle myoblasts to analyze MEF2 target genes (Wales *et al.* 2014). These studies revealed a regulation of the phosphatase gene *Dusp6* by p38MAPK-MEF2 signaling (Wales *et al.* 2014). It has been demonstrated that MEF2 proteins regulate distinct gene programs in mammalian skeletal muscle differentiation (Estrella *et al.* 2015). While these studies

show that only MEF2A is absolutely required for skeletal muscle differentiation, each MEF2 isoform regulates a significant subset of non-overlapping genes. Although not functionally tested as direct targets of MEF2, the preferential sensitivity of certain genes to specific MEF2 isoforms suggests that each MEF2 factor transcriptionally activates a different subset of target genes to regulate distinct gene programs in skeletal muscle differentiation.

The repertoire of MEF2 target genes has expanded in the past decade based on genome-wide expression studies, and our lab has also contributed to the identification of a number of MEF2 targets. Microarray analysis of MEF2A KO hearts coupled with *in vitro* promoter characterization identified both *Myomaxin* (*Xirp2*/*Cmya3*) and *Myospryn* (*Cmya5*) as target genes of MEF2 (Durham *et al.* 2006, Huang *et al.* 2006). MEF2A has been identified as a regulator of a costamere gene program in cardiac muscle. The costamere is a macromolecular complex linking the myofibrils to the myocyte membrane. Fifty-five known costamere-localized genes were found to be dysregulated in *Mef2a* KO hearts. Additionally, this global downregulation of costamere-localized genes was observed in MEF2A-deficient neonatal rat ventricular myocytes (NRVMs) but not when MEF2D protein levels were depleted via shRNA-mediated knockdown. These results show a MEF2 isoform-specific regulation of cardiac gene programs (Ewen *et al.* 2011). In a separate set of experiments, cell-cycle and differentiation programs were found to be antagonistically regulated in an isoform-specific manner in cardiomyocytes (Desjardins & Naya 2017). In these experiments, both MEF2A and MEF2D were individually necessary for myocyte survival, whereas MEF2C was dispensable. Additionally, MEF2A

or MEF2D deficiency triggered activation of cell cycle genes and downregulation of terminal differentiation markers. Conversely, MEF2C deficiency in NRVMs antagonistically regulated cell cycle genes and differentiation gene programs compared to MEF2A and MEF2D (Desjardins & Naya 2017).

Recent research shows that MEF2 regulates the expression of the *Gtl2-Dio3* non-coding RNA (ncRNA) locus (Snyder *et al.* 2013). This cluster harbors several long non-coding RNAs (lncRNAs) and a mega-cluster of microRNAs. A subset of these microRNAs target the Wnt signaling pathway in the process of skeletal muscle regeneration in *Mef2a*-null mice (Snyder *et al.* 2013).

1.2.5 MEF2 loss-of-function mouse models

Overlapping expression patterns and functional redundancy among the MEF2 family members complicates dissecting the specific function of each vertebrate gene. *Mef2c* was the first gene of the *Mef2* family to be inactivated by gene knockout in mice, and *Mef2c*-null mice die at E9.5, displaying underdevelopment of the ventricles as well as cardiac looping abnormalities (Lin *et al.* 1997). These studies demonstrate a role for MEF2C in early heart development and that MEF2C is absolutely required at this timepoint during embryogenesis. Conditional *Mef2c* KO mice were generated to allow for temporal and tissue-specific analysis of the cardiac phenotype since global knockout of the *Mef2c* gene results in early embryonic lethality (Vong *et al.* 2005). Delayed *Cre recombinase*-mediated removal of *Mef2c* in the myocardium using an *alpha myosin heavy chain* driver resulted in viable offspring. This result demonstrates that while *Mef2c*

is required for early development of the heart, *Mef2c* is dispensable after looping morphogenesis (Vong *et al.* 2005)

Mef2d-null mice do not display any obvious abnormalities under normal conditions, but display major alterations in cardiac remodeling upon stress (Kim *et al.* 2008, Potthoff & Olson 2007). *Mef2b*-null mice appear normal (Black & Olson 1998). The lack of an observable cardiac-related phenotype in *Mef2b* KO mice indicates that MEF2B does not have an essential role in the heart, as compared to other MEF2 isoforms. While MEF2B expression was detected in cardiac and skeletal muscle of developing mouse embryos, MEF2B expression was not detected in adult striated muscle (Morisaki *et al.* 1997).

Mef2a mutant mice fall into two phenotypic classes. The first class of *Mef2a*-null mice die perinatally between postnatal days 5 (P5) and P10. These mutant mice exhibit cytoarchitectural defects and right ventricular dilation (Naya *et al.* 2002). Defective cytoarchitecture in these hearts results from the misregulated expression of genes encoding proteins that localize to the costamere (Ewen *et al.* 2011). The costamere, a macromolecular complex, is perturbed in perinatal *Mef2a*-null hearts. The second class of mice survive to adulthood without any obvious structural defects in the heart. Instead these mutant mice exhibit mitochondrial deficiency and conduction abnormalities (Naya *et al.* 2002). While the *Mef2a*-null perinatal phenotype has been characterized, not much is known about the defective gene programs and cellular processes in the adult *Mef2a* KO heart.

1.3 The mammalian heart

1.3.1 Cardiogenesis

The formation of the mammalian heart can be broken down into four main stages (Figure 1.2). In response to cues from adjacent endoderm (*e.g.*, bone morphogenetic protein [BMP] and Wnt signaling molecules), cardiac progenitor cells are specified in the anterior lateral mesoderm and migrate to the ventral midline during vertebrate embryogenesis (Schultheiss *et al.* 1995). These signals are conserved across species and activate the expression of *Nkx2-5* in vertebrates and *tinman* in flies (Harvey 1996). To date, NKX2-5 and Tinman are the earliest markers of the cardiac lineage in vertebrates and flies, respectively (Harvey 1996).

After converging at the ventral midline and forming a cardiac crescent, cardiomyoblasts organize into a functional linear heart tube. GATA family factors are involved in the formation of the linear heart tube, and loss of these GATA signals prevents proper formation of a linear heart tube, a defect known as cardiac bifida and results in embryonic lethality (Kuo *et al.* 1997, Molkentin *et al.* 1997, Reiter *et al.* 1999). After proper formation of the linear heart tube, the heart undergoes the critical event of rightward looping. Rightward looping of the linear heart places the systemic (left) and pulmonary (right) ventricles, as well as the atria, in their correct, three-dimensional orientation. The underlying factors governing rightward looping are still unknown.

In the final stage of cardiogenesis, each chamber is now distinguishable and in the correct position. The heart then goes through the process of chamber segmentation,

cardiac valve formation, and chamber growth. In these final stages of cardiac development, maturation of the ventricles is dependent specifically on MEF2C function.

1.3.2 Chamber specification and differentiation

An important process in cardiogenesis is the proper specification of each chamber in the heart. Chamber identity and development are tightly regulated by a network of various transcription factors expressed throughout the heart (Figure 1.3). One example is the transcription factor COUP-TFII. Knockout of COUP-TFII in cardiomyocytes produced ventricular-like chambers in place of atrial chambers (Wu *et al.* 2013). Cardiomyocytes from these "ventricularized" chambers displayed physiological and morphological properties more closely resembling ventricular myocytes as opposed to atrial myocytes (Wu *et al.* 2013). Additionally, this chamber-identity switch was accompanied by dysregulation of 2,584 genes, many of which are differentially expressed between wild-type atria and ventricles. Similarly, the bHLH transcriptional repressor Hrt2 is necessary for the suppression of atrial genes in the ventricular myocardium (Xin *et al.* 2007). While *Hrt2* KO mice die perinatally from cardiac abnormalities, conditional KO of *Hrt2* in cardiomyocytes results in the activation of atrial genes in the ventricular myocardium. Conversely, expression of *Hrt2* in atrial cardiomyocytes is sufficient to repress atrial cardiac genes (Xin *et al.* 2007).

1.3.3 Cardiac chamber morphogenesis

Proper formation of the mammalian heart involves precisely coordinated morphogenetic and differentiation processes that give rise to an organ with multiple, well-defined anatomical structures. Gene inactivation studies of cardiac-related transcription factors have revealed a number of genes required for the proper formation of the mammalian heart. As mentioned previously, *Mef2c*-null mice die at E9.5 displaying underdevelopment of the ventricles as well as cardiac looping abnormalities (Lin *et al.* 1997). *Nkx2.5* is expressed in the precardiac mesoderm and is one of the earliest markers of the cardiac muscle lineage (Srivastava & Olson 2000). Mice lacking Nkx2.5 display abnormal heart morphogenesis and embryonic lethality at around E9.5. While proper formation of the heart tube was observed, *Nkx2.5* KO mice failed to undergo cardiac looping (Lyons *et al.* 1995). Mice lacking *Pitx2* die before birth, displaying left-right asymmetry, chamber remodeling, atrial and ventricular septal defects in the heart (Gage *et al.* 1999, Liu *et al.* 2001). Mice with haploinsufficiency of the transcription factor *Tbx5* (*Tbx5*$^{del/+}$) were viable and displayed enlarged atria as well as conduction abnormalities and abnormal gene expression patterns (Bruneau *et al.* 2001). However, *Tbx5* KO mice (*Tbx5*$^{del/del}$) did not survive past embryonic day 10.5. *Tbx5* KO mice also displayed impaired cardiac differentiation. In *Tbx5* KO mice, expression of *Nkx2.5* decreased at E8.5, and by E10 *Nkx2.5* transcript levels were almost undetectable (Bruneau *et al.* 2001). Taken together, these observations provide evidence for a network of interdependent transcriptional regulatory factors involved in proper cardiac chamber formation in the developing heart.

1.3.4 MEF2 in atrial and ventricular tissue differences

The atria and ventricular chambers are the two main tissues in the mammalian heart. These two tissues serve different functions in the cardiovascular system. The primary role of the ventricles is to facilitate the distribution of blood to the lungs for oxygenation (pulmonary ventricle) and to the organs in the body (systemic ventricle) by pumping blood through the circulatory system. The atrial chambers of the heart receive and pump the blood into the ventricles. For the most part, atrial and ventricular myocytes have similar functions in both chambers, but surprisingly, they do not express the same genes. It is known that certain transcription factors expressed in the heart facilitate chamber identity such as COUP-TFII (Pereira *et al.* 1999, Wu *et al.* 2013). Various studies have shown that atrial and ventricular chambers, and to an extent left and right sides of respective chambers, have differential gene expression (Tabibiazar *et al.* 2003, Zhao *et al.* 2002). In a similar study, promoters of genes that are differentially expressed throughout the heart were analyzed, and promoters of atrial-enriched genes were found to contain MEF2 transcription factor binding sites (Zhao *et al.* 2002). Moreover, it was suggested that MEF2 plays a role in the differential expression of key genes throughout the heart, and more specifically, in the atrial chambers of the heart. However, the conclusions drawn from those studies are not entirely convincing due to the lack of proper controls and additional quantifications. A more thorough investigation is needed regarding chamber-specific roles for MEF2A as suggested by these researchers (Zhao *et al.* 2002).

Interestingly, although MEF2 factors have been shown to be expressed in both atria and ventricular chambers for the heart, MEF2 proteins have been implicated in the regulation of atrial and ventricular chamber-restricted genes. Expression of a minimal enhancer of the *Mlc2v* gene in the ventricles was shown to be dependent on a MEF2 site (Ross *et al.* 1996). The atrial chamber-enriched gene *ANF* was shown to be co-regulated by MEF2 and GATA-4 and by MEF2A and PITX2C (Morin *et al.* 2000, Toro *et al.* 2004). MEF2C has been shown to regulate the enhancers of the *BOP* and *Hcn4* genes in the second heart field and atrioventricular conduction system, respectively (Phan *et al.* 2005, Vedantham *et al.* 2013). Taken together, these observations suggest that MEF2 factors are necessary to coordinate proper cardiac chamber-dependent gene expression.

1.3.5 Chamber-related diseases in the heart

The differential chamber-dependent regulation of cardiac genes may provide a mechanism by which a diseased heart regionally reprograms gene expression according to a specific insult. In this instance, modulation of MEF2 activity through preferential interaction with coregulators would drive a chamber-specific gene regulatory response as part of the pathological remodeling of the heart. A MEF2-dependent transgene, a reporter that responds to all MEF2 isoforms, showed preferential atrial activation when mice were treated with various cardiac insults such as isoproterenol, angiotensin II, and thyroid hormone (Zhao *et al.* 2002). The immediate early and widely expressed bZip transcription factor ATF3 was also shown to be preferentially upregulated in the atrial chambers of mice treated with angiotensin II whereas adrenergic stimulation induced

ATF3 similarly in all chambers (Hasin *et al.* 2011). Based on these observations it is likely that additional TFs in the heart control differential chamber activity in response to specific pathological stimuli.

1.4 MEF2-interacting transcriptional co-regulators

MEF2 proteins are primarily transcriptional activators, and MEF2 transcription factors interact with transcriptional co-regulators for precise regulation of target genes. Studies provide evidence that MEF2 is involved in interactions with transcriptional co-factors that modulate the activity of MEF2 proteins (Feng *et al.* 2015, Van Rooij *et al.* 2010, Toro *et al.* 2004). Here, I discuss the different interactions that MEF2 proteins participate in with other transcriptional co-regulators. These interactions include chromatin remodeling proteins, repressive effects, and synergistic activation of target genes. I also discuss potential co-regulators that have been shown to interact with MEF2 proteins at some capacity. In Chapter 3 I will show that MEF2A interacts with these cofactors to further modulate and regulate the activity of target genes.

1.4.1 Modulation of MEF2 transcriptional activity

Histone deacetylase complexes (HDACs) remove the acetyl groups from histones to condense the chromatin to reduce expression of certain genes. MEF2 is known to interact with class IIa HDACs and forms repressive complexes on MEF2 target genes such as matrix metalloproteinase 10 (*Mmp10*), myoglobin, and myogenin (Bassel-Duby *et al.* 1992, Bertos *et al.* 2001, Chang *et al.* 2006, Cheng *et al.* 1993). Protein kinases

regulated by calcium signals phosphorylate these class IIa HDACs. This phosphorylation then promotes nuclear-to cytoplasmic translocation of these HDACs. Phosphorylation-mediated translocation of HDACs out of the nucleus then relieves the HDAC-mediated transcriptional repressive effects and leads to the activation of MEF2 (McKinsey & Olson 2005, Zhang *et al.* 2002). These types of interactions provide a mechanism for the modulation of expression of MEF2 target genes in response to physiological and pathological signaling (Potthoff & Olson 2007).

Another interaction showing negative modulation of MEF2 activity is with the early growth response protein 1 (EGR1) (Feng *et al.* 2015). In these studies, a bioinformatics approach was used to identify cis-elements as binding sites for transcriptional co-regulators of MEF2A-dependent costamere genes (Ewen *et al.* 2011), and the early growth response (EGR) family was identified as a candidate co-regulator. EGR1 was found to be a potent repressor of MEF2A activity. These repressive effects were observed in both non-cardiac and cardiac cells. Additionally experiments showed that EGR1 and MEF2A interact *in vivo* in co-immunoprecipitation studies, and that costamere-localized genes are upregulated in EGR1-depleted NRVMs.

Previous findings in the field provide evidence that interactions between MEF2 transcription factors and other proteins on upstream regulatory regions of genes result in synergistic transcriptional activation. Some examples of this include MEF2A and PITX2C in oral epithelial cells (Toro *et al.* 2004). These findings report both isoform-specific and cell-specific synergistic activation. Interaction between the bHLH protein MASH1 and MEF2C has been shown to promote synergistic activation of transcription

through either the MASH1 or the MEF2 site in *in vitro* reporter assays (Black *et al.* 1996). These studies demonstrate that the MEF2 domain is necessary for MASH1/MEF2C interaction, and that either DNA-binding site is able to promote synergistic activation involving both factors. It has also been shown that MEF2 isoforms –A, –C, and –D functionally interact with GATA-4 to cooperatively activate the ANF promoter (Morin *et al.* 2000). These findings demonstrate an additional layer of regulation that MEF2 interactions provide. Both repressive and synergistic activation effects provide evidence of the fine-tuning of transcriptional activity that MEF2 proteins can undergo.

1.4.2 Potential MEF2A transcriptional co-regulator interactions

Here I discuss three sets of transcription factors with known expression and roles in the adult heart: HAND factors, Nkx2.5, and estrogen receptors. Aside from their roles in cardiac development and homeostasis, these transcription factors have distinct expression patterns in the heart. In Chapter 3, I present data that show that *Mef2a* KO mice display preferential gene dysregulation in a chamber-dependent manner in the adult heart. Additionally, bioinformatics analysis of upstream regulatory regions from promoters of these MEF2A-sensitive genes revealed an enrichment of HAND, Nkx, and estrogen receptor transcription factor binding sites, also aligning with each factor's expression pattern in the heart. Altogether, these findings make HAND proteins, Nkx2.5, and estrogen receptors as promising candidates as co-regulators of MEF2A transcriptional activity *in vivo*.

1.4.2.1 The bHLH HAND factors

The basic helix-loop-helix (bHLH) factors HAND1 (eHAND) and HAND2 (dHAND) are members of the Twist family of bHLH proteins. HAND factors function as either homo– or heterodimers binding to consensus sequences known as E-boxes (CANNTG) (Barnes & Firulli 2009, Conway *et al.* 2010, Firulli 2003). Previous studies describe the complementary expression of HAND1 and HAND2 in the left and right ventricles, respectively (Srivastava *et al.* 1997). Additional studies have expanded the expression patterns of both HAND proteins, describing HAND1 expression in the myocardial cuff on the cardiac outflow tract, and HAND2 expression in myocardium, endocardium, and epicardium (Firulli *et al.* 2000). *Hand2*-null mice die between E9.5 and E10.5 from cardiac and vascular defects (Srivastava *et al.* 1997, Yamagishi *et al.* 2000). The cardiac-related phenotypes in *Hand1*-null mice are more difficult to interpret due to extra-embryonic mesoderm that results in lethality between E8.0 and E9.0 (Firulli *et al.* 1998, Riley *et al.* 1998). In these studies, heart morphology is altered but extra-embryonic effects make it difficult to interpret these results.

HAND proteins have been shown to interact with MEF2 factors. In previous studies HAND2 interacts with MEF2C (Zang *et al.* 2004). Using the atrial natriuretic peptide (ANF; *Nppa*) promoter, HAND2 and MEF2C synergistically activated expression in transfected HeLa cells (Zang *et al.* 2004). Additional GST-pulldown and immunoprecipitation assays show that HAND2 and full-length MEF2C are able to interact *in vitro* and *in vivo*. Additional studies have shown that HAND1 and MEF2A

interaction results in synergistic activation of the ANF promoter (Morin *et al.* 2005). HAND1 is recruited to the promoter via a physical interaction with MEF2A.

In light of these observations, it possible that HAND factors interact with MEF2A and this interaction modulates and adds an extra layer of regulation to MEF2A-dependent genes in the ventricular chambers of the mammalian heart.

1.4.2.2 NKX2.5

NKX homeobox factors are a family of evolutionarily conserved proteins. In *Drosophila*, *tinman* (*Nkx2.5*) is used a marker of cardiogenesis (Harvey 1996). NKX homeobox and MEF2 factors have been shown to interact. In co-immunoprecipitation studies, NKX2.5 and MEF2C interact *in vitro* (Vincentz *et al.* 2008). MEF2 factors and NKX2.5 have a similar expression pattern in the developing heart and target similar genes (Vincentz *et al.* 2008). Since MEF2C and NKX2.5 have been shown to interact and their spatial and temporal expression patterns are similar, it is possible that NKX2.5 and MEF2 factors cooperatively regulate genes in the heart. More specifically, it is possible that NKX2.5 and MEF2A coordinately regulate a subset of MEF2A-dependent genes in the heart.

1.4.2.3 Estrogen receptors

Estrogen receptor alpha (ERα) and estrogen receptor beta (ERβ) are two nuclear estrogen receptors encoded by the *Esr1* and *Esr2* genes, respectively (Luo & Kim 2016). ERα and ERβ expressed in the heart are active and are involved in the regulation of gene

expression (Knowlton & Lee 2012). Estrogen receptors are expressed in both cardiac fibroblasts and myocytes (Grohé *et al.* 1997). While ERα and ERβ are both expressed in the heart, their expression patterns are different. While no observable difference were present between male and female adult rat ventricles, subcellular fractionation shows greater localization of ERβ protein in the nucleus of ventricular myocytes *in vivo*, and female mice show higher levels of ERα in the ventricles and higher levels of ERβ in the atrial chambers (Lizotte *et al.* 2009)

To date there are no data to support that MEF2 and estrogen receptor proteins physically interact to regulate target genes. However, estrogen receptors have been shown to be downstream targets of MEF2 signaling. Female mice lacking class IIa HDAC5 and HDAC9 are protected against maladaptive cardiac remodeling after myocardial infarction, where normally there is an increase in expression of gene sensitive to estrogen levels (Van Rooij *et al.* 2010). Others studies have confirmed up-regulation of ERα during human heart failure (Mahmoodzadeh *et al.* 2006). Additionally, *Ers1* was shown to be a direct target of MEF2C. Interestingly, ERα interacts with the MEF2 binding domain of class II HDACs *in vitro* (Van Rooij *et al.* 2010). Estrogen receptors have also been shown to activate ANF in the rat heart (Jankowski *et al.* 2001).

Keeping in mind the expression and role of estrogen receptors in the heart, global transcriptome analysis in *Mef2a* knockout hearts coupled with bioinformatics analysis point to estrogen receptors as appealing candidates for interacting partners to modulate MEF2 transcriptional activity.

1.5 A novel direct-target gene of MEF2A

1.5.1 Bex1

The brain expressed x-linked gene 1 (*Bex1*) gene is located on the X-chromosome in rodent and human genomes, and *Bex1* RNA is expressed in the brain, heart, and liver (Alvarez *et al.* 2005). Initial experiments on BEX1 linked this small adaptor-like protein to the cell cycle and neurotrophin signaling in PC12 cells (Vilar *et al.* 2006). In these studies, a screen identified BEX1 as an interacting protein with the intracellular domain of the p75 neurotrophin receptor (p75-NTR). In PC12 cells, *Bex1* levels oscillated during the cell cycle, and downregulation of *Bex1* expression inhibited PC12 differentiation in response to nerve growth factor (NGF) (Vilar *et al.* 2006).

Several loss-of-function analyses have been performed to determine the role of BEX1 in other cell types. *Bex1* KO mice appear to develop normally and are fertile, but were found to perform poorly in treadmill exercises compared to wild-type control mice (Koo *et al.* 2007). Intramuscular cardiotoxin injection, a widely used model for muscle regeneration studies, in *Bex1* KO mice showed prolonged cell proliferation and delayed cell differentiation. These studies indicated that *Bex1* plays a role in skeletal muscle regeneration (Koo *et al.* 2007). Myoblasts harvested from *Bex1* KO mice showed a defect in myoblast-myotube fusion *in vitro* (Jiang *et al.* 2016). While some studies have begun to uncover the role of BEX1 in neuronal and myocyte cell types, overall information on BEX1 is lacking.

1.5.2 *Bex1* in the heart

To date there are several dozen research articles about Bex1, and only a few of these link *Bex1* to the heart. Therefore not much is known about Bex1 in the heart, and *Bex1* studies are lacking in the cardiac biology field. There is evidence to support that *Bex1* is involved in the proper development of the heart. Mice lacking the p75-NTR gene show cardiac innervation defects (Habecker *et al.* 2008). Since the BEX1 protein is downstream of the p75-NTR, it is likely that perturbation of BEX1 also leads to cardiac defects. In a single-cell resolution of temporal gene expression study performed on developing hearts (E9.5 – P21), *Bex1* RNA was one of the top ten enriched transcripts in the left ventricular chamber of E14.5 mice (DeLaughter *et al.* 2016). Altogether, *Bex1* has been shown to be expressed in the brain and in the heart, an expression pattern similar to the MEF2 proteins. Therefore, it is possible that MEF2 regulates BEX1 expression and links itself to neurotrophin signaling and the cell cycle in the heart.

1.6 Thesis rationale

Atrial and ventricular chambers have differing specified roles in the function of the mammalian heart although gene expression and cytoarchitecture of myocytes in these tissues do not differ greatly. MEF2 proteins are key regulators of differentiation and gene programs in cardiomyocytes. While studies have shown the importance of MEF2, most research has focused on the ventricular chamber, and is somewhat biased in this regard.

This dissertation is presented in two parts. The work in Chapter Three focuses on dissecting the mechanisms behind the differential regulation of MEF2A-dependent genes and cellular pathways between atrial and ventricular chambers of the heart. MEF2

proteins interact with numerous transcriptional co-regulators that modulate the transcriptional activity on target genes. In this chapter, I present data indicating that MEF2A transcriptional activity is modulated by chamber-dependent expression of transcriptional co-regulators. This additional layer of transcriptional control is responsible for the chamber-dependent regulation of molecular pathways downstream of MEF2A. The research in Chapter Four focuses on the gene *Bex1*, a candidate target of MEF2A. BEX1 is an intracellular adaptor protein involved in neurotrophin signaling and the cell cycle. Additionally, *Bex1* function has been implicated in muscle regeneration and myocyte fusion, functions similar to the role of MEF2A in skeletal muscle. These findings suggest a role for BEX1 in the ventricular myocardium, and potentially link MEF2A to neurotrophin signaling and the cell cycle in ventricular cardiomyocytes. This work suggests that neurotrophin signaling and the cell cycle are regulated by MEF2A through its interaction with the *Bex1* gene in cardiomyocytes.

The primary goal of the research presented in this thesis is to uncover the differential regulation of target genes and cellular pathways by MEF2A in the adult mammalian heart. By doing so, we will characterize the functional role of MEF2A in adult cardiac chambers. Additionally, we begin to understand the mechanism of the chamber-dependent differential regulation of MEF2A transcriptional activity in the adult heart. This research will also contribute to the knowledge of differential regulation of other transcription factors in the developing and adult heart.

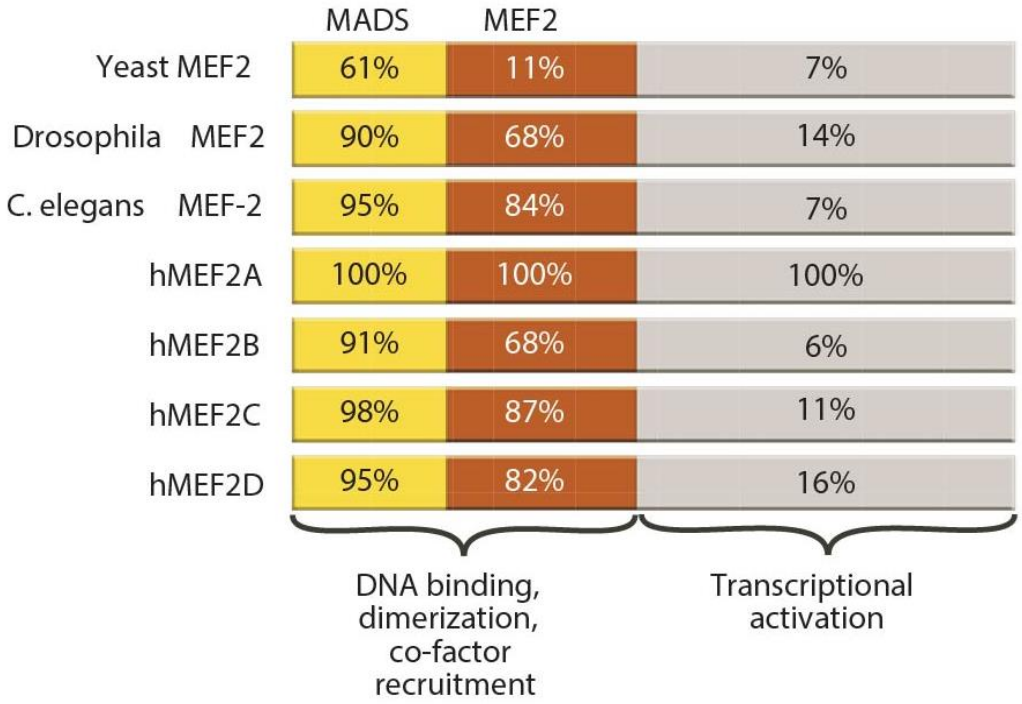

Figure 1.1 Amino acid sequence identity of MEF2 proteins. For each MEF2 protein domain across several species, amino acid sequence identity percentage is compared to human MEF2A (hMEF2A). With the exception of yeast MEF2, MADS-box and MEF2-domains of MEF2 proteins across different species shows high percentage amino acid sequence identity. The transcriptional activation domain is divergent across all species and within human isoforms. Image adapted from (Potthoff & Olson 2007).

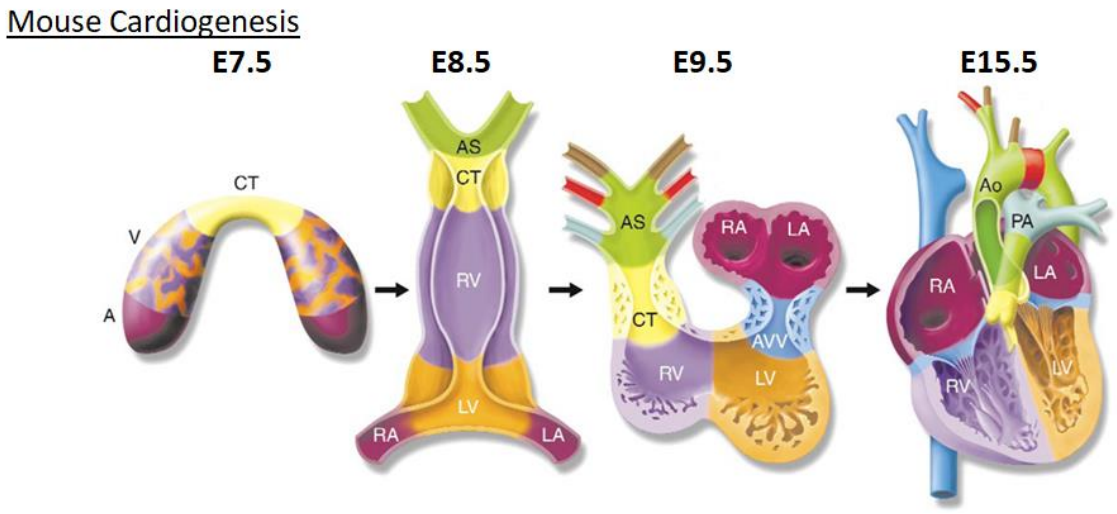

Figure 1.2 The four main stages of mammalian heart development. From left to right: Cardiac progenitor cells migrate from the anterior lateral mesoderm and converge at the ventral midline to form a cardiac crescent at embryonic day 7.5 (E7.5). The cardiac crescent cells extend to form a functional linear heart tube (E8.5), which then undergoes rightward looping (E8.5). After cardiac looping, each chamber is now correctly positioned and each cardiac chamber undergoes maturation and growth (E15.5). A, atrium; Ao, aorta; AVV, atrioventricular valve segment; CT, conotruncal segment; LA, left atrium; LV, left ventricle; PA, pulmonary artery; RA, right atrium; RV, right ventricle; V, ventricle. Image adapted from (Srivastava & Olson 2000).

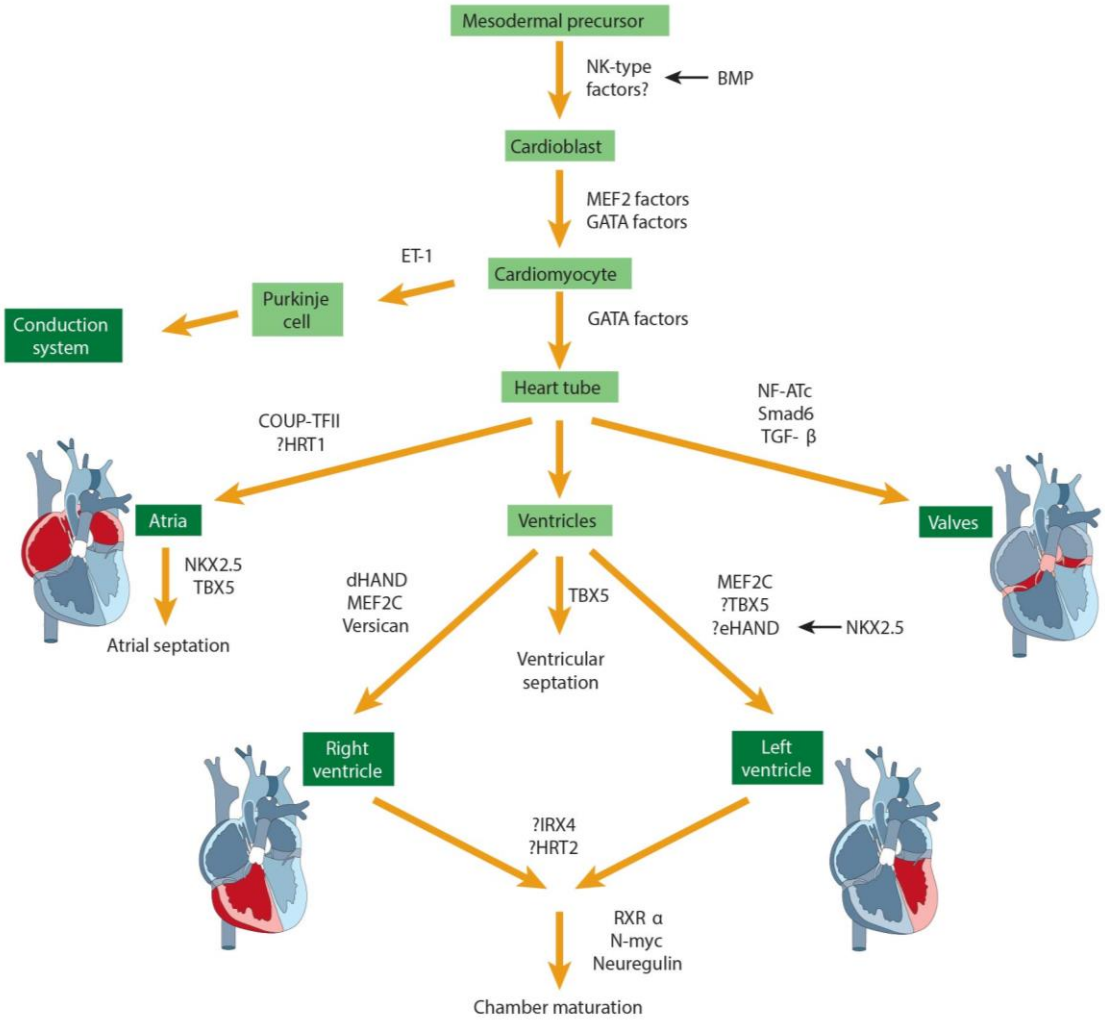

Figure 1.3 Atrial and ventricular chambers expresses different transcriptional regulators. During mammalian cardiogenesis, the expression of different regulatory proteins are necessary for proper cardiac chamber development, septation, and maturation. Regulatory factors necessary for specific stages in mammalian cardiogenesis are indicated beside each arrow. Image adapted from (Srivastava & Olson 2000).

CHAPTER TWO: Materials and Methods

2.1 Mouse colony maintenance and tissue preparation

Experimental procedures on animals used in these studies were approved by the Boston University Institutional Animal Care and Use Committees (IACUC) (Protocol numbers 11-001, 13-048, and 16-019). These studies were performed in accordance with the principals of animal care and experimentation in the Guide for the Care and Use of Laboratory Animals.

2.1.1 Mouse husbandry

For MEF2A knockout studies, one *Mef2a* heterozygous-null (*Mef2a*$^{+/-}$) sire and dam were used as a breeding pair. For *Mef2a* overexpressing transgenic studies, one sire of *Mef2a*$^{+/-}$;Tg(αMHC:*Mef2a*) genotype and one dam of *Mef2a*$^{+/-}$ genotype were used as a breeding pairs. Pups from each litter were weaned at 21 days of age. Tail clippings 2 mm in length were collected from each pup for genomic DNA isolation. Pup ears were notched in specific positions for identification purposes. Food, water, and bedding were overseen by the technicians and staff at the Boston University Charles River Campus Animal Science Center.

2.1.2 Tail clipping and genomic DNA isolation

Clipped tails were placed in 1.5 mL microcentrifuge tubes containing 200 μL Tail Lysis Buffer containing Proteinase K (10 mM Tris, pH 8.0; 25 mM EDTA, pH 8.0;

100 mM NaCl; 1% SDS, 200 μg/mL Proteinase K). Tails were incubated at 55 °C for at least 12 h to overnight. 200 μL of 1:1 phenol:chloroform was added to each tube, and tubes were vigorously shaken for 15 – 20 sec to ensure proper mixing. 150 μL of the aqueous layer from each sample was transferred to a clean tube, and to each tube 375 μL of ice-cold 100% ethanol was added. Tubes were vigorously shaken for 15-20 sec to ensure proper mixing. Samples were centrifuged at 13,500 rpm for 5 min at room temperature, and the supernatant was removed from each tube. Pellets were washed with 300 μL of ice-cold 70% ethanol, and samples were centrifuged at 13,500 rpm for 1 min at room temperature. The supernatant was removed from each tube, and pellets were allowed to air dry completely for at least 30 min. DNA pellets were redissolved in 200 μL of sterile water and then stored at -20 °C.

2.1.3 Genotyping

Genomic tail DNA was subjected to PCR using allele-specific primers. 1 μL of genomic tail DNA was added to a PCR containing 1 μL primer mix, 2 μL 10 mM dNTPs, 2.5 μL 10X Thermopol Buffer (New England Biolabs), 0.25 μL Taq Polymerase (New England Biolabs), and 18.25 μL sterile water. For detecting *Mef2a* WT and mutant alleles, primer mixes were created by combining 25 μL 100 μM *Mef2a* forward primer, 25 μL 100 μM *Neomycin* forward primer, and 50 μL 100 μM *Mef2a* reverse primer. For detecting *Mef2a* transgenic allele, primer mixes were created by combining 25 μL 100 μM HGH-*Mef2a* forward primer, 25 μL 100 μM HGH-*Mef2a* reverse primer, 12.5 μL 100 μM IL-2 forward primer, 12.5 μL 100 μM IL-2 reverse primer, and 25 μL

sterile water. General thermocycling parameters (PTC-100 Thermal Cycler, MJ Research) were as follows: *1*, 95 °C for 4:00 min; *2*, 95 °C for 30 sec; *3*, 60 °C for 30 sec; *4*, 68 °C for 30 sec; *5*, go to step *2* for 29 additional cycles; *6*, 68 °C for 5:00 min; *7*, hold at 4 °C; *8*, end program. 4 μL of 6X Orange-G DNA loading dye (1 ml 50X TAE buffer [2 M Tris, 2.5 M sodium acetate, 50 mM EDTA pH 8.0], 75 mg Orange-G, 30 mL 100% glycerol, final volume to 50 mL with deionized water) was added to each completed genotyping reaction, and samples were electrophoresed on a 0.8% agarose gel in 1X TAE buffer (40 mM Tris, 50 mM sodium acetate, 1 mM EDTA pH 8.0). Genotyping gels were imaged on a Bio-Rad imaging station under UV light.

2.1.4 Tissue dissection

Mice were euthanized in the Boston University Animal Science Center. Atria, ventricles, and additional tissues were carefully dissected and thoroughly rinsed with 1X PBS to remove blood. Tissues were used for RNA extraction, protein extraction, cyrosectioning, or chromatin immunoprecipitation (ChIP) as described below.

2.1.5 RNA isolation

Dissected tissues were homogenized in 1 mL of Trizol reagent (Life Technologies) using a Polytron homogenizer for 30 sec. Homogenized tissue samples were transferred into a 1.7 mL microcentrifuge tube, and 0.2 mL chloroform was added to each sample. Tubes were closed tightly, shaken vigorously for 30 sec, and then incubated at room temperature for 3 min. Tubes were centrifuged at 13,500 rpm for

10 min at 4 °C. The top aqueous layer from each sample was transferred into a new 1.7 mL microcentrifuge tube, and to each sample 0.5 mL isopropanol was added. Tubes were closed tightly, shaken for 30 sec, and were incubated at -20 °C for at least 1 h for RNA precipitation. Precipitated samples were centrifuged at 13,500 rpm for 30 min at 4 °C. The supernatant from each tube was carefully removed, and each pellet was washed with 1 mL 70% ethanol and subsequently centrifuged at 13,500 rpm for 5 min at 4 °C. The supernatant from each tube was carefully removed, and pellets were allowed to air dry for 10 min. Pellets were resuspended in 20 μL of sterile nuclease-free water. RNA concentration was determined using a Nanodrop (Thermo Fisher Scientific).

2.1.6 Protein extraction

Dissected and cleaned tissues were cut into smaller pieces and each was placed into a 1.7 mL microcentrifuge tube. For atria and ventricles, 50 μL and 1 mL of complete ELB (50 mM HEPES, 250 mM M NaCl, 5 mM EDTA, 0.1% NP-40, 1 mM PMSF, 1 mM DTT, and 1X protease inhibitor (Roche)) was added to each tube, respectively. Tissue pieces in complete ELB were further homogenized using a disposable microcentrifuge pestle. Protein lysates were allowed to incubate on ice for 10 min, and then clarified by centrifuging at 13,500 rpm for 10 min at 4 °C. Clarified protein lysate supernatants were transferred to a clean 1.7 mL microcentrifuge tube, and samples were stored at -80 °C. Samples probed for Histone H3 were sonicated using Digital Sonifer 450 (Branson) prior to centrifugation.

2.1.7 Tissue preparation for cryosectioning

Dissected and rinsed tissues were placed in a 15 mL conical tube filled with 10 mL sucrose solution (30% sucrose, 1X PBS) to cryoprotect samples. Tissues in sucrose solution were incubated at 4 °C, and tissues were gently squeezed repeatedly with forceps for 15 sec every hour until tissues were no longer buoyant (approximately 4 h). Tissues were recovered from sucrose solution, quickly rinsed in 1X PBS, and placed into aluminum foil molds (1 cm x 1 cm x 1 cm) containing Tissue-Tek O.C.T. compound (Sakura Fine-Tek). A small freezing bath using dry ice and isopentane was prepared, and embedded tissues were partially submerged until O.C.T. compound turned opaque. Embedded and frozen tissues were stored at -80 °C.

2.1.8 Tissue preparation for chromatin-immunoprecipitation

Dissected tissue and rinsed tissues were frozen slowly by placing tissues over a piece of aluminum foil on top of dry ice pellets. Once completely frozen, tissue samples were collected and placed in a pre-chilled ceramic mortar. Tissues were pulverized using a ceramic pestle, and small amounts of liquid nitrogen were continuously added during pulverization procedure to prevent samples from thawing. Frozen, pulverized tissue samples were collected into a 1.7 mL microcentrifuge tube and stored at -80 °C.

2.2 Recombinant DNA Techniques

2.2.1 Preparing chemically competent *E. coli*

DH5α cells were plated on a Lysogeny Broth (LB) agar plate (10 g/L casein peptone, 5 g/L yeast extract, 5 g/L sodium chloride, 15 g/L agar) and incubated for 12 – 16 h at 37 °C. 5 mL LB (10 g/L casein peptone, 5 g/L yeast extract, 5 g/L sodium chloride) was inoculated with a singly colony and incubated in a shaking incubator at 225 rpm for 12 – 16 h at 37 °C. The entire liquid culture was transferred into 200 mL LB and DH5α cells were grown to an undiluted absorbance reading between 0.4 and 0.6 at 600 nm wavelength. Cells were harvested by centrifugation at 3,000 *g* for 5 min at 4 °C. Cells were resuspended in 20 mL of chilled 10 mM NaCl. To each sample 80 mL of chilled 100 mM $CaCl_2$ was added, and cells were centrifuged at 3,000 *g* for 5 min at 4 °C. The cell pellet was resuspended in 80 mL of chilled 100 mM $CaCl_2$, and incubated on ice for 30 to 60 min. Cells were centrifuged at 3,000 *g* for 5 min at 4 °C. The cell pellet was resuspended in 17 mL 100 mM $CaCl_2$ supplemented with 3 mL 100% glycerol. DH5α aliquots were generated by aliquoting 100 μL of cell suspension into 1.7 mL microcentrifuge tubes, which were then flash frozen using liquid nitrogen and stored at -80 °C.

2.2.2 Transforming chemically competent *E. coli*

DH5α aliquots were thawed on ice for 15 – 20 min. 100 – 200 ng of plasmid DNA (5 – 10 μL of ligation reaction) was then added to each aliquot of cells and samples were mixed gently. The DH5α/DNA mixture was incubated on ice for 10 min. Competent cells were heat shocked in a 42 °C water bath for 30 sec, then immediately placed on ice for 2 min. 500 μL LB was added to transformed bacteria and the mixture was transferred

to a 14 mL snap-cap tube. Tubes were incubated in a shaking incubator at 225 rpm for 1 h at 37 °C.

For plasmid DNA, 100 µL of bacteria were plated on LB agar plates containing the appropriate antibiotic selection drug. For ligation reactions, bacteria were transferred to a clean 1.7 mL microcentrifuge tube and pelleted by centrifugation at 6,000 *g* for 1 min at room temperature. The supernatant was discarded from each tube leaving behind approximately 100 µL of LB. Recovered cells were gently resuspended in the remaining 100 µL of LB and plated on LB agar plates containing the appropriate antibiotic selection drug. LB agar plates were incubated overnight at 37 °C. After confirmation of colony growth, LB agar plates were stored in the cold room at 4 °C.

2.2.3 Plasmid purification

For mini preps, 3 mL of antibiotic supplemented LB was inoculated with a single colony. Inoculated tubes were placed in a shaking incubator at 225 rpm for 12 – 16 h at 37 °C. 1.5 mL of culture was transferred into a 1.7 mL microcentrifuge tube, and tubes were centrifuged at 13,500 rpm for 1 min. The supernatant was decanted from each tube, and pellets were resuspended with 100 µL Resuspension Buffer (50 mM glucose, 10 mM EDTA pH 8.0, 25 mM Tris pH 8.0). 200 µL Lysis Buffer (0.2 M NaOH, 1% SDS) was added to each tube and immediately inverted 6 – 8 times. The lysis reaction was allowed to proceed for no longer than 5 min, and 150 µL Neutralization Buffer (3 M potassium acetate, 2 M acetic acid) was then added to each tube and immediately inverted 6 – 8 times. 400 µL phenol/chloroform was added to each tube and shaken by hand for 30 –

60 sec. Samples were centrifuged at 13,500 rpm for 1 min at room temperature. 400 μL of the aqueous phase from each sample was transferred into a new 1.7 mL microcentrifuge tube. 1 mL (2.5 volumes) of ice cold 100% ethanol was added to each tube, mixed by shaking, and tube were centrifuged at 13,500 rpm for 30 min at 4 °C. The supernatant from each tube was discarded, and DNA pellets were washed with 200 μL 70% ethanol. Samples were centrifuged at 13,500 rpm for 1 min at room temperature. The supernatant from each tube was discarded, and DNA pellets were allowed to air dry for 30 min. Air-dried pellets were resuspended in 25 μL sterile water containing 100 μg/mL of RNase. Mini preps were incubated for 15 min at 37 °C for complete RNA degradation. Samples were stored at -20 °C.

For midi preps, 3 mL of antibiotic supplemented LB was inoculated with a single colony. Inoculated tubes were placed in a shaking incubator at 225 rpm for 12 – 16 h at 37 °C. 100 mL of antibiotic supplemented LB was inoculated with 3 mL of previously grown inoculated culture. 100 mL of inoculated culture was placed in a shaking incubator at 225 rpm for 12 – 16 h at 37 °C. Cells were harvested by centrifugation at 6,000 *g* for 15 min at 4 °C. Plasmid DNA was isolated using the NucleoBond Midiprep Kit (Macherey-Nagel) following the manufacturer's instructions. Plasmid DNA concentration was determined using a NanoDrop, and plasmid DNA was stored at -20 °C. A list of plasmids used in this thesis can be found in Table 2.2.

2.2.4 Polymerase chain reaction

For cloning purposes, Q5 High-Fidelity DNA Polymerase was used (New England Biolabs). 10 µL 5X Q5 Reaction Buffer, 1 µL 10 mM dNTPs, 2.5 µL 100 µM forward primer, 2.5 µL 100 µM reverse primer, 1 ng template DNA, 0.5 µL Q5 High-Fidelity DNA Polymerase, and sterile nuclease-free water up to a final reaction volume of 50 µL was added and mixed in a 0.65 mL PCR tube. General thermocycling parameters (PTC-100 Thermal Cycler, MJ Research) were as follows: *1*, 98 °C for 30 sec; *2*, 98 °C for 30 sec; *3*, annealing temperature for 30 sec; *4*, 72 °C for proper extension time; *5*, go to step *2* for 29 additional cycles; *6*, 72 °C for 2:00 min; *7*, hold at 4 °C; *8*, end program. Optimal annealing temperatures were calculated using NEB T_m calculator (https://tmcalculator.neb.com), and extension times were dependent on product length.

2.2.5 Nucleic acid purification for PCR products

For intermediate clean-up of PCR products before restriction digestion, phenol/chloroform extraction was used. PCRs were transferred to a 1.7 mL microcentrifuge tube and sterile nuclease-free water was added to a final volume of 200 µL. An equal volume of 1:1 phenol:chloroform was added to each sample and mixed vigorously for 30 sec. Samples were centrifuged at 13,500 rpm for 3 min at room temperature. The aqueous phase was transferred to a new 1.7 mL microcentrifuge tube, and 20 µL 3 M sodium acetate pH 5.2, 2 µL 20 mg/mL glycogen, and 500 µL cold 100% ethanol was added to each sample. Samples were incubated at -20 °C for 1 h. Tubes were centrifuged at 13,500 rpm for 30 min at 4 °C. The supernatant from each sample was removed and the pellet was washed with 250 µL cold 70% ethanol. Samples were

centrifuged at 13,500 rpm for 2 min at room temperature. The supernatant from each sample was removed and the pellets were allowed to air dry for 15 – 20 min. Air-dried pellets were resuspended in 20 μL of sterile nuclease-free water.

2.2.6 Restriction digestion

Typically, DNA was digested using restriction enzymes from New England Biolabs. 5 μL of appropriate 10X NEB Buffer, 2 μg plasmid DNA or 20 μL cleaned PCR product, 10 units of each restriction enzyme (0.5 – 1 μL each depending on activity concentration), and sterile nuclease-free water was added to a final reaction volume of 50 μL. Samples were incubated for 1 h at the appropriate incubation temperature. For restriction digestions using incompatible enzymes, an intermediate phenol/chloroform-based nucleic acid purification step as described above was applied in between each restriction digestion procedure.

2.2.7 Gel extraction

Digested plasmid DNA and PCR products were prepared for gel electrophoresis by adding 10 μL 6X Orange-G loading buffer to each sample. Samples were loaded onto a 0.8% agarose gel in 1X TAE buffer (40 mM Tris, 50 mM sodium acetate, 1 mM EDTA pH 8.0). Bands of interest were excised using a clean razor blade, and gel slices were transferred to 1.7 mL microcentrifuge tubes. DNA of interest from each gel slice was extracted using the QIAquick Gel Extraction Kit (QIAGEN) following the

manufacturer's instructions. The DNA concentration of gel extraction samples was determined using a NanoDrop, and samples were stored at -20 °C.

2.2.8 Ligation

Digested insert and vector were mixed at an equimolar ratio for a total of no greater than 250 ng DNA. The volume was adjusted to 7 µL with sterile water. To each ligation reaction, 1 µL 10 mM ATP, 1 µL 10X T4 DNA Ligase Buffer (New England Biolabs), and 1 µL T4 DNA Ligase (New England Biolabs) was added. Ligation reactions were incubated for 12 – 16 h at 16 °C. 5 – 10 µL of ligation reactions were used to transform chemically competent *E. coli*.

2.3 Primary cardiomyocyte isolation and cell culture techniques

2.3.1 Neonatal rat ventricular myocyte isolation

Neonatal rat ventricular myocytes (NRVMs) were extracted from two day-old Sprague Dawley neonatal rats (Charles River Labs, Strain Code 400). Neonatal rats were euthanized and decapitated. A ¼ inch incision was cut into the sternum of the neonatal rat, and angled to the left of the torso. Hearts were extracted and immediately placed into 1X HBSS (Life Technologies) in a 50 mL conical tube and placed on ice. After processing all of the neonatal rats, the hearts were transferred to a biosafety cabinet. 1X HBSS was aspirated, and dissected hearts were transfected to a 6-cm dish with 5 mL of cold 1X HBSS. Atrial chambers were removed and discarded, and ventricles were cut into 3 – 4 pieces and then transferred to a new 6-cm dish containing 5 mL of cold 1X

HBSS. Ventricles were washed by transferring tissue pieces from one 6-cm dish to another 6-cm dish containing 5 mL of cold 1X HBSS. Ventricle pieces were washed for an additional 5 times. Ventricle pieces were finally transferred to a 100 mL glass bottle containing 0.6 mg/mL trypsin (Life Technologies) and incubated overnight at 4 °C.

The next day 10 mL 10% FBS containing 1X DMEM was added to each trypsinzed heart solution, and samples were incubated in a shaker at 100 rpm for 3.5 min at 37 °C. The supernatant was discarded and 10 mL collagenase solution (1 mg/mL collagenase type 2 (Worthington, Cat# LS004176), 1X HBSS, pre-warmed to 37 °C immediately before use) was added. Tissues were collagenase treated in a shaker at 100 rpm for 6 min at 37 °C. Subsequent supernatant fractions containing NRVMs were collected in a 50 mL conical tube and placed on ice. Collagenase treatment and supernatant collection steps were repeated 7 times. NRVMs were centrifuged at 1,000 rpm for 4 min at room temperature and supernatant was discarded. The cell pellet was resuspended in 20 mL 10% FBS containing 1X DMEM, centrifuged at 1,000 rpm for 4 min at room temperature, and the supernatant was discarded. The cell pellet was resuspended in 10 mL 10% FBS containing 1X DMEM and plated onto a 10-cm dish. NRVMs were incubated for 1 h at 37 °C in a 5% CO_2 incubator (first pre-plate). NRVMs from the first pre-plate were collected and transferred to a new 10-cm dish. NRVMs were incubated for 1 h at 37 °C in a 5% CO_2 incubator (second pre-plate). NRVMs from the second pre-plate were collected and the concentration of cells in the suspension was determined using a hemocytometer. NRVMs were plated at seeding density of 300,000

cells/well in growth media (1X DMEM, 10% FBS, 1X penicillin/streptomycin/glutamine) for a 6-well plate.

The next day dead cells were removed by changing to new growth media. The following day, growth media was replaced with Nutridoma media (0.5X Nutridoma, 1X penicillin/streptomycin/glutamine, 1X DMEM). NRVMs were transfected as described below (Section 2.3.4).

2.3.2 Standard cell culture

HEK293T cells were cultured in 10-cm dishes in growth media (1X DMEM, 10% FBS, 1X penicillin/streptomycin/glutamine), 1X in an incubator at 37 °C with 5% CO_2. Near confluency, cells were detached from dish using 1 mL warm 0.25% trypsin (Life Technologies) for 2 min at room temperature. Cells were resuspended in 5 mL growth media (1X DMEM, 10% FBS, 1X penicillin/streptomycin/glutamine) and passaged at a ratio of 1:5 to 1:10. For experiments, HEK293T cells were plated at a density of 80,000 cells/well in a 6-well plate

2.3.3 PEI transfections

A maximum of 2 μg of DNA was transfected per well in a 6-well plate, and a PEI:DNA ratio of 6 μL 1 mg/mL PEI: 1 μg DNA. Experiments were performed in technical triplicate (3 wells per condition), and for each condition PEI was added to 300 μL warmed 1X DMEM and incubated for 5 min at room temperature. DNA was added to each mixture and incubated for an additional 15 min at room temperature.

Growth media from each well was removed, and cells were washed with 2 mL 1X PBS. 1X PBS was removed from each well, and 2 mL of transfection media (10% FBS, 1X DMEM, antibiotic-free) was transferred into each well. The PEI/DMEM/DNA transfection mixture was evenly distributed among triplicate wells. 24 h post-transfection, transfection media was replaced with growth media, and cells were incubated for an additional 24 h before being used for protein extraction.

2.3.4 FuGENE 6 transfections

A maximum of 2 μg of DNA was transfected per well in a 6-well plate, and a FuGENE 6:DNA ratio of 3 μL FuGENE 6: 1 μg DNA. Experiments were performed in technical triplicate (3 wells per condition), and for each condition FuGENE 6 was added to 300 μL warmed 1X DMEM and allowed to incubate for 5 min at room temperature. DNA was added to each mixture and allowed to incubate for an additional 15 min at room temperature. Growth media from each well was removed, and cells were washed with 2 mL 1X PBS. 1X PBS was removed from each well, and 2 mL of transfection media (10% FBS, 1X DMEM, antibiotic-free) was transferred into each well. FuGENE 6/DMEM/DNA transfection mixture was evenly distributed among triplicate wells. 24 h post-transfection, transfection media was replaced growth media, and cells were incubated for an additional 24 h before being used for protein extraction.

2.3.5 RNA isolation

For 10-cm dishes, the media was removed by aspiration and dishes were washed once with 1X PBS. 1X PBS was aspirated, and 1 mL of Trizol reagent (Life Technologies) was added to each dish and placed on ice. Cells in Trizol reagent were scraped using a cell scraper, and samples were transferred to a 1.7 mL microcentrifuge tube. 0.2 mL chloroform was added to each sample. Tubes were closed tightly, shaken vigorously for 30 sec, and then incubated at room temperature for 3 min. Tubes were centrifuged at 13,500 rpm for 10 min at 4 °C. The top aqueous layer from each sample was transferred into a new 1.7 mL microcentrifuge tube, and to each sample 0.5 mL isopropanol was added. Tubes were closed tightly, shaken for 30 sec, and incubated at -20 °C for at least 1 h for RNA precipitation. Precipitated samples were centrifuged at 13,500 rpm for 30 min at 4 °C. The supernatant from each tube was carefully removed, and each pellet was washed with 1 mL 70% ethanol and subsequently centrifuged at 13,500 rpm for 5 min at 4 °C. The supernatant from each tube was carefully removed, and pellets were allowed to air dry for 10 min. Pellets were resuspended in 20 μL of sterile nuclease-free water. RNA concentration was determined using a Nanodrop (Thermo Fisher Scientific).

2.3.6 Protein extraction

For luciferase assays, 350 μL of 1X Passive Lysis Buffer (Promega) was added to each well in a 6-well plate. Plates were continuously agitated on a horizontal shaker for 20 min at 4 °C. Protein lysates from each well were transferred to a 1.7 mL microcentrifuge tube and clarified by centrifugation at 13,500 rpm for 10 min at 4 °C.

Clarified protein lysate supernatants were transferred to a clean 1.7 mL microcentrifuge tube, and samples were stored at -80 °C.

2.4 Nucleic acid-based techniques

2.4.1 Microarray sample preparation

Total RNA was isolated from wild-type and knockout cardiac chambers separately (WT atria, WT ventricles, KO atria, and KO ventricles) and pooled (n=7 per pool). Pooled RNA samples were diluted to a concentration of 150 ng/µl using RNase-free sterile water and submitted to the Boston University Microarray Core Facility. Samples were processed and applied to individual GeneChip® Gene 1.0 ST Array System for Mouse (Affymetrix) arrays.

2.4.2 cDNA synthesis

For cDNA synthesis, 2 µg of RNA was brought to a final volume of 9.3 µL with sterile nuclease-free water in a 0.65 mL PCR tube. To each tube, 6 µL 10 mM dNTPs and 6.7 µL 15.4 µM random primers was added, incubated for 5 min at 65 °C, and incubated on ice for 5 min. To each tube, 6 µL 5X M-MLV Reaction Buffer, 1 µL M-MLV reverse transcriptase (Promega), and 1 µL RNasin (Promega) was added, and samples were incubated for one hour at 37 °C. cDNA samples were stored at -20 °C.

2.4.3 Reverse transcriptase-polymerase chain reaction

Synthesized cDNA was used for RT-PCR. 1 µL of cDNA was added to a PCR containing 1 µL primer mix, 2 µL 10 mM dNTPs, 2.5 µL 10X Thermopol Buffer (New England Biolabs), 0.25 µL Taq Polymerase (New England Biolabs), and 18.25 µL sterile water. Primer mixes for gene-specific primers were generated by mixing 25 µL 100 µM forward primer, 25 µL 100 µM reverse primer, and 50 µL 100 µM sterile nuclease-free water. General thermocycling parameters were as follows: *1*, 95 °C for 4:00 min; *2*, 95 °C for 30 sec; *3*, annealing temperature for 30 sec; *4*, 68 °C for 30 sec; *5*, go to step *2* for a number of additional cycles; *6*, 68 °C for 5:00 min; *7*, hold at 4 °C; *8*, end program. Appropriate annealing temperatures were determined using the online NEB T_m calculator (https://tmcalculator.neb.com), and additional cycles needed were individually determined for each gene to prevent saturation of amplicon signal. 4 µL of 6X Orange-G DNA loading dye was added to each reaction, and samples were electrophoresed on a 0.8% agarose gel in 1X TAE buffer. Genotyping gels were imaged on a Bio-Rad imaging station under UV light. Densitometry analysis was performed on the imaging software ImageJ.

2.4.4 Quantitative RT-PCR

Relative gene expression levels were measured by qRT-PCR. Quantitative RT-PCR was performed in triplicate wells. Briefly, 15 µL SYBR Green Master Mix (Applied Biosystems), 4 µL sterile nuclease-free water, 6 µL primer mix, and 5 µL diluted cDNA were mixed in 0.65 mL microcentrifuge tubes. Quantitative RT-PCR assays were performed in technical triplicate by pipetting 8.5 µL into each of three wells of a 384-well

plate. Quantitative RT-PCR reactions were performed and read in a 7900HT sequence detection system (Applied Biosystems). qRT-PCR data were analyzed using the ΔΔCT method (Livak & Schmittgen 2001). For quality control purposes, primer melting curves of Applied Biosystems SDS files were checked for single melting peaks, and 5 μL samples of final qPCRs were electrophoresed on a 1% agarose gel in 1X TAE to check for single band amplicons.

2.4.5 Chromatin immunoprecipitation

For chromatin immunoprecipitation, 100 mg of frozen pulverized tissue was transferred to a 1.7 mL microcentrifuge tube and kept frozen on dry ice. 1 mL of freshly prepared 1% formaldehyde in 1X PBS was added and cells were fixed for precisely 9.5 min to avoid over fixation. Immediately 143 μL 1 M glycine was added and samples were gently inverted for 5 min at room temperature. Tubes were centrifuged at 3,000 rpm for 5 min at 4 °C, supernatant was discarded, and cells were resuspended in 1 mL cold 1X PBS. Tubes were centrifuged again at 3,000 rpm for 5 min at 4 °C, supernatant was discarded, and cells were resuspended in 642 μL cold 1X PBS. The cell suspension was transferred to a 2 mL microcentrifuge tube and 642 μL ChIP Lysis Buffer (50 mM HEPES pH 7.5, 140 mM NaCl, 1 mM EDTA pH 8, 1% Triton X-100, 0.1% sodium deoxycholate, 0.1% SDS) and 214.2 μL 7X protease inhibitors (Roche) was added to the sample. Samples were incubated on ice for 20 min. Cells were sonicated until an average chromatin size of ~350 bp was obtained. 25 μg DNA of sonicated chromatin, 20 μL bead volume of Protein-G beads, 500 μL 7X protease inhibitors, 100 μL 100 mM PMSF,

100 μL 100 mM DTT was transferred to at 15 mL conical tube and the final volume was adjusted to 10 mL with IP Dilution Buffer (0.01% SDS, 1.1% Triton X-100, 1.2 mM EDTA, 16.7 mM Tris pH 8.1, 167 mM NaCl). 100 μL of immunoprecipitation was removed and used as 1% INPUT and then 3 μg of MEF2A or IgG antibodies were added to each immunoprecipitation reaction. Immunoprecipitations were incubated overnight at 4 °C on a Nutator. The next day, samples were centrifuged at 2,000 *g* for 10 min at 4 °C to pellet beads-antibody-protein-chromatin complexes. Pellets were resuspended in 1 mL Wash Solution I (0.1% SDS, 1% Triton X-100, 2 mM EDTA, 20 mM Tris pH 8.1, 150 mM NaCl) and incubated for 5 min at 4 °C on a Nutator. Samples were centrifuged at 2,000 *g* for 3 min at 4 °C. Pellets were resuspended in 1 mL Wash Solution II (0.1% SDS, 1% Triton X-100, 2 mM EDTA, 20 mM Tris pH 8.1, 500 mM NaCl) and incubated for 5 min at 4 °C on a Nutator. Samples were centrifuged at 2,000 *g* for 3 min at 4 °C. Pellets were resuspended in 1 mL Wash Solution III (250 mM LiCl, 1% NP-40, 1% deoxycholate, 1 mM EDTA, 10 mM Tris pH 8.1) and incubated for 5 min at 4 °C on a Nutator. Samples were centrifuged at 2,000 *g* for 3 min at 4 °C. Pellets were resuspended in 1 ml of 1X TE, incubated for 5 min at room temperature on a Nutator, centrifuged at 2,000 *g* for 3 min at room temperature for a total of three times. Pellets were resuspended in 250 μL Elution Buffer (1% SDS, 100 mM sodium bicarbonate), vortexed for 45 sec, and incubated on a Nutator for 15 min at room temperature. Samples were centrifuged at 2,000 *g* for 5 min, and the supernatant was saved in a 1.7 mL microcentrifuge tube. Elution and centrifugation steps were repeated an additional time, and a second round of 250 μL elution volume was combined with the previous elution tube. Elutions were

cleaned using phenol/chloroform extraction. Cleaned immunoprecipitation chromatin was analyzed using qPCR.

Immunoprecipitation CT values (CT_{IP}) were normalized to 1% input CT values ($CT_{1\%IN}$). Briefly, 1% input CT values were adjusted to 100% input CT values ($CT_{100\%IN}$) by subtracting 6.64, *i.e.*, $\log_2(100)$. Then, $CT_{100\%IN}$ values were subtracted from CT_{IP} values ($\Delta CT_{100\%IN - IP}$). Percent chromatin immunoprecipitated relative to total input chromatin was obtained by calculating 2 raised to the power of $\Delta CT_{100\%IN - IP}$, then multiplied by 100%.

2.5 Biochemical Assays

2.5.1 Luciferase assay

Clarified protein lysates from HEK293T cells and NRVMs were used for luciferase assays. For each sample, 10 μL clarified protein lysate was dispensed into a 1.7 mL clear microcentrifuge tube. To each sample, 50 μL of luciferase substrate reagent (Promega) was added, vortexed briefly for 5 sec to ensure mixing, and liquid was collected to the bottom of the tube with rapid downward flicking motion. Luminescence was measured on the GloMax 20/20 single tube luminometer (Promega). Luminescent readings were integrated over 10 sec. Luciferase activity readings were individually normalized using either β-galactosidase activity or Bradford assay readings (Schagat *et al.* 2007).

2.5.2 β-galactosidase assay

Clarified protein lysates from HEK293T cells were used for β-galactosidase assays. For each sample, 10 μL clarified protein lysate was dispensed into a 1.7 mL microcentrifuge tube. To each sample, 135 μL Master Mix (6.6 mM sodium phosphate dibasic, 4.4 mM sodium phosphate monobasic, 1.1 mM KCl, 100 μM $MgSO_4$, 977.8 μg/mL ortho-Nitrophenyl-β-galactosidase, 28.6 mM β-mercaptoethanol) was added, and reactions were vortexed and collected at the base of the tube. Once sufficiently yellow in color, reactions were halted by adding 250 μL 1 M sodium carbonate and vortexed. 200 μL of halted reactions were transferred into a 96-well plate and read on a spectrophotometer at a wavelength of 420 nm.

2.5.3 Bradford assay

For generating a protein standard curve, 5 μL sample volumes containing 0 – 5 μg of bovine serum albumin in 0.5 μg increments were dispensed into separate wells in a 96-well plate. For protein concentration determination in clarified lysates, 5 μL sample volumes were dispensed into separate wells. To each well 200 μL of diluted Bradford reagent (Bio-Rad, diluted 1:5 in deionized water) was added to each well, and Bradford reactions were incubated for a minimum of 2 min. Bradford assay plate was read on a spectrophotometer at a wavelength of 595 nm.

2.5.4 SDS polyacrylamide gel electrophoresis

Protein samples were resolved on denaturing SDS polyacrylamide gels. For each lane, 15 μg of clarified lysate was transferred to a 1.7 mL microcentrifuge tube and

brought to a final volume of 30 μL with deionized water. To each sample, 5 μL of 6X SDS-PAGE loading dye (250 mM Tris pH 6.8, 10% SDS, 40% glycerol, 5% β-mercaptoethanol, 0.02% bromophenol blue) was added and samples were denatured by heating at 95 °C for 10 min. Samples were loaded onto an discontinuous gel (5% stacking gel, 10% resolving gel), and 80 V of current were applied through the stacking gel, and 180 V of current were applied through the resolving gel until the bromophenol blue dye front reached the lower tenth of the gel. SDS polyacrylamide gels were removed from the glass plates for western blotting.

2.5.5 Western blotting

Protein samples were transferred onto a PVDF membrane (Bio-Rad) in transfer buffer (20 mM Tris, 150 mM glycine, 20% methanol) at 100 V for one hour. Western blot membranes were blocked overnight at 4 °C in 1X TBS (50 mM Tris pH 7.5, 150 mM NaCl) containing 5% nonfat dry milk. Membranes were then incubated in 1X TBS containing 5% nonfat dry milk and suitably diluted primary antibodies with shaking for one hour at room temperature. Membranes were washed for 5 min for a total of three times in 1X TBST (1X TBS containing 0.1% Tween-20). Blots were then incubated in 1X TBST and suitably diluted secondary antibodies with shaking for one hour at room temperature. Membranes were washed for 5 min for a total of three times in 1X TBST. Proteins of interest were detected using Western Lighting Chemiluminescent Reagent (Perkin-Elmer) and autoradiography film. Primary antibodies used include the following: anti-pFAK (1:500; Santa Cruz), anti-FAK (1:1,000; Santa Cruz), anti-TRAF6 (1:1,000;

Santa Cruz), anti-MEF2A (1:2,000; Santa Cruz), anti-GAPDH (1:1,000; Santa Cruz), anti-Histone H3 (1:5,000; Cell Signaling Technology). Secondary antibodies used include the following: horseradish peroxidase conjugated goat anti-rabbit (1:10,000; PerkinElmer), and horseradish peroxidase conjugated goat anti-mouse (1:10,000; PerkinElmer).

2.5.6 Electrophoretic mobility shift assay

Double-stranded oligos were generated by combining 2.5 μg of sense primer, 2.5 μg of anti-sense primer, and 5 μL of NEB Buffer 2, and then adjusting the final volume to 50 μL with sterile nuclease-free water. Samples were incubated on a heat block for 20 min at 65 °C. The heat block was turned off and samples were allowed to cool to room temperature (approximately 1.5 – 2 h). Double-stranded oligos were labeled by combining 15 μL of sterile nuclease-free water, 20 ng of double-stranded oligos, 2.5 μL NEB Buffer 2, 2.5 μL ATG mix, 2.5 μL dCTP [α-^{32}P], and 1 μL Klenow into a 1.7 mL microcentrifuge tube, and samples were incubated for 1 – 2 h at room temperature. To each labeled oligo, 25 μL of 1X TE buffer (10 mM Tris, 1 mM EDTA) and cleaned over a G-25 column (Roche). Counts per minute (cpm) were obtained for each labeled-double stranded oligo and 15 μg clarified protein lysate, 0.5 μL poly(dI-dC), 1 μL 10X gel shift buffer (250 mM Tris pH 7.5, 800 mM NaCl, 350 KCl, 10 mM DTT), and 1 μL labeled oligo (~50,000 cpm) was combined in a 1.7 mL microcentrifuge tube and brought to a final volume of 20 μL using sterile protease-free nuclease-free water. Samples were incubated for 15 min at room temperature. 6X DNA loading dye (30% glycerol, 0.35%

xylene cyanol, 0.25% bromophenol blue) was added to each sample and resolved over a 5% non-denaturing polyacrylamide gel. Gels were dried on a gel dryer for one hour at 80 °C. Dried gels were exposed to a phosphor screen overnight and screens were imaged on a Typhoon scanner (GE Healthcare Life Sciences). Oligo sequences used for EMSA are found in Table 3.6.

2.6 Immunofluorescent techniques

2.6.1 Cryosectioning

Tissues embedded in O.C.T. compound prepared from Section 2.1.7 were transferred from -80 °C to -20 °C for 4 h to allow to reach appropriate cryosectioning temperature. Tissues were sectioned at thickness of 16 μm (Leica CM 1850), and cryosections were carefully transferred onto charged slides. Cryosections were stored at -80 °C for long-term storage.

2.6.2 Immunohistochemistry

Sixteen micron cryosections were fixed in PHEM fixative (4% formaldehyde, 60 mM PIPES, 20 mM HEPES, 10 mM EGTA, 2 mM $MgCl_2$, 3% sucrose, pH 7.2) for 15 min. PHEM fixative was removed and sections were washed once in 1X PBS. Tissue sections were permeabilized in permeabilization buffer (0.3% Triton X-100, 1X PBS) for 30 min. Permeabilization buffer was removed and sections were blocked for one hour in blocking buffer (10% BSA, 0.3% Triton X-100, 1X PBS). Blocking buffer was removed and sections were incubated with primary antibody suitably diluted in antibody dilution

buffer (1% BSA, 0.3% Triton X-100, 1X PBS) for 1 hour. Sections were washed three times in 1X PBS. Sections were incubated with secondary antibody suitably diluted in antibody dilution buffer for 1 hour. Sections were wash three times in 1X PBS and then mounted using media containing DAPI (Vectashield). Image fluorescence intensities were quantified using ImageJ. Briefly, MEF2A-positive nuclei were traced, and DAPI and MEF2A signal intensities from each channel were extracted. MEF2A signal intensity was normalized to respective DAPI signal intensity, and average normalized MEF2A signal was quantified for wild-type atria and ventricles.

Primary antibodies used include the following: anti-MEF2A (1:200; Santa Cruz); anti-PECAM (CD31; 1:200; R&D Systems) and anti-WT1 (1:200; Santa Cruz) antibodies were kindly gifted by Dr. William Pu (Boston Children's Hospital). Secondary antibodies used include the following: Alexa Fluor 568® goat anti-rabbit (1:200; Invitrogen), Alexa Fluor 488® donkey anti-goat (1:200; Invitrogen), and Alexa Fluor 488® goat anti-mouse (1:200; Invitrogen).

2.7 Computational and statistical methods

2.7.1 Genomatix software

Transcription factor enrichment analysis was performed on the proximal promoter regions of genes preferentially dysregulated in each chamber using MatInspector (www.genomatix.com). Analysis was limited to regions within 50 bp of predicted MEF2 binding sites to enrich for potential transcription factor co-regulator interactions. The analytical background was composed of a cross-section of genomic promoter sequences

to discriminate between enriched motifs and generic promoter regions. Resulting enriched motifs were sorted by Z-score, with a Z-score greater than positive 2.0 being considered significantly enriched.

2.7.2 Statistical methods

Statistically significant differences between two populations of data were determined using two-tailed Student's *t*-test. *P*-values of < 0.05 were considered to be statistically significant.

Genotyping primers

Primer	***Sequence* (*5' → 3'*)**
Mef2a Fwd	GCTAGCCAACATTTCACCTTTGAGATCT
Mef2a Rev	CAACGATATCCGAGTTCGTCCTGCTTTC
Neomycin Fwd	TTGGCTACCCGTGATATTGCTGAAGAGC
HGH-*Mef2a* Fwd	GTCTGACTAGGTGTCCTTCT
HGH-*Mef2a* Rev	CGTCCTCCTGCTGGTATAG
IL-2 Fwd	TGGCATCGATTACCTCAGTCCCCCT
IL-2 Rev	CCAGAACATGCCGCAGAGGTCCA

Table 2.1 Genotyping primers used in this thesis. Primers are listed 5' to '3'. Annealing temperatures for genotyping reactions were determined using NEB T_m calculator (https://tmcalculator.neb.com).

Reporter constructs

Plasmid	*Source*
pGL3Basic-1.5kb-*Xirp2*-Luciferase	(Huang *et al.* 2006)
pGL3Basic-0.3kb-*Xirp2*-Luciferase	(Huang *et al.* 2006)
pGL3Basic-*Bex1*-Luciferase (proximal enhancer)	*Cloned in-lab*
pGL3Promoter-*Bex1*-Luciferase (distal enhancer)	(Medrano & Naya 2017)
pGL3Promoter-*Itga7*-Luciferase	(Medrano & Naya 2017)

Overexpression constructs

Plasmid	*Source*
pCMV-β-galactosidase	(Snyder *et al.* 2013)
pCDNA1-MEF2A	Dr. Tod Gulick (Sanford Burnham Med. Research Institute)
pCGN-HA-Nkx2.5	*Previously cloned in-lab* (Dr. Christine Snyder)
pCDNA3-HAND1	Dr. Anthony Firulli (Indiana U. School of Med.)
pCDNA3-HAND2	Dr. Anthony Firulli (Indiana U. School of Med.)
pCR3.1-ERα	Dr. Sang Jun Han (Baylor College of Med.)
pCMV-3Tag-9-ERβ	Dr. Sang Jun Han (Baylor College of Med.)

Table 2.2 Reporter and overexpression plasmids used in this thesis. Reporter plasmids and overexpression plasmids were previously cloned in-lab or received from outside investigators as noted in the table above.

CHAPTER THREE: MEF2A modulates different signaling pathways in atria and ventricles of the heart

This research was originally presented in the *Journal of Biological Chemistry*. **Medrano JL**, Naya FJ (2017). The transcription factor MEF2A fine-tunes gene expression in the atrial and ventricular chambers of the adult heart. *J Biol Chem* doi: 10.1074/jbc.M117.806422 [Epub ahead of print]

3.1 Introduction

The atrial and ventricular chambers of the mammalian heart have distinct anatomical and functional properties that are necessary for the coordinated and efficient pumping of blood. These differences arise from morphogenetic events coupled to cell specification pathways within myocyte and non-myocyte lineages that create the atria and ventricles from a linear heart tube (Buckingham *et al.* 2005, Moorman & Christoffels 2003). Moreover, these developmental programs lead to regional gene expression patterns that are unique to the atrial and ventricular chambers (Barth *et al.* 2005, Ng *et al.* 2010, Tabibiazar *et al.* 2003). The importance of these gene expression patterns is highlighted by cardiac defects in mouse model systems that display distinct atrial and ventricular chamber dysregulation (Bruneau *et al.* 2001, Singh *et al.* 2005, Tessari *et al.* 2008, Wang *et al.* 2010, Wu *et al.* 2013, Xin *et al.* 2007).

The establishment of atrial and ventricular identity from cardiomyocyte precursors occurs early in the developing heart (Evans *et al.* 2010, Paige *et al.* 2015,

Später *et al.* 2014). Throughout development these gene programs undergo dynamic gene regulation to ultimately express a fixed, compartment-specific gene expression pattern postnatally. Investigating the transcriptional regulation of chamber-restricted genes has led to the identification of a number of enhancers and transcription factors required for distinct regional expression patterns in the heart (Habets *et al.* 2002, Lien *et al.* 1999, Reecy *et al.* 1999, Searcy *et al.* 1998, Tanaka *et al.* 1999).

The myocyte enhancer factor 2 (MEF2) family of transcription factors includes key regulators of cardiac muscle differentiation and development (Desjardins & Naya 2016, Potthoff & Olson 2007). Interestingly, MEF2 proteins have been implicated in the regulation of atrial and ventricular chamber-restricted genes (Ross *et al.* 1996, Small & Krieg 2004). Based on their reported uniform expression throughout the heart it is unlikely that MEF2 proteins alone drive chamber-specific gene programs. Nevertheless, these observations suggest that MEF2 proteins play an important modulatory role in the regional expression of cardiac genes.

Previously, we described the variable penetrance of cardiac defects in global MEF2A knockout (KO) mice. Perinatal MEF2A-deficient hearts displayed dilation of the right and left ventricles including structurally compromised cardiomyocytes (Ewen *et al.* 2011, Naya *et al.* 2002). By contrast, adult MEF2A mutant hearts did not display ventricular dilation, but interestingly showed compensatory activation of a MEF2-dependent reporter that was largely restricted to the ventricles. Because both young and adult mutant hearts display predominantly ventricular phenotypes these observations suggest that the atria and ventricles are differentially affected by the loss of MEF2A.

In this chapter, I discuss about the cardiac chamber-dependent transcriptional regulation of MEF2A-sensitive genes in the adult heart. To delve deeper into a potential regional requirement of MEF2A in the heart, we performed genome-wide expression profiling of atrial and ventricular chambers from adult MEF2A KO mice. We found that genes uniformly expressed throughout the heart displayed preferential chamber dysregulation to the loss of MEF2A. Only a small fraction of the dysregulated genes throughout the heart were similarly affected in both atria and ventricles of MEF2A mutant hearts. To understand the transcriptional basis of this regional gene dysregulation pattern, we computationally analyzed the promoter regions of genes preferentially dysregulated in the atrial and ventricular chambers, and identified a distinct complement of transcription factor binding sites in each gene set. Our results demonstrate that MEF2A is required for proper atrial and ventricular gene expression but does not confer chamber identity. These findings provide insight into the complex transcriptional mechanisms of region-specific cardiomyocyte gene expression in the mammalian heart.

3.2 Differential gene dysregulation in cardiac chambers of MEF2A knockout mice.

Global MEF2A deficiency in mice results in two distinct cardiac phenotypes (Naya *et al.* 2002). Most MEF2A knockout (KO) mice (~80%) die perinatally and display various cardiac defects including dilation of the right and left ventricles. A subset of KO mice survive to adulthood and also have cardiac abnormalities. However, these adult mutant hearts do not display ventricular dilation, instead a MEF2-responsive lacZ reporter is primarily upregulated in the right and left ventricles, likely resulting from

stress-induced activation of MEF2D (Naya *et al.* 2002). Given the predominant ventricular phenotypes in MEF2A mutant hearts, we hypothesized that the atria and ventricles have a differential requirement for MEF2A in cardiac chamber gene regulation.

To characterize potential differences in cardiac chamber gene regulation mediated by MEF2A, we dissected atrial (left and right combined) and ventricular (left and right) tissue from adult wild-type (WT) and MEF2A KO hearts, and analyzed the extracted RNA via microarray. As shown in Figure 3.1, this analysis revealed a total of 686 genes dysregulated by at least 1.5-fold. Interestingly, the scatter plots suggested a greater number of genes dysregulated in MEF2A KO atria compared to KO ventricles. Indeed, detailed examination of the 686 dysregulated genes revealed that 481 genes (70%) were preferentially dysregulated in the atrial chambers of MEF2A KO hearts, even though the vast majority of these genes were uniformly expressed in the atrial and ventricular chambers of WT hearts (Figure 3.2**,** Appendix A.1). By contrast, only 158 genes (23%) were preferentially dysregulated in mutant ventricles, and the majority of these did not display chamber-enriched expression in WT hearts. The remaining 47 genes (7%) were dysregulated by at least 1.5-fold in both chambers of the mutant hearts. Chamber-enriched genes, *i.e.*, genes displaying 2.0-fold or more expression in one WT chamber relative to the other, accounted for a small percent of the dysregulated genes in each KO chamber (Table 3.1).

While the atrial chambers had more dysregulated genes, the extent of dysregulation was similar in each compartment. Genes preferentially affected in the atria were dysregulated on average by 1.76-fold and genes preferentially affected in the

ventricles were dysregulated on average by 1.87-fold (Table 3.2). Interestingly, the average fold dysregulation was far greater for those genes affected in both chambers: 2.4-fold in atria and 2.6-fold in ventricles. Although there were more dysregulated genes in MEF2A KO atria, the proportion of up- and down-regulated genes was similar in both KO atria and ventricles (Table 3.3). Taken together, this expression profiling analysis revealed differential chamber sensitivity of genes to the loss of MEF2A despite its reported uniform expression throughout all chambers of the heart. Furthermore, most genes sensitive to the loss of MEF2A in both chambers were dysregulated in a similar direction. Finally, the abundance of preferentially dysregulated genes in MEF2A KO atria is in stark contrast to the more obvious ventricular phenotypes in these mutant hearts.

3.3 Validation of MEF2A-sensitive genes

To confirm the differential chamber sensitivity, we examined a subset of genes from each of the dysregulated gene sets by qRT-PCR. All genes selected for this analysis are expressed throughout the heart but showed preferential dysregulation in one chamber or were affected in both. As depicted in Figure 3.3 A, *Arhgef19*, *Chrdl2*, *Clic6*, *Itga7*, and *Shisa6* were significantly dysregulated in the atria, but not in the ventricles. Likewise, expression of *Bex1*, *Fbxo44*, *Fgf16*, *Pknox2*, and *Slitrk4* was dysregulated in the ventricles, but not in the atria (Figure 3.3 B). Finally, *Aqp4*, *Arhgap20*, *Asb4*, *Fgf14*, and *Pde7a* genes were significantly dysregulated, either up- or down-regulated in both atria and ventricles of the heart (Figure 3.3 C).

3.4 Top canonical dysregulated pathways

To determine whether the preferentially dysregulated genes function in distinct pathways we performed Ingenuity® Pathway Analysis (IPA, Qiagen) on the three gene sets. As shown in Table 3.4, those genes preferentially dysregulated in MEF2A KO atria function in fibrosis, stem cell pluripotency, and adhesion. Genes dysregulated primarily in the mutant ventricles function in amino acid metabolism and endocytosis signaling. The cohort dysregulated in both chambers function in folate transformation and ubiquitination pathways, though enrichment in these processes was modest given the small number of genes in this category. These results suggest that dysfunction in adult MEF2A KO hearts arises not from a globally defective pathway but the cumulative effect of abnormal regulation of distinct cellular processes in each cardiac compartment.

3.5 Dysregulated pathways *in vivo*

To assess whether these cellular processes were perturbed in a chamber-specific fashion, we analyzed expression or activity of selected components from the canonical pathways identified in the IPA (Table 3.4) in MEF2A KO hearts. Specifically, we subjected atrial and ventricular tissue lysates from adult wild-type and MEF2A KO hearts to western blot analysis for FAK (Focal adhesion kinase) and TRAF6 (TNF receptor associated factor 6). Among their roles in diverse signal transduction cascades, FAK and TRAF6 activities are modulated by the integrin/adhesion and MSP-RON (Macrophage stimulating protein – Recepteur d'Origine Nantais) pathways, respectively (Franchini

2012, Li *et al.* 2015, Mitra & Schlaepfer 2006, Yao *et al.* 2013). Adhesion was among the top dysregulated pathways in MEF2A KO atria whereas MSP-RON, a receptor tyrosine kinase pathway involved in cancer and inflammation (Li *et al.* 2015, Yao *et al.* 2013), was the top dysregulated pathway in mutant ventricles. As shown in Figure 3.4 and Figure 3.5, we detected a modest but significant downregulation of phosphorylated FAK, an indicator of its activity, in MEF2A KO atria but not ventricles. Conversely, TRAF6 was preferentially and significantly downregulated in the ventricles of adult MEF2A mutant hearts. These data highlight the distinct cellular responses of the cardiac chambers to the loss of a broadly expressed transcription factor and provide support for differential gene regulatory activity of MEF2A in the atria and ventricles of the heart.

3.6 MEF2A expression is similar throughout the adult heart

A previous study described enrichment of MEF2A protein in the atrial chambers of the adult mouse heart (Zhao *et al.* 2002). Since a majority of the dysregulated genes were preferentially affected in the atria we sought to determine whether this expression pattern could explain the differential sensitivity to MEF2A. Initially, we examined *Mef2a* transcript levels in both cardiac chambers. RT-PCR analysis revealed similar transcript levels of *Mef2a* between adult wild-type atrial and ventricular cardiac chambers (Figure 3.6). This is in contrast to a previous report describing enrichment of MEF2 protein in the atrial chambers in adult mice (Zhao *et al.* 2002). Additionally, we analyzed expression of *Mef2a* splice isoforms (Yu *et al.* 1992), but found no difference in any alternatively spliced transcripts between atrial and ventricular tissue.

To address the discrepancy between observed *Mef2a* transcript levels and previously reported atrial enrichment of MEF2A protein levels, we compared MEF2A protein levels between atria and ventricles by performing immunohistochemistry on adult cardiac sections using anti-MEF2A antibody (Santa Cruz sc-313). Similar to a previously published report (Zhao *et al.* 2002), MEF2A immunoreactivity appeared higher in the atrial chambers compared to the ventricles of the heart (Figure 3.7). Because the increased signal in the atria may reflect the higher density of atrial myocytes, owing to their smaller size, we normalized the MEF2 signal to DAPI-positive cells in each chamber. On normalization of MEF2A-positive myocytes to nuclear DAPI-positive cells, a similar fold difference was observed between WT atria and ventricles (Figure 3.8). In a complementary set of experiments, MEF2A protein levels were evaluated by western blotting using whole tissue lysates from each cardiac chamber. Again, MEF2A protein levels appeared higher in atrial lysates compared to ventricular lysates (Figure 3.9). However, MEF2A protein levels were found to be similar between atria and ventricles when normalized to the nuclear protein histone H3 (Figure 3.10). To further define the expression domain of MEF2A in the adult heart, we co-stained adult cardiac sections with epicardial or endocardial markers. As shown in Figure 3.11, MEF2A signal did not overlap with that of either PECAM (endocardium) or WT1 (epicardium). Nuclear MEF2A signal was mainly localized to the myocardium in adult wild-type hearts. These results clearly demonstrate that MEF2A is not preferentially expressed in the atria of the adult heart and the apparent chamber-specific differences can be explained by the different sizes and densities of atrial and ventricular myocytes per mass of tissue.

Moreover, MEF2A is restricted to the myocardium in the atria and ventricles thereby ruling out expression differences arising from additional regions of the adult heart.

3.7 MEF2 DNA binding in vitro and in vivo

We next asked whether differences in MEF2 DNA-binding activity could account for the preferential dysregulation of MEF2A-sensitive genes in *Mef2a* KO hearts. Initially, electrophoretic mobility shift assays were performed to evaluate MEF2 binding from atrial and ventricular lysates in vitro. Similar to the western blot analysis, gel shift assays using whole tissue lysates from each chamber showed greater MEF2 DNA-binding activity in atrial lysates (Figure 3.12 left panel). As a control we used a probe harboring the CaRG element, the consensus binding site for SRF, a cardiac TF uniformly expressed in the heart (Figure 3.12 right panel) (Belaguli *et al.* 1997, Miano 2003). Because SRF also showed this differential DNA-binding pattern, after normalization there was no significant difference in MEF2 binding activity (Figure 3.12 right graph). Moreover, the reduction in MEF2 DNA-binding activity from MEF2A KO atrial and ventricular lysates appeared to be similar (Figure 3.13). These results demonstrate that total MEF2 DNA-binding activity does not differ between the cardiac chambers.

Next, we examined endogenous MEF2 genomic binding to promoter regions of selected dysregulated genes to determine whether differences in MEF2A binding in vivo could help explain the observed preferential dysregulation. For this analysis, we focused on the same set of dysregulated genes described in Figure 3.3. Predicted MEF2 sites (Figure 3.14 left chart) were identified in the upstream regions of these genes based on

available ENCODE MEF2A ChIP-seq data (accession numbers ENCSR806JZK and ENCSR867SDZ) and the MEF2 consensus sequence (5'-YTAWWWWTAG-3'). We chose to analyze the 5,000 bp proximal promoter of these genes to identify candidate MEF2 enhancers based on previous promoter analysis studies performed in our lab (Estrella *et al.* 2015, Huang *et al.* 2006). While there was slight variability in the MEF2 consensus sequence these minor differences did not group together with genes displaying similar preferential dysregulation. Chromatin immunoprecipitation (ChIP) was performed on cross-linked atrial and ventricular tissue from adult wild-type hearts using MEF2A antibodies (Santa Cruz) that we previously reported preferentially recognize MEF2A (Snyder *et al.* 2013). As shown in Figure 3.14, MEF2A associates at the predicted MEF2 sites. Multiple attempts to assess binding of MEF2A to these genes in ventricular tissue by ChIP were unsuccessful. Nevertheless, the similarity of MEF2A association to these genomic regions in WT atrial chambers, whose genes display differences in chamber sensitivity, does not explain the differential chamber dysregulation profile.

To bolster the in vivo ChIP analysis and demonstrate that the dysregulated target genes are directly regulated by MEF2A, we cloned the genomic regions harboring the candidate MEF2 binding site from a representative gene in each category: Itga7 (preferentially dysregulated in the atria) and Bex1 (preferentially dysregulated in the ventricles). As shown in Figure 3.15, transfection of MEF2A significantly stimulated the activation of both pGL3p-Itga7 (2.9-fold) and pGL3p-Bex1 (2.3-fold) in HEK293T cells.

3.8 Candidate MEF2A co-factors

The lack of any obvious difference in MEF2A expression or binding activity between atria and ventricles suggests that differential sensitivity of genes in the cardiac chambers results from the ability of MEF2A to interact with a distinct set of cofactors. Toward this end, we performed transcription factor (TF) binding motif analysis using MatInspector (Genomatix) on dysregulated genes from each group (*i.e.*, promoters of genes preferentially dysregulated in KO atria, promoters of genes preferentially dysregulated in KO ventricles, and promoters of genes dysregulated in KO atria and ventricles). This analysis revealed a distinct set of enriched TF binding sites in each gene set (Table 3.5).

Of the top enriched TF binding sites in each cardiac chamber category, we focused on those bound by the estrogen receptor (ER, V$EREF), NKX homeodomain (V$NKXH), and the HAND family (V$HAND). The ER binding site was found to be overrepresented in genes preferentially dysregulated in the atria, the NKX homeodomain site was enriched in the preferential ventricular cohort, and the HAND binding site was found in genes dysregulated in both chambers. The ER is known to have a protective effect on the heart (Van Rooij *et al.* 2010), and differences in cardiac chamber expression of ER isoforms (α and β) have been reported (Lizotte *et al.* 2009). Members of the NKX and HAND family are core cardiac TFs important in cardiac gene regulation and development (Akazawa & Komuro 2005, Bartlett *et al.* 2010, Firulli 2003, Vincentz *et al.* 2011). While the primary cardiac NKX member, Nkx2.5, is not enriched in a specific cardiac chamber a null mutation of this gene in mice results in ventricular morphogenesis defects (Tanaka *et al.* 1999). Similarly, mutations in HAND genes result in cardiac

chamber morphogenesis defects (Firulli *et al.* 2010, Srivastava *et al.* 1997). While the two primary gene products, HAND1 and 2, are each expressed in distinct chambers, when taken together HAND transcriptional activity is present throughout all compartments of the heart (Thattaliyath *et al.* 2002).

3.9 Transcriptional cooperativity between MEF2A and candidate co-factors

To test potential transcriptional cooperativity between MEF2A and the candidate TFs (estrogen receptors, Nkx2.5, and HAND factors), we used the 1.5 kb proximal promoter of the *Xirp2* (myomaxin and Xinβ) gene as a readout. Although this gene was not part of the differential gene set it is an established, direct target of MEF2A and harbors multiple DNA binding sites for these candidate TFs (Figure 3.16). The 1.5 kb proximal promoter of *Xirp2* contains two predicted estrogen response elements, four predicted Nkx2.5 response elements, and two predicted HAND-binding sites (Figure 3.16).

As shown in Figure 3.17, the 1.5 kb *Xirp2*-luciferase reporter was significantly activated by MEF2A alone (2.1 – 2.8-fold). This reporter was also activated by ERβ (1.6-fold, *top graph*), Nkx2.5 (1.4-fold, *middle graph*), and HAND2 (4.5-fold, *bottom graph*) individually. By contrast, the 1.5 kb *Xirp2* reporter was not significantly activated by ERα (upper graph) or HAND1 (lower graph) alone. However, co-transfection of MEF2A with ERβ, Nkx2.5, and HAND2, and to a lesser extent HAND1, resulted in significant cooperative activity.

To demonstrate that MEF2A and these TFs function cooperatively in cardiac muscle we performed the same reporter gene analysis in neonatal rat ventricular myocytes (NRVMs). Because the 1.5 kb *Xirp2*-luciferase reporter showed an exceedingly high basal activity in NRVMs in the absence of any transfected TF, we used a 0.3 kb *Xirp2*-luciferase reporter (Figure 3.16 lower schematic). This minimal promoter, which contains the conserved -75 MEF2 site and lacks all but a single predicted binding site for ER, Nkx2.5, and HAND, displayed lower basal activity in NRVMs (data not shown). ERα, Nkx2.5, HAND1, or HAND2 individually did not significantly activate the 0.3 kb *Xirp2*-luciferase reporter (Figure 3.18), whereas ERβ alone had a modest but significant effect on the reporter (1.7-fold, *top graph*). Co-transfection of MEF2A with ERβ, Nkx2.5, and HAND2, and to a lesser extent ERα and HAND1 resulted in significant cooperative activation. Co-transfection of MEF2A with Nkx2.5 resulted in cooperative activation of at least 4.2-fold over individual activation from MEF2A or Nkx2.5 alone. Similarly, co-transfection of MEF2A with ERβ and MEF2A with ERα resulted in cooperative activation of at least 4.6-fold and 2.9-fold over activation from individual transfections, respectively. Finally, co-transfection of MEF2A with HAND2 and MEF2A with HAND1 resulted in cooperative activation of at least 3.1-fold and 2.0-fold over activation from individual transfections, respectively. It is interesting to note that in both HEK293T cells and NRVMs, ERβ and HAND2 displayed higher cooperative activity compared to ERα and HAND1 protein isoforms. These results demonstrate that MEF2A interacts with at least three TFs predicted to have enriched binding sites in the preferentially dysregulated gene sets between the atria and ventricles.

3.10 Discussion

Defining the molecular mechanisms by which atrial and ventricular cardiomyocytes develop their distinct cellular and functional properties is essential for refining approaches to promote specific myocyte lineages from precursor populations, including embryonic and induced pluripotent stem cells, and for directed reprogramming of cardiomyocytes. In this report we demonstrate that genes uniformly expressed throughout the adult heart are differentially sensitive to the loss of MEF2A. This preferential dysregulation is predicted to affect distinct pathways in the cardiac chambers of MEF2A KO mice making the mutant phenotype far more complex than previously recognized (Naya *et al.* 2002). Taken together, our results suggest that proper chamber gene regulation in the heart is not only driven by lineage restricted TFs, but also by broadly expressed cardiac TFs that impart robustness to gene expression patterns in myocytes within each compartment.

It is intriguing that genes expressed uniformly throughout the heart display preferential chamber sensitivity to a broadly expressed transcription factor such as MEF2A. This is not entirely surprising since cardiac genes display dynamic spatiotemporal expression patterns in development, reflecting the activity of multiple enhancers (Christoffels *et al.* 2004, Dupays & Mohun 2016, Rana *et al.* 2013). The core cardiac TFs Nkx2.5 and MEF2C are prime examples of genes that undergo chamber-dependent transcriptional regulation. Both TFs are uniformly expressed throughout the developing heart yet analysis of their transcriptional regulatory regions has uncovered

enhancers active in distinct compartments in the developing heart (Barnes *et al.* 2016, Lien *et al.* 1999, Reecy *et al.* 1999, Searcy *et al.* 1998, Tanaka *et al.* 1999). While each enhancer is active in a specific compartment, their collective activity drives uniform expression through the heart. Perhaps the preferential dysregulation of MEF2A target genes reflects region-specific enhancers embedded in these genes that are dependent on MEF2 transcriptional activity.

It is curious that there were more dysregulated genes in the atria even though MEF2A KO hearts appear to have more prominent ventricular phenotypes. It is possible that the collection of genes dysregulated in the ventricular chambers, based on their function in myocytes and despite the relatively small number, triggers a more readily observable defect in this compartment. Alternatively, the pathology caused by the cohort of dysregulated atrial genes may be subtle or the atrial chambers may be more resistant to changes in gene expression. For example, cellular adhesion was among the top dysregulated pathways in the MEF2A KO atria. We examined the localization of N-cadherin, a prototypical adhesion molecule important in the heart, in adult MEF2A KO atria and did not find significant differences compared to wild-type. Similarly, the extent of fibrosis in these mutant hearts was highly variable and did not appear to be significantly different between atria and ventricles (data not shown). More detailed analyses will be required to determine the specific cellular defects in MEF2A mutant hearts.

MEF2 has been implicated in chamber-specific gene expression. An enhancer of the Mlc2v gene was shown to be active in the ventricles of the mouse heart. This minimal

enhancer harbors a MEF2-binding site and when mutated ventricular expression is lost (Ross *et al.* 1996). In addition, the atrial-enriched ANF gene has been shown to be co-regulated by GATA4 and MEF2 (Morin *et al.* 2000) and MEF2A and Pitx2 (Toro *et al.* 2004). MEF2C is required for the proper regulation of enhancers of the *Hcn4* and *BOP* genes in the atrioventricular conduction system and right ventricle, respectively (Phan *et al.* 2005, Vedantham *et al.* 2013). Finally, though not functionally tested, the atrial *Mlc2a* and *sarcolipin* genes harbor candidate MEF2 sites in their upstream regulatory regions (Small & Krieg 2004). Taken together, these observations strongly suggest that MEF2 proteins function to coordinate proper cardiac chamber gene expression.

Regarding the computational analysis of MEF2A-sensitive cardiac chamber gene programs, prior studies have shown that MEF2 proteins collaborate with the NKX and HAND family of transcription factors. MEF2C and Nkx2.5 were shown to genetically interact and required for proper ventricular chamber development in mice (Vincentz *et al.* 2008). Moreover, these factors functioned cooperatively to activate heterologous promoters. Our computational analysis is consistent with these observations suggesting that Nkx binding sites are significantly enriched in genes displaying preferential dysregulation in ventricular chambers in MEF2A KO hearts. In a similar fashion, MEF2A and MEF2C were each shown to interact with HAND proteins (Morin *et al.* 2005). HAND proteins display an intricate expression pattern in the developing heart. HAND1 is expressed in the myocardial cuff on the cardiac outflow tract. HAND2 is expressed in myocardium, endocardium, and epicardium as well as the underlying pharyngeal mesoderm of the second heart field. Thus, our analysis revealing

overrepresentation of the HAND E-box motif in genes that are dysregulated by MEF2A KO in both chambers seems logical based on the reported spatiotemporal expression patterns. Presumably, MEF2A interacts with specific HAND protein isoforms to regulate genes in distinct regions of the heart. Because MEF2 interacts with both HAND proteins we observe similar dysregulation of this gene cohort in both cardiac chambers.

Expression of estrogen receptor isoforms has been described in the heart of adult rodents. In rats, ERα mRNA is more abundant in atria compared to ventricles whereas ERβ is uniformly expressed (Jankowski *et al.* 2001). However, in mice, ERα protein appears to be more abundant in ventricles, but similar to the rat study ERβ is expressed in both chambers. These expression patterns do not strictly correlate with the overrepresentation of ER binding sites in the atrial preferentially dysregulated genes in MEF2A KO hearts. This suggests that additional mechanisms beyond MEF2-ER cooperativity are required for the observed chamber sensitivity of these genes.

This study has identified a preferential gene regulatory response of MEF2A in chambers of the adult mouse heart. Characterization of transcriptional pathways in the chambers of the heart will lead to a deeper understanding of the mechanisms of region-specific cardiomyocyte function. This information can be used to develop therapies that selectively target dysfunctional regions of the heart in diseases such as atrial fibrillation or arrhythmogenic right ventricular cardiomyopathy.

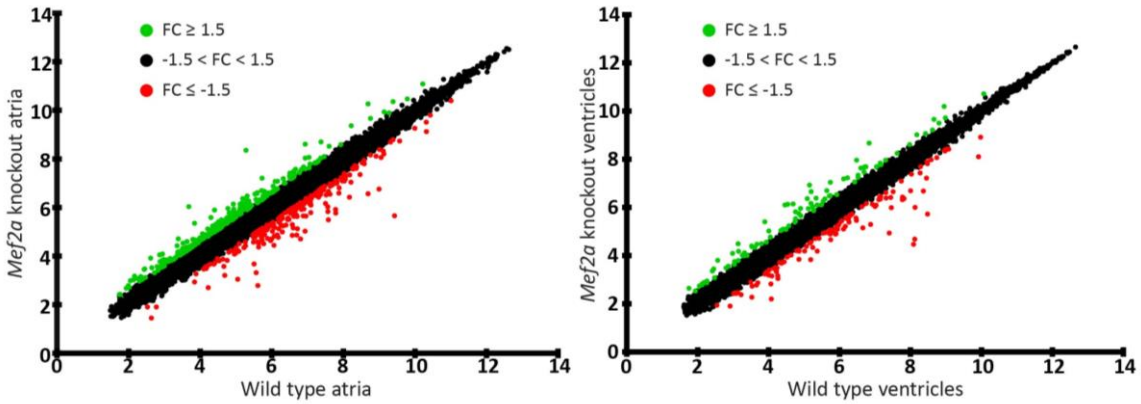

Figure 3.1 MEF2A differentially regulates genes in the adult mouse heart. Scatter plots depicting gene expression differences in MEF2A KO atria and ventricles. Wild-type (WT) and MEF2A KO atria microarray intensities (*left graph*), and WT and MEF2A KO ventricles microarray intensities (*right graph*) were plotted against one another. In each graph, genes upregulated by at least 1.5-fold in MEF2A KO mice are plotted in green (FC ≥ 1.5), genes downregulated by at least -1.5-fold in MEF2A KO mice are plotted in red (FC ≥ -1.5), and genes with no greater than 1.5-fold difference in either direction are plotted in black (-1.5 < FC < 1.5). Of the 21,212 gene probe sets on the Mouse Affymetrix GeneChip® Gene 1.0 ST Array System, 686 well-annotated genes were dysregulated by at least 1.5-fold or greater in adult MEF2A KO hearts.

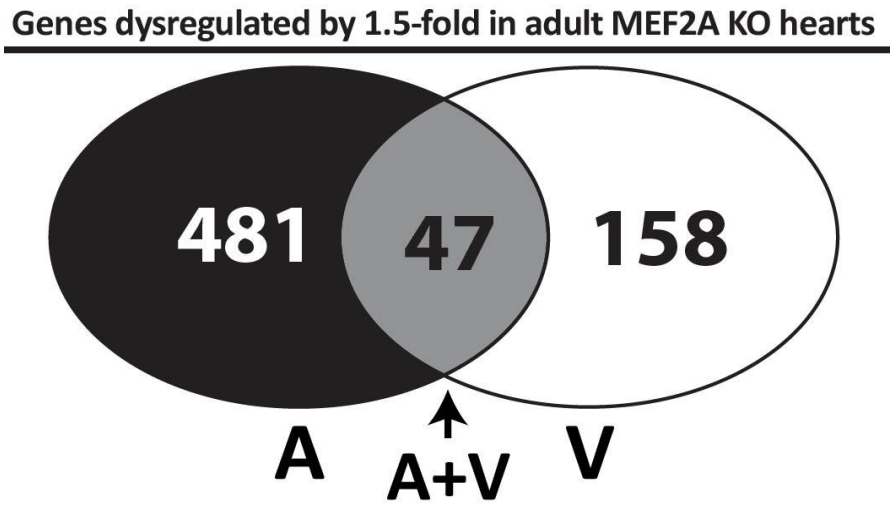

Figure 3.2 MEF2A regulates distinct and overlapping genes in the adult heart. Venn diagram summarizes dysregulated gene expression profiles in KO atria (A), KO ventricles (V), and both (A+V). Of the 21,212 gene probe sets on the Mouse Affymetrix GeneChip® Gene 1.0 ST Array System, 686 well-annotated genes were dysregulated by at least 1.5-fold in adult *Mef2a* KO hearts as compared to WT control hearts. Of the 686 dysregulated genes in the *Mef2a* KO hearts, 481 were preferentially dysregulated in *Mef2a* KO atria, 158 were preferentially dysregulated in *Mef2a* KO ventricles, and 47 were dysregulated in both *Mef2a* KO atria and ventricles.

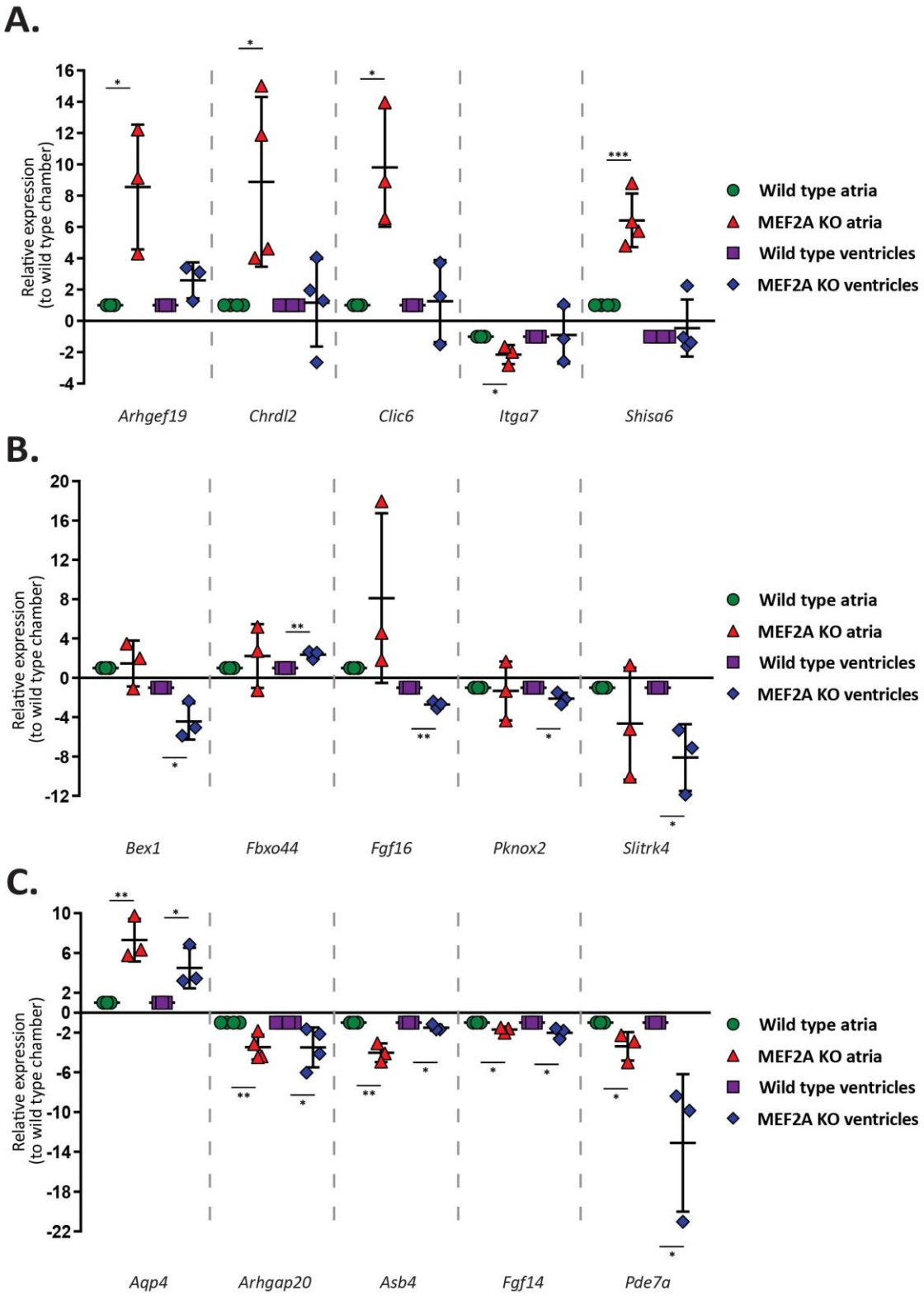
A.
Relative expression
(to wild type chamber)
16
14
12
10
8
6
4
2
0
-2
-4
Arhgef19
Chrdl2
Clic6
Itga7
Shisa6
Wild type atria
MEF2A KO atria
Wild type ventricles
MEF2A KO ventricles
B.
Relative expression
(to wild type chamber)
20
16
12
8
4
0
-4
-8
-12
Bex1
Fbxo44
Fgf16
Pknox2
Slitrk4
Wild type atria
MEF2A KO atria
Wild type ventricles
MEF2A KO ventricles
C.
Relative expression
(to wild type chamber)
10
6
2
0
-2
-6
-10
-14
-18
-22
Aqp4
Arhgap20
Asb4
Fgf14
Pde7a
Wild type atria
MEF2A KO atria
Wild type ventricles
MEF2A KO ventricles

Figure 3.3 MEF2A-sensitive genes display cardiac-chamber specific dysregulation in adult MEF2A KO hearts. ***A***, Quantitative RT-PCR analysis revealed that *Arhgef19*, *Chrdl2*, *Clic6*, *Itga7*, and *Shisa6* were preferentially dysregulated in adult MEF2A KO atria by more than 2-fold when compared to their expression in KO ventricles. Expression levels for each gene in KO atria and ventricles were normalized to their respective WT cardiac region. ***B***, Quantitative RT-PCR analysis revealed that *Bex1*, *Fbxo44*, *Fgf16*, *Pknox2*, and *Slitrk4* were dysregulated in KO ventricles by more than 2-fold compared to KO atrial tissue. ***C***, Quantitative RT-PCR analysis revealed that *Aqp4*, *Arhgap20*, *Asb4*, *Fgf14*, and *Pde7a* were dysregulated by more than 1.5-fold in both KO atria and ventricles. KO gene expression comparisons for atrial and ventricular tissues were performed using WT littermate controls. Error bars represent standard deviation ($n \geq 3$); *, $p < 0.05$; **, $p < 0.01$; ***, $p < 0.001$.

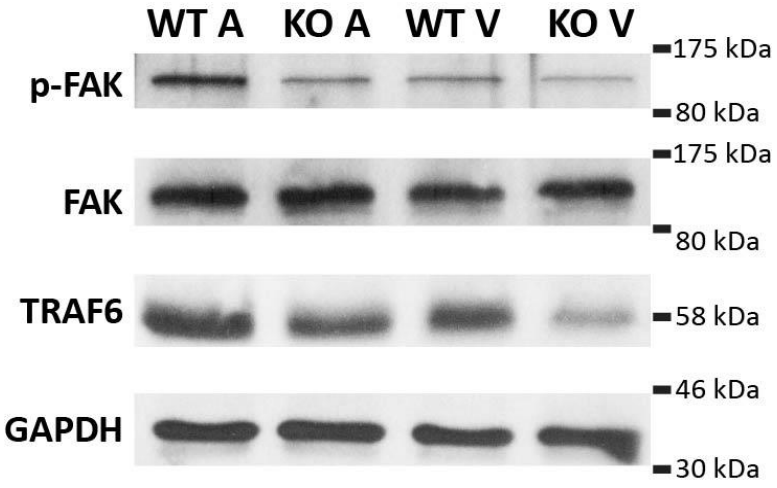

Figure 3.4 Atria and ventricles of adult MEF2A KO hearts each display perturbations in distinct signaling pathways. Immunoblot analysis of phospho-FAK (p-FAK) and total FAK, TRAF6, and GAPDH proteins levels in WT and KO samples in atrial and ventricular lystates. 15 μg of cleared lysate was loaded onto each lane.

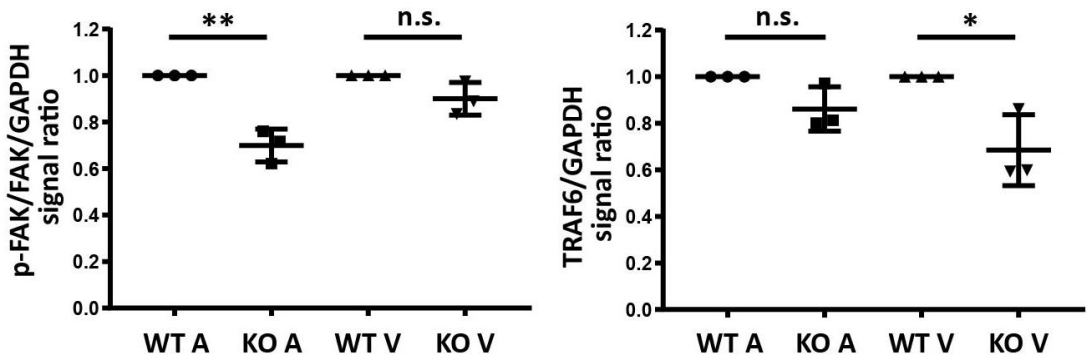

Figure 3.5 Preferential dysregulation of cell signaling pathways in cardiac chambers of MEF2A KO mice. Quantification of p-FAK and TRAF6 protein signals in WT and KO samples in atrial and ventricular lysates. p-FAK levels were normalized to total FAK levels before normalizing to GAPDH levels, and TRAF6 levels were normalized to GAPDH levels. Quantified KO levels were normalized to respective WT levels for each tissue comparison. Error bars represent standard deviation (n = 3); n.s., not significant; *, $p < 0.05$; **, $p < 0.01$.

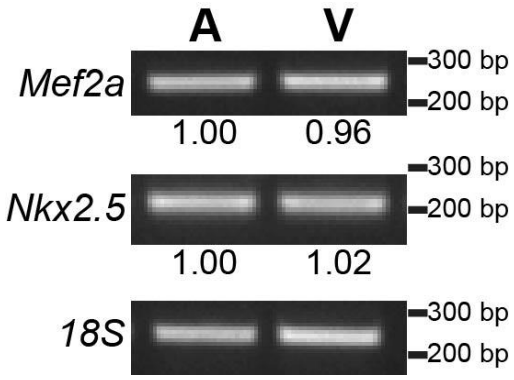

Figure 3.6 *Mef2a* displays similar mRNA levels in adult wild-type hearts. RT-PCR analysis of *Mef2a*, *Nkx2.5*, and *18S* mRNA levels in WT atria and ventricles. Numbers below *Mef2a* and *Nkx2.5* bands represent average band intensity when normalized against *18S* (*n* = 4, quantifications normalized to atrial tissue).

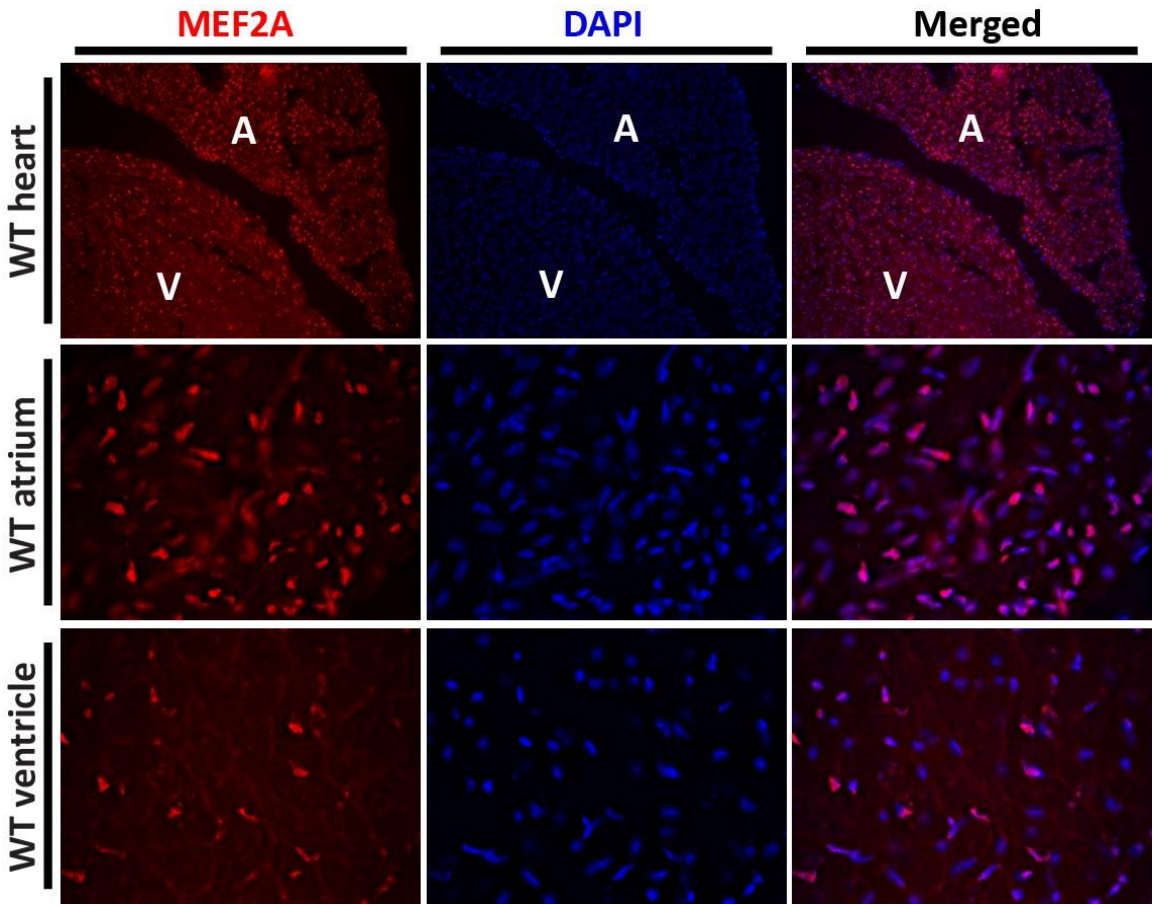

Figure 3.7 MEF2A protein is expressed in atrial and ventricular chambers of adult wild-type hearts. Immunohistochemical detection of MEF2A expression (red) in WT atria and ventricles, counterstained with DAPI (blue). 10X WT atrium and ventricle (*top panels*; A = atrium; V = ventricle), 60X WT atrium (*middle panels*), and 60X WT ventricle (*bottom panels*) fluorescent images were acquired.

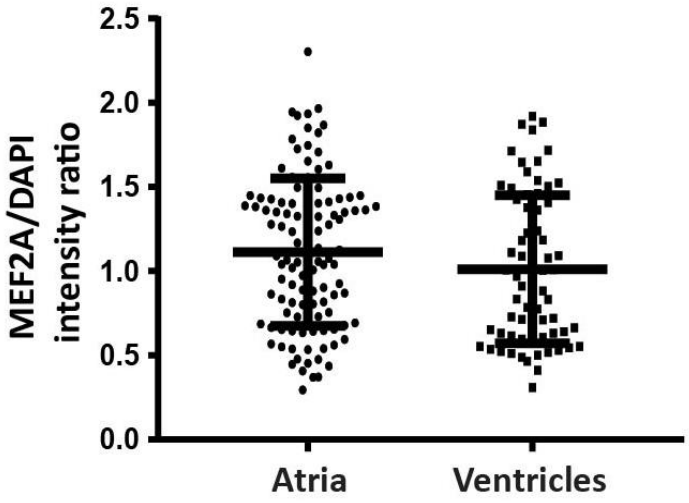

Figure 3.8 Immunofluorescent MEF2A levels are similar between wild-type atrial and ventricular chambers. Quantification of MEF2A nuclear signal using 60X WT atrium and ventricle images. MEF2A signal was normalized to total DNA (DAPI) signal. Average MEF2A/DAPI signal was normalized to WT ventricles. Error bars represent standard deviation.

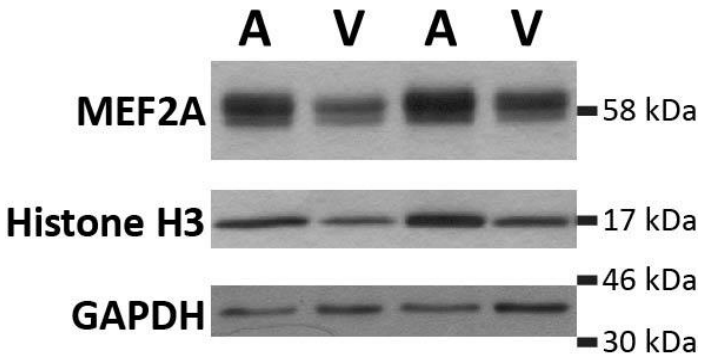

Figure 3.9 MEF2A levels appear enriched in WT atrial chambers. Immunoblot analysis of MEF2A, Histone H3, and GAPDH protein levels in WT atrial and ventricular lysates. 15 μg of cleared lysate was loaded in each lane.

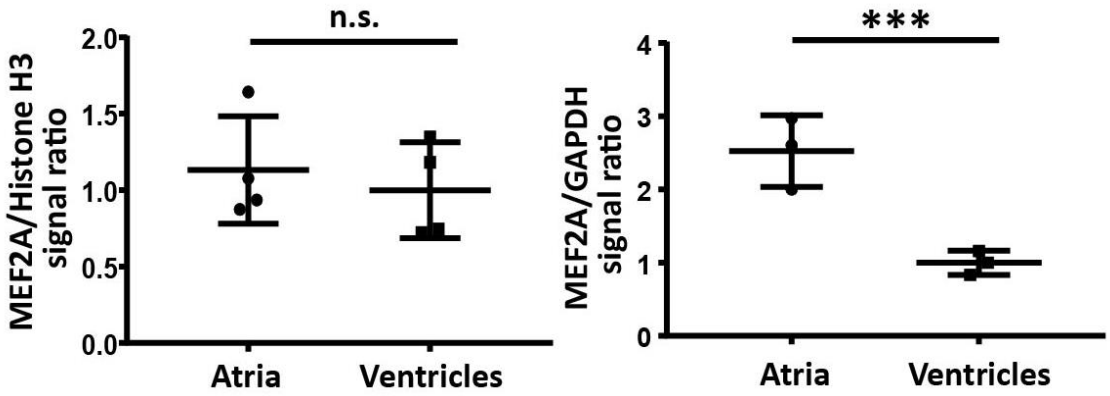

Figure 3.10 MEF2A levels normalized to nuclear control are similar between atrial and ventricular chambers. Quantification of MEF2A protein signal in atrial and ventricular lysates. MEF2A signal was normalized to total Histone H3 levels (*left graph*), or to GAPDH levels (*right graph*) for each lane. Error bars represent standard deviation ($n \geq 3$); n.s., not significant; ***, $p < 0.001$.

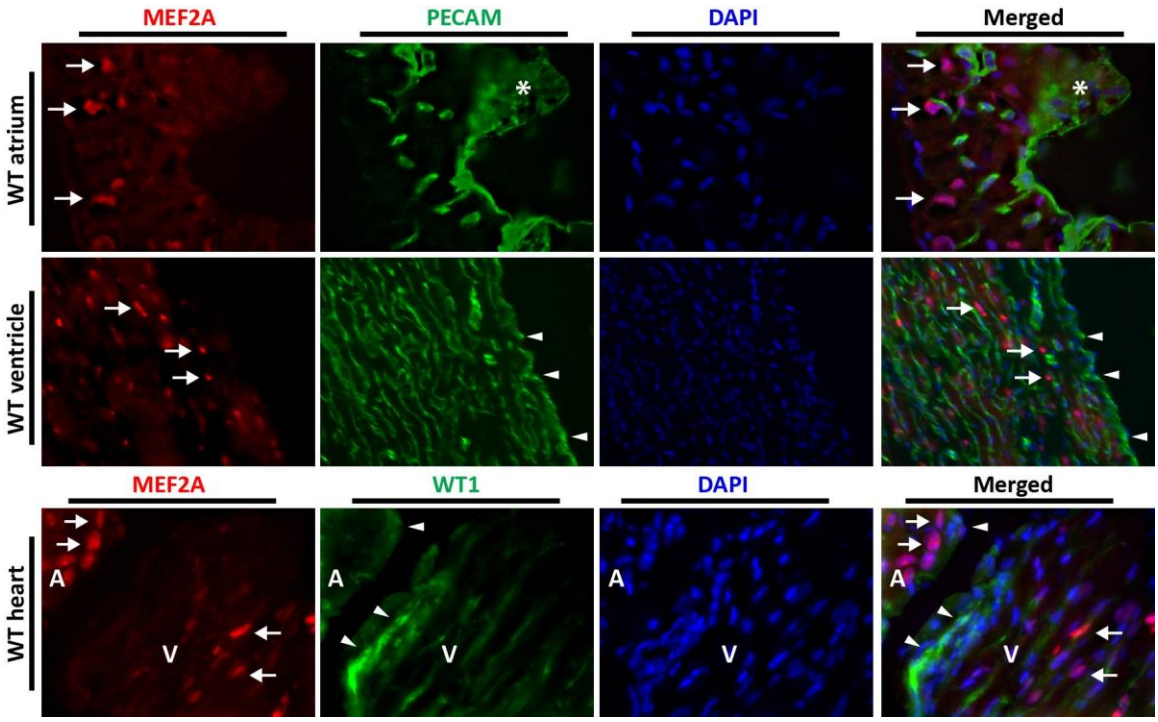

Figure 3.11 MEF2A protein is restricted to the myocardium in adult hearts. Immunohistochemical detection of MEF2A in myocardium but not epicardium or endocardium in WT atria and ventricles. MEF2A (red), PECAM (green; *top and middle panels*), and WT1 (green; *bottom panels*) counterstained with DAPI (blue). 60X WT atrium (*top panels*), 40X WT ventricle (*middle panels*), and 10X WT atrium and ventricle (*bottom panels*) fluorescent images were acquired (arrows indicate MEF2A-positive nuclei; the asterisk indicates PECAM staining; arrowheads indicate PECAM and WT1 focused staining in middle and bottom panels respectively; A = atrium; V = ventricle).

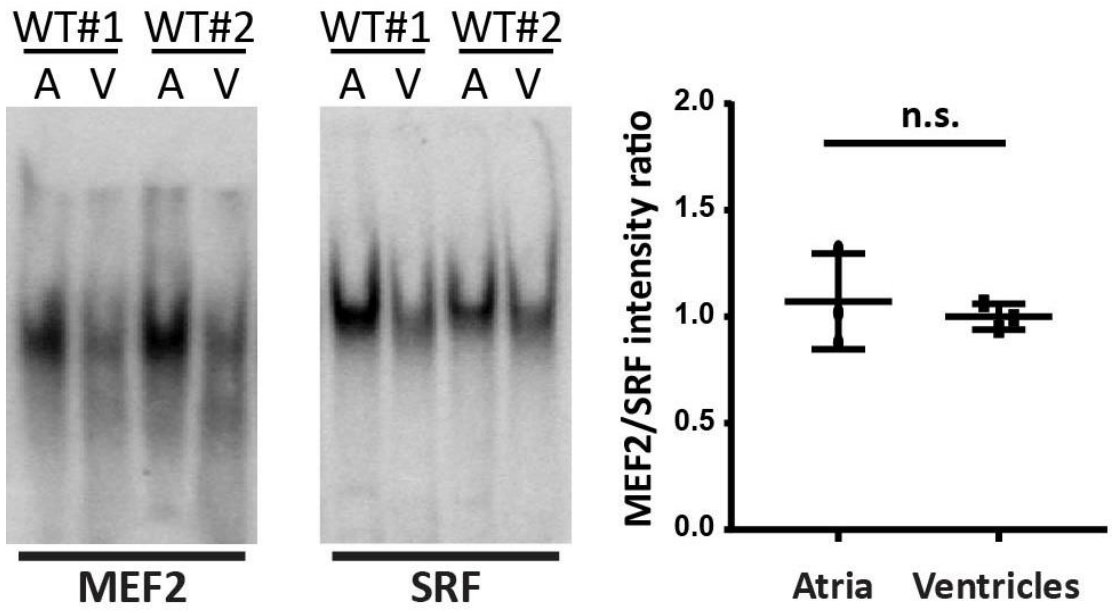

Figure 3.12 MEF2A DNA-binding activity. Electrophoretic mobility shift assays of MEF2 (*left panel*) and SRF (*right panel*) DNA-binding activity in lysates from WT atria and ventricles. Quantification of MEF2 DNA-binding activity relative to SRF binding activity (*right graph*). Average fold change was normalized to WT ventricles. Oligo sequences used for EMSA are found in Table 3.6. Error bars represent standard deviation of biological replicates; n.s., not significant.

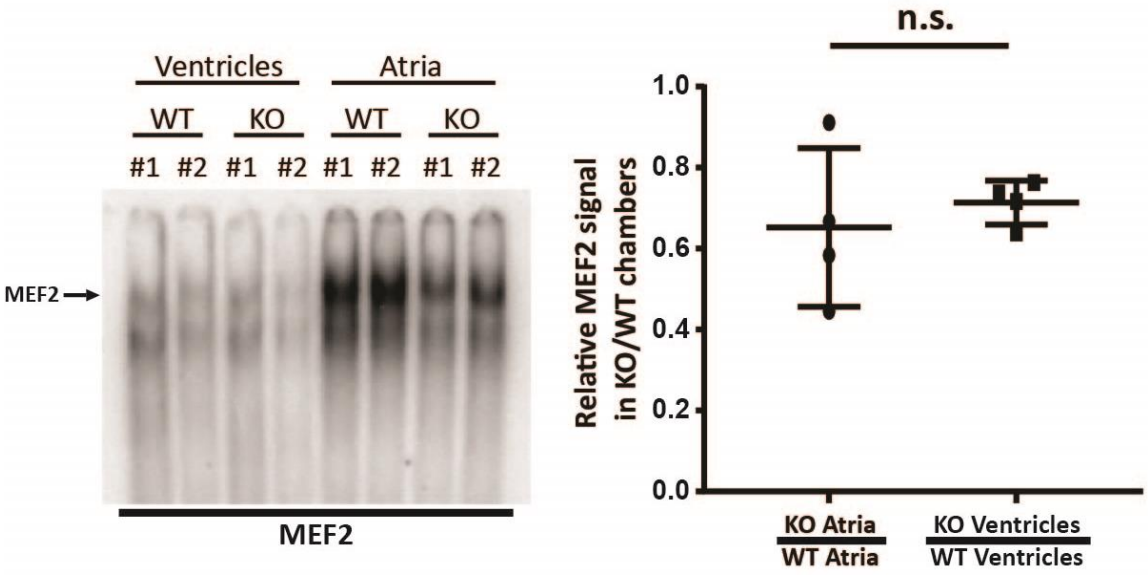

Figure 3.13 MEF2 DNA-binding activity is reduced in MEF2A KO hearts. Gel shift assay of MEF2 DNA binding activity in lysates from WT and KO cardiac chambers. MEF2 KO/WT chamber gel shift signal reduction quantification (*right graph*). MEF2 DNA-binding activity signal in KO chambers was normalized against respective WT chamber. Error bars represent standard deviation of biological replicates; n.s., not significant.

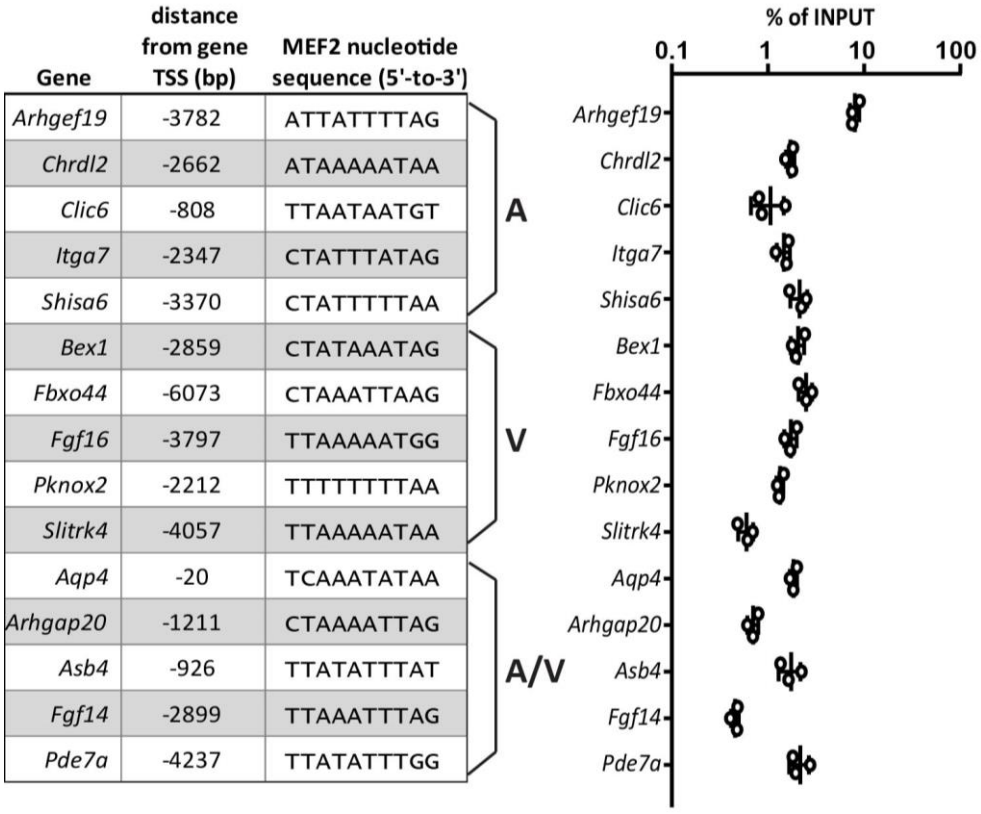

Figure 3.14 MEF2A associates with chromatin containing predicted MEF2 enhancers of dysregulated genes *in vivo*. 5,000 bp upstream regulatory region for 15 MEF2A-sensitive genes were scanned for predicted MEF2 sites using the Integrative Genomics Viewer (Broad Institute), ENCODE experimental datasets (accession numbers ENCSR806JZK and ENCSR867SDZ), and the MEF2 consensus sequence 5'-*YTAWWWWTAG*-3'. For *Fbxo44*, an optimal MEF2 site was located upstream of the original -5,000 bp search parameter. Formaldehyde fixed and sonicated chromatin was isolated from *Mef2a* WT whole hearts. ChIP assay was performed with a MEF2A polyclonal antibody, and immunoprecipitated chromatin was subjected to quantitative PCR with primers designed to amplify ~100 bp of promoter sequence containing predicted MEF2 sites. Error bars represent standard deviation of technical triplicates of qPCR samples.

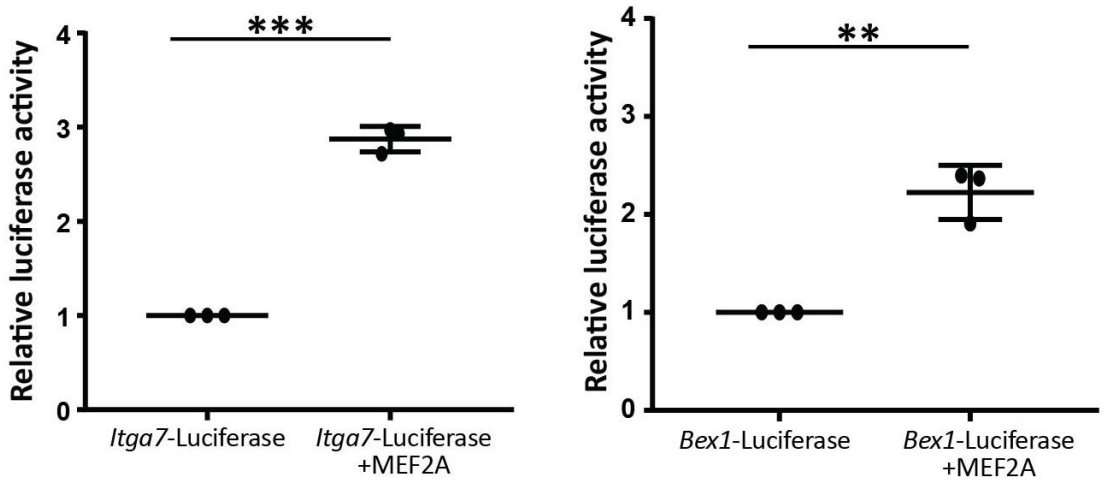

Figure 3.15 Transcriptional activation of predicted MEF2 enhancers in MEF2A-sensitive genes. MEF2A-dependent activation of a luciferase reporter harboring a 500 bp upstream genomic region surrounding a MEF2 binding site (-2347) of the *Itga7* gene (*left graph*). MEF2A-dependent activation of a luciferase reporter harboring a 500 bp genomic region surrounding a MEF2 binding site (-2859) of the *Bex1* gene (*right graph*). Error bars represent standard deviation of biological replicates; **, $p < 0.01$; ***, $p < 0.001$.

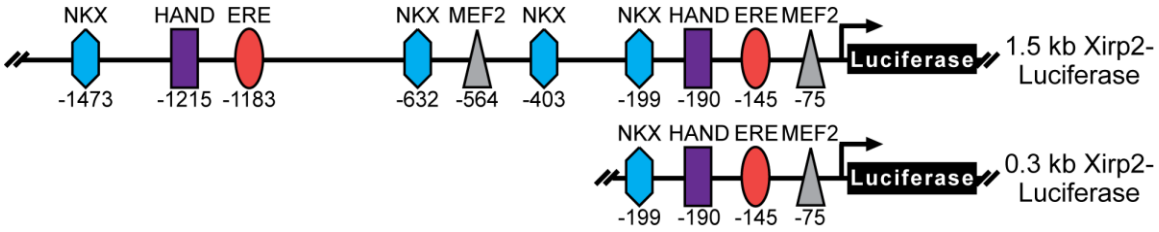

Figure 3.16 *Xirp2*-Luciferase constructs used in this study. Schematic of the pGL3basic-1.5kb-*Xirp2*-Luciferase construct (top), and the pGL3basic-0.3kb-*Xirp2*-Luciferase construct (bottom). The functional MEF2 (-75), and predicted EREF, HAND, and NKXH binding sites position are shown relative to the luciferase reporter gene.

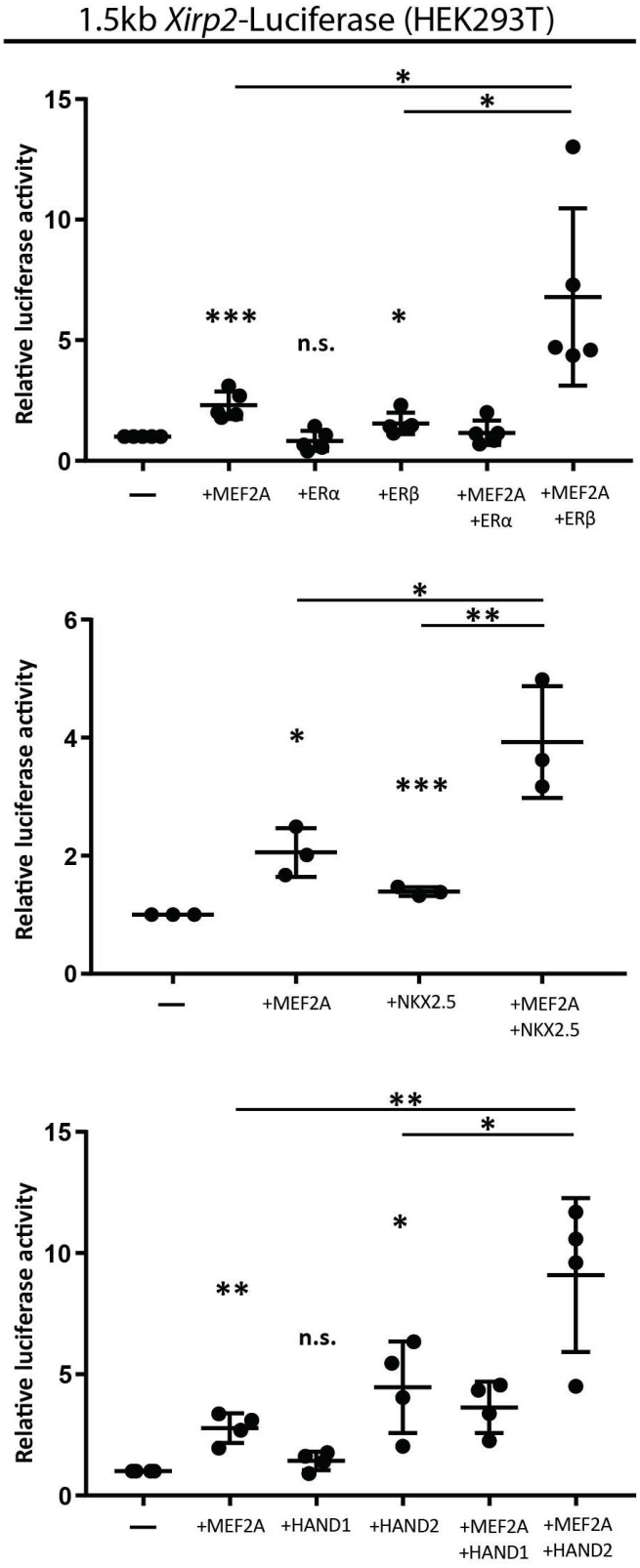
1.5kb Xirp2-Luciferase (HEK293T)
Relative luciferase activity
15
10
5
0
*
*
***
n.s.
*
—
+MEF2A
+ERα
+ERβ
+MEF2A +ERα
+MEF2A +ERβ
Relative luciferase activity
6
4
2
0
*
**
*
***
—
+MEF2A
+NKX2.5
+MEF2A +NKX2.5
Relative luciferase activity
15
10
5
0
**
*
**
n.s.
*
—
+MEF2A
+HAND1
+HAND2
+MEF2A +HAND1
+MEF2A +HAND2

Figure 3.17 MEF2A cooperatively interacts with transcription cofactors in HEK293T cells. Activation of the 1.5 kb *Xirp2*-luciferase reporter in HEK293T cells by MEF2A (top, middle, bottom graphs), ERα and β expression constructs (*top*), NKX2.5 expression construct (*middle*), or HAND expression constructs (*bottom*). Fold changes are normalized to reporter-alone condition (1.0) in each graph. Fold-change activation with overexpression plasmids over 1.5kb-*Xirp2*-Luciferase reporter alone are: 2.3 (+MEF2A), 0.8 (+ERα), 1.5 (+ERβ), 1.2 (+MEF2A +ERα), and 6.8 (+MEF2A +ERβ) (*top graph*); 2.1 (+MEF2A), 1.4 (+NKX2.5), and 4.0 (+MEF2A +NKX2.5) (*middle graph*); 2.8 (+MEF2A), 1.4 (+HAND1), 4.5 (+HAND2), 3.6 (+MEF2A +HAND1), 9.1 (+MEF2A +HAND2) (*bottom graph*). Error bars represent standard deviation ($n \geq 3$); n.s., not significant; *, $p < 0.05$; **, $p < 0.01$; ***, $p < 0.001$.

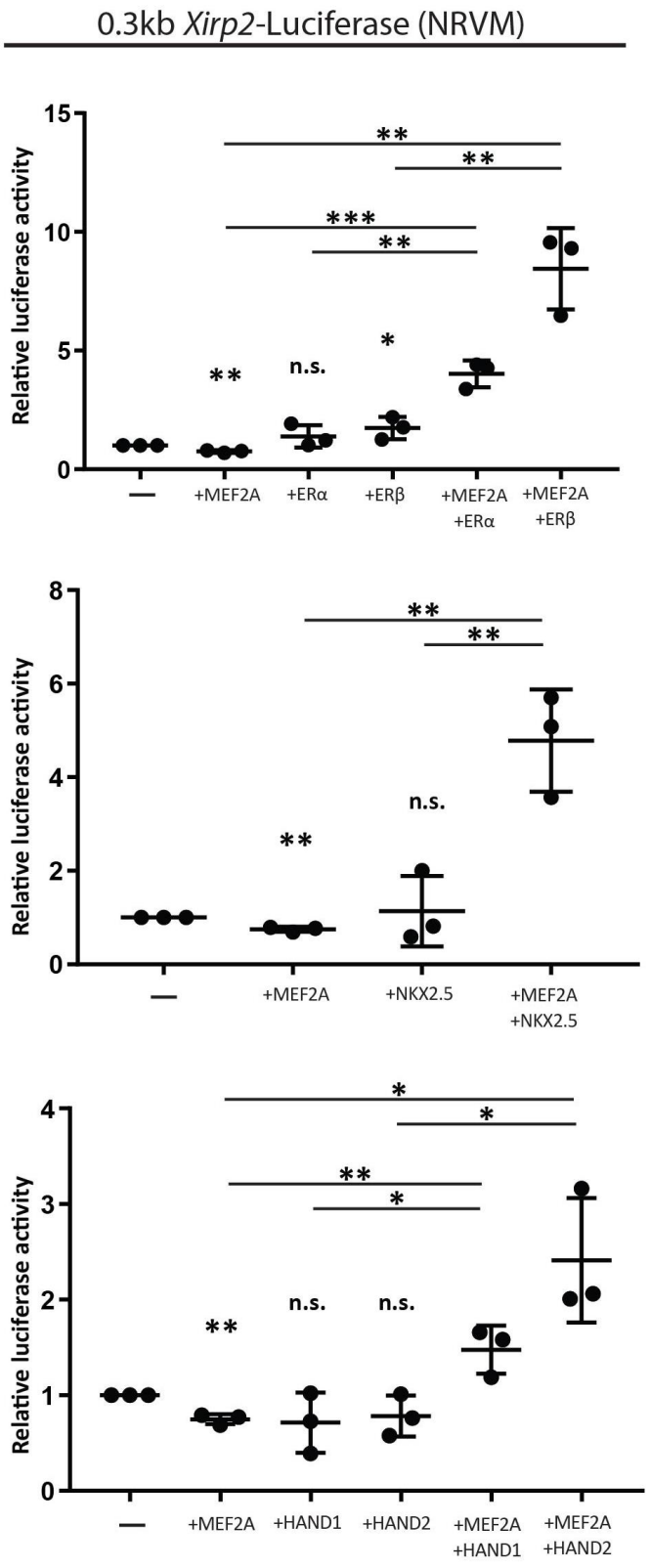
0.3kb Xirp2-Luciferase (NRVM)
Relative luciferase activity
15
10
5
0
**
**
***
**
*
**
n.s.
—
+MEF2A
+ERα
+ERβ
+MEF2A +ERα
+MEF2A +ERβ
Relative luciferase activity
8
6
4
2
0
**
**
**
n.s.
—
+MEF2A
+NKX2.5
+MEF2A +NKX2.5
Relative luciferase activity
4
3
2
1
0
*
*
**
*
**
n.s.
n.s.
—
+MEF2A
+HAND1
+HAND2
+MEF2A +HAND1
+MEF2A +HAND2

Figure 3.18 MEF2A cooperatively interacts with transcription cofactors in neonatal rat ventricular myocytes. Activation of the 0.3 kb *Xirp2*-luciferase reporter in NRVMs by MEF2A (top, middle, bottom), ERα and β expression constructs (*top*), NKX2.5 expression construct (*middle*), or HAND expression constructs (*bottom*). Fold changes are normalized to reporter-alone condition (1.0) in each graph. Fold-change activation with overexpression plasmids over 0.3kb-*Xirp2*-Luciferase reporter alone are: 0.8 (+MEF2A), 1.4 (+ERα), 1.7 (+ERβ), 4.0 (+MEF2A +ERα), and 8.4 (+MEF2A +ERβ) (*top graph*); 0.8 (+MEF2A), 1.1 (+NKX2.5), and 4.8 (+MEF2A +NKX2.5) (*middle graph*); 0.8 (+MEF2A), 0.7 (+HAND1), 0.8 (+HAND2), 1.5 (+MEF2A +HAND1), 2.4 (+MEF2A +HAND2) (*bottom graph*). Error bars represent standard deviation ($n = 3$); n.s., not significant; *, $p < 0.05$; **, $p < 0.01$; ***, $p < 0.001$.

Preferentially dysregulated in KO atria:	**481 /686 (70%)**
Non-enriched	391 /481 (81%)
Atrial enriched	68 /481 (14%)
Ventricular enriched	22 /481 (5%)
Preferentially dysregulated in KO ventricles:	**158 /686 (23%)**
Non-enriched	110 /158 (70%)
Atrial enriched	19 /158 (12%)
Ventricular enriched	29 /158 (18%)
Dysregulated in both KO atria and ventricles:	**47 /686 (7%)**
Non-enriched	29 /47 (62%)
Atrial enriched	10 /47 (21%)
Ventricular enriched	8 /47 (17%)

Table 3.1 A majority of MEF2A-sensitive genes are similarly expressed throughout wild-type hearts. Of the total 686 dysregulated genes between WT and KO hearts, 481 genes (70%) were preferentially dysregulated in KO atria, 158 genes (23%) were preferentially dysregulated in KO ventricles, and the remaining 47 genes (7%) were dysregulated in both KO cardiac chambers. These genes were further categorized based on their chamber expression profile (chamber enrichment is specified as 2.0-fold or greater expression in one chamber relative to the other) in WT hearts. Most of the preferentially dysregulated genes are similarly expressed in both atria and ventricles of WT hearts.

Gene set	Average fold dysregulation ± SD	
	Atrial	Ventricular
Preferentially dysregulated in atria (481)	1.76 ± 0.46	1.15 ± 0.11
Preferentially dysregulated in ventricles (158)	1.19 ± 0.14	1.87 ± 0.86
Dysregulated in both atria and ventricles (47)	2.64 ± 2.06	2.44 ± 1.73

Table 3.2 Average fold dysregulation of preferentially dysregulated genes. Average fold dysregulation of each three gene sets. Averages are calculated as absolute values.

Gene dysregulation	# upregulated	# downregulated	
preferentially in KO atria (481)	262	219	
preferentially in KO ventricles (158)	74	84	
	# upregulated in both chambers	# downregulated in both chambers	# in opposing directions
in both KO atria and ventricles (47)	15	26	6

Table 3.3 Directionality of gene dysregulation in MEF2A KO cardiac chambers. Analysis of direction of dysregulation in each gene set. Similar number of genes were up- and down-regulated in each. 6 out of the 47 genes dysregulated in both KO atria and ventricles are up- and downregulated in different chamber types.

Top Canonical Pathways

Name	p-value	Ratio
MEF2A KO atria only		
Hepatic Fibrosis	2.74E-04	13/197
Human Embryonic Stem Cell Pluripotency	2.07E-03	9/134
Agranulocyte Adhesion and Diapedesis	6.63E-03	10/189
GADD45 Signaling	6.87E-03	3/19
Nicotine Degradation II	7.77E-03	5/59
MEF2A KO ventricles only		
MSP-RON Signaling Pathway	3.97E-03	3/46
Tryptophan Degradation X (Mammalian, via Tryptamine)	6.78E-03	2/18
Glutamine Biosynthesis	6.93E-03	1/1
Clathrin-mediated Endocytosis Signaling	9.39E-03	5/185
Cellular Effects of Sildenafil (Viagra)	1.25E-02	4/129
MEF2A KO atria & ventricles		
Folate Transformations I	6.44E-03	1/9
Protein Ubiquitination Pathway	1.6E-01	1/242

Table 3.4 Top canonical pathways dysregulated in MEF2A KO hearts. Three gene sets (481 genes dysregulated in KO atria, 158 genes dysregulated in KO ventricles, and 47 genes dysregulated in KO atria and ventricles) were analyzed using the Qiagen Ingenuity Pathway Analysis. The top affected canonical pathways are listed for each gene set. Ratios for each pathway report the number of dysregulated genes from each data set (*numerator*) and the total number of associated genes (*denominator*). In a separate KEGG Pathway analysis, cell adhesion was the top pathway predicted to be dysregulated in the set of genes preferentially dysregulated in MEF2A KO atria.

V$MEF2 & secondary TF paired module	TF description	Fold over representation / Z-score in promoters of genes dysregulated		
		preferentially in MEF2A KO atria	preferentially in MEF2A KO ventricles	in MEF2A KO atria and ventricles
V$CLOX	CLOX and CLOX homology (CDP) factors	1.7 / 18.96		
V$EREF	Estrogen response elements	2.22 / 19.14		
V$HBOX	Homeobox transcription factors	1.32 / 13.88		
V$SF1F	Vertebrate steroidogenic factor	3.3 / 28.42		
V$BRN5	Brn-5 POU domain factors		1.58 / 13.08	
V$DMRT	DM domain-containing transcription factors		1.65 / 11.48	
V$HOXF	Paralog hox genes 1-8 from the four hox clusters A, B, C, D		1.45 / 12.48	
V$NKXH	NKX homeodomain factors		1.59 / 12.96	
V$BHLH	bHLH transcription factors expressed in muscle, intestine and stomach			1.91 / 5.67
V$CART	Cart-1 (cartilage homeoprotein 1)			1.39 / 5.83
V$HAND	Twist subfamily of class B bHLH transcription factors			1.77 / 5.66
V$HOXC	HOX - PBX complexes			1.57 / 5.63
V$LEFF	LEF1/TCF			1.6 / 5.42
V$LHXF	Lim homeodomain factors	1.3 / 14.81	1.46 / 12.86	
V$OCT1	Octamer binding protein	1.36 / 17.17	1.47 / 12.95	
V$CAAT	CCAAT binding factors	1.9 / 19.67		1.78 / 5.21
V$HOMF	Homeodomain transcription factors		1.36 / 11.22	1.41 / 7
V$BRNF	Brn POU domain factors	1.29 / 15.05	1.47 / 13.71	1.35 / 5.53
V$FKHD	Fork head domain factors	1.31 / 16	1.53 / 15.6	1.39 / 6.31
V$SORY	SOX/SRY-sex/testis determining and related HMG box factors	1.38 / 18.48	1.56 / 15.51	1.36 / 9.03

Table 3.5 Candidate co-factor analysis of MEF2A-dependent genes. The 5,000 bp proximal promoters from the three dysregulation gene sets were analyzed for predicted MEF2 sites, and then analyzed for additional neighboring transcription factor binding sites within 50 bp of predicted MEF2 sites (Genomatix). In each gene set, over representation (*number left of slash*) and Z-score (*number right of slash*) for each MEF2-TF module is calculated (Z-score greater than 2 is considered statistically significant). Over representation is the fold increase of MEF2-TF module found in each promoter dataset compared to a background promoter dataset. For each gene set, the top 10 overrepresented MEF2-TF modules are listed and rearranged according to representation in each gene set. The three co-factor families studied in this chapter are estrogen receptors (V$EREF family weight matrices), Nkx2.5 (V$NKXH family weight matrices), and HAND proteins (V$HAND family weight matrices). Individual positional weight matrices for each family can be accessed in the Genomatix Matrix Family Library (Version 3.3; www.genomatrix.de).

RT-PCR

Gene	Forward primer	Reverse primer
Mef2a	ACACGCATAATGGATGAGAGGAACCGAC	CAACGATATCCGAGTTCGTCCTGCTTTC
Mef2a (Exon 5,7, 8)	GTCCACTCTCGGAGGACAGATTCAGCAAAC	***CATTTGGCACCGTGAGGTCTGTAGTGCTC***
Mef2a (Exons 6-8)	GCGACAGCCCAGACCCTGATACTTCATATG	***CATTTGGCACCGTGAGGTCTGTAGTGCTC***
Mef2a (Exons 9, 10)	ATGGATTTGTAAACTCAAGGGCCTCTC	CAACTCCAATTCCTCTTCCTCCGA
Nkx2-5	TTTTACCCGGGAGCCTACGGT	TGTTGCTTGAAGCGCCGCT
Rn18s	CATTCGAACGTCTGCCCTAT	CCTCCAATGGATCCTCGTTA

qRT-PCR

Gene	Forward primer	Reverse primer
Arhgap20	GCCCCGCGAGATGCAATGCC	GGTGTGTGCTAGAACCCCGCCA
Arhgef19	CTTGGCTACAACCCCATTGC	GAAATGGCGGCCTTAGAGAC
Aqp4	CAGGGAAGGCATGAGTGACAG	TGCTGAGACTGCCTTCCAGA
Asb4	GTGCCAAGCAGTTGGTGTTG	TCCACGTAGAAGGCAACCAG
Bex1	AGAGGAGAAGGCAAGGATAGG	TGGCTCCCTTCTGATGGTATC
Chrdl2	GCCCAGACAGCCTACACCGCTT	GCCGGTGAGCAGCCGGAAGT
Clic6	GAGAATGGCCCAGCATTGGA	ATGCTCTCGCCGTCATAACC
Fbxo44	CCAGAGGAACCTCCTTCACA	CATTCATCGCCTCCGTTCAC
Fgf14	GCAGATGCACCCCGATGGAGC	CCTGGATGGCAACAACGCGCA
Fgf16	AGACTTCGCCCACCTGAA	ACAGCCAAGCTGATAAATTCCA
Itga7	ATGCTCACCAGCCCAGCACCC	AACGGCTGCCCACTCAATGCG
Pde7a	GGACCTCTGGTTGATCCAATG	ATGTACGGATGGGAACCTCTT
Pknox2	TCCTGCAGAATTCCCCCAAT	CCACCTGACACGACTTGAGA
Shisa6	GACTCCAGGTGATCGTCAGT	GGAGAGGTCATAGGGTTCCG
Slitrk4	TAGAGAGCATCGCGGAAACT	CACGGTCTTTGAGCAGCTTT
Rn18s	TCGGAACTGAGGCCATGATT	TTGGCAAATGCTTTCGCTCT

ChIP-qPCR

Gene	Forward primer	Reverse primer
Arhgap20	GCACCCCTGATTCACAGATGTA	CCCACAAAGACACACCTACACA
Arhgef19	AGCCCGAGCAAATATCAAGTCA	CCAACAGGGACCAATCCTACA
Aqp4	TGGGAGTCAGATTACGGGCA	TGATTGCCACATGGTGCAGAA
Asb4	TGACGTAGGAGCAAAGGATCG	AGGCTTGTCAGGGAGGAGTA
Bex1	ATGTGTTACAGGGAGACTGGAAA	GGCAAGCACTCTAACAACCG
Chrdl2	ATGAGTTCAAACCCCTTGCAC	TCCACAACAGACAATGCTGGA
Clic6	GAGTGTGTCTGTGTCTTGGAAGTTATGCTAG	CACACACATAACTTACATATAGCACACACAAGC
Fbxo44	GGGTGACCAACAGTAGCGT	GGGGTAGGGGAGGTCGTT
Fgf14	CATGTTAACTTAAGTTCCAGACTCTTAAGTTTCATTTTGG	CAGATTTTTACTACCAATCTTCACAAGCATCTAAGACC
Fgf16	CGAGAAACTAGGTATCAAAAAACCAGACAGTCC	GGAACCTGGGTCCTTTAGTAATCAATGC
Itga7	TTCTTTCCCTCCCTTACCCCA	TTTGAGAAGTCACCTCACCCG
Pde7a	TCCCCTACCCATGACAGAGC	GCTTGATTCCGTGCTGGTCT
Pknox2	GCTGATGACCCAGCTAGTGA	AGGATTTAGATGTGGCACCCA
Shisa6	ATGCTTACTCTGGATGGCAGG	AAGCCAACTGGAAATCACCTCC
Slitrk4	CTGGAAGAGGCTCTTTTCATGATCTAATGTG	AATGTTGCTTCCCTTTTCTCAGTAAATAAAGATCAC

EMSA oligonucleotides

TF	Oligonucleotide	Reverse complement
MEF2	AGGTGGGCTATTTTTAGGGA	AGGTTCCCTAAAAATAGCCC
SRF	CCGGGAACAGGTCCATGTATGGAAGCGAAAG	CCGGCTTTCGCTTCCATACATGGACCTGTTC

Table 3.6 Primers used for gene dysregulation in MEF2A KO mice. A list of RT-PCR and quantitative RT-PCR primers used for expression analysis, and oligonucleotides used for gel electrophoretic shift assays. All sequences are listed 5’ to 3’. Sequences listed in bold font indicate identical primers.

CHAPTER FOUR: *Bex1* is a target of MEF2A signaling

Parts of this research are in preparation for a submission to the open access journal *PLOS One*.

4.1 Introduction

Proper formation of the mammalian heart is dependent on coordinated gene expression. Members of the myocyte enhancer factor-2 (MEF2) family of transcription factors play a critical role in the expression of gene programs, and cardiac-specific cellular pathways (Desjardins & Naya 2016). Research from the Naya Lab has continually expanded the function of MEF2 isoforms through characterization studies of target genes and MEF2-sensitive cellular pathways. MEF2 proteins have been found to control a costamere gene program in cardiac muscle, cytoarchitectural target genes including *Myomaxin* and *Myospryin*, the *Gtl2-Dio3* non-coding RNA locus, and cell cycle related target genes such as *Pten* (Clark & Naya 2015, Durham *et al.* 2006, Estrella *et al.* 2015, Ewen *et al.* 2011, Huang *et al.* 2006). Additionally, MEF2 isoforms have been documented to display antagonistic roles in regulating cell cycle and differentiation gene programs in cardiac myocytes (Desjardins & Naya 2017). These characterization studies include global transcriptome analysis in loss-of-function and gain-of-function models, paired with DNA binding activity, predicted binding site characterization, and transcriptional activation assays.

In this chapter I discuss experiments related to *Bex1* as a about the potential MEF2 target gene. In the microarray study described in Chapter Three, *Bex1* is the fourth-most preferentially dysregulated gene in *Mef2a* knockout (KO) ventricles, with no enrichment in wild-type (WT) atria or ventricles (Appendix A.1.2.3). The *Bex1* gene encodes a 128 amino acid protein in mice and interacts with the intracellular domain of the p75 neurotrophin receptor (Figure 4.1). This interaction with the p75 neurotrophin links the BEX1 protein to both neurotrophin signaling and the cell cycle (Vilar *et al.* 2006). Through various promoter analysis and transcriptional activation studies, we show that *Bex1* is a direct target gene of MEF2A. The results described in this chapter also suggest that the BEX1 protein has a role in the nucleus of cardiomyocytes, and that MEF2A is involved in neurotrophin signaling and the cell cycle through its interaction with the *Bex1* gene.

4.2 Overlapping expression of *Bex1* and MEF2 in mouse tissues

To establish a more comprehensive expression pattern of *Bex1* in mice, I examined *Bex1* transcript levels in several tissues. Messenger RNA was collected from smooth muscle (stomach), skeletal muscle (tibialis anterior), cardiac atria and ventricles, brain, lung, kidney, and liver, and semi-quantitative RT-PCR was performed using *Bex1*-specific primers (Figure 4.2). *Bex1* mRNA expression levels were lowest in liver samples, and all samples were normalized to this value. Skeletal muscle and cardiac ventricles showed the highest levels of *Bex1* expression, 5.5- and 2.6-fold higher relative to *Bex1* expression levels in liver, respectively. Cardiac atria and brain showed less *Bex1*

expression than in skeletal muscle and cardiac ventricles, but both were approximately 2.1-fold higher compared to liver. These results show that *Bex1* expression patterns in the adult mouse overlaps with the expression pattern of MEF2. While ubiquitously expressed, MEF2 factors are highly expressed in cardiac, skeletal, and smooth muscle tissues, and to a lesser extent, in the brain (Black & Olson 1998, Desjardins & Naya 2016, Potthoff & Olson 2007). This overlapping expression pattern between *Mef2* factors and *Bex1* transcripts supports the hypothesis that *Bex1* is a target of MEF2.

4.3 *Bex1* is coordinately dysregulated in various MEF2A models

The microarray experiment described in Chapter Three showed that *Bex1* mRNA levels are downregulated by 2.1-fold in *Mef2a* KO ventricles as compared to WT ventricles (Appendix A.1.2.3). Data from our lab also confirm that *Bex1* is coordinately dysregulated in other MEF2A loss- and gain-of-function models. In separate microarray experiments, our lab has observed downregulation of *Bex1* in MEF2A loss-of-function studies. Knocking down MEF2A in neonatal rat ventricular myocytes (NRVMs) resulted in a 3.9-fold downregulation of *Bex1* mRNA levels (Desjardins & Naya 2017). Using whole hearts in *Mef2a* KO and *Mef2a* overexpression transgenic models, *Bex1* was downregulated by 2.5-fold and upregulated by 4.0-fold, respectively (unpublished data). These results demonstrate that *Bex1* is sensitive to the levels of MEF2A in cardiomyocytes, and we hypothesized that *Bex1* is a direct target gene of MEF2A.

4.4 *Bex1* mRNA levels are sensitive to MEF2A levels *in vivo*

To further characterize the MEF2A-dependent dysregulation of *Bex1* in the adult heart, I took advantage of two MEF2A models used in our lab: the *Mef2a* knockout and transgenic *Mef2a* overexpressor mouse lines. I isolated mRNA from wild-type, *Mef2a* heterozygous, *Mef2a* homozygous-null, wild-type possessing a single transgenic *Mef2a* overexpressor allele, and *Mef2a* homozygous-null possessing a single transgenic *Mef2a* overexpressor allele (Figure 4.3). Compared to wild-type levels, *Mef2a* heterozygous and homozygous-null mice showed a 1.7-fold and 1.9-fold reduction in *Bex1* mRNA expression levels, respectively. Mice that harbor a single transgenic allele overexpressing *Mef2a* in the wild-type background [$Mef2a^{+/+}$; Tg(αMHC:*Mef2a*)] showed a 1.5-fold increase in *Bex1* transcripts via RT-PCR. Interestingly, mice that contain a single transgenic overexpressor allele in the homozygous-null background [$Mef2a^{-/-}$; Tg(αMHC:*Mef2a*)] show *Bex1* levels similar to those observed in wild-type mice. While loss of a single wild-type allele is sufficient to reduce *Bex1* mRNA expression levels by nearly 50% as demonstrated in *Mef2a* heterozygous- and homozygous-null mice, the transgenic allele is sufficient to restore *Bex1* expression to near wild-type levels in the homozygous-null background. These results further demonstrate that *Bex1* is sensitive to levels of MEF2A in the adult heart, and support our hypothesis that *Bex1* is a target of MEF2A.

4.5 *Bex1* regulatory sequences respond to MEF2A levels *in vitro*

To identify MEF2-responsive elements in the mouse *Bex1* promoter, I subjected the 5,000 bp proximal promoter region upstream of the transcription start site (TSS) to a

transcription factor binding site search (http://rulai.cshl.edu/TRED). Searching for predicted MEF2 binding sites using a MEF2 positional weight matrix (http://jaspar.genereg.net/) revealed one candidate site 995 bp upstream of the TSS (5'-CTATATTTAT-3'; proximal MEF2 binding site) and a second candidate site 2,859 bp upstream of the TSS (5'-CTATAAATAG-3'; distal MEF2 binding site). It is interesting to note that while the distal MEF2 binding site in the *Bex1* promoter had a higher score (TRED score = 8.78) than the proximal MEF2 binding site (TRED score = 7.24), alignments of the mouse *Bex1* regulatory sequences show that this distal MEF2 site is not conserved across several mammalian species including human, rat, and mouse (Figure 4.4). However, the proximal MEF2 site is conserved across eight different species in the alignment (Figure 4.4)

To characterize the candidate MEF2 binding sites, I subcloned promoter fragments containing the proximal MEF2 and distal MEF2 site into luciferase reporter constructs (pGL3-Basic and pGL3-Promoter, respectively). Although the predicted proximal MEF2 binding site was conserved across several mammalian species, it showed a modest 1.5-fold activation over basal levels when transfected with human MEF2A over-expression plasmids in HEK293T cells. While the distal MEF2 binding site was not conserved across mammalian species, it showed higher transcriptional activation. The predicted distal MEF2 binding site showed 2.3-fold activation over basal levels when transfected with human MEF2A over-expression plasmids in HEK293T cells (Figure 4.5). These data show that human MEF2A can transcriptionally activate the *Bex1* gene through two upstream MEF2 enhancer sites.

4.6 MEF2A binds to Bex1 upstream regulatory regions *in vivo*

To support the reporter activation studies of the proximal and distal MEF2 binding sites, I subjected chromatin isolated from adult mouse ventricles to immunoprecipitation followed by quantitative PCR (ChIP-qPCR) to assess MEF2A occupancy on the *Bex1* promoter.

Using a MEF2 antibody which has higher preferentially affinity to MEF2A than to other MEF2 isoforms (Snyder *et al.* 2013), ChIP-qPCR studies revealed that 1.3% of input chromatin containing the proximal MEF2 binding site co-immunoprecipitates with MEF2A, while 2.0% of input chromatin containing the distal MEF2 site co-immunoprecipitates with MEF2A (Figure 4.6). As a negative control, 0.3% of input chromatin containing the proximal MEF2 binding site and 0.1% of input chromatin containing the distal MEF2 site co-immunoprecipitated when using rabbit IgG antibody. These results suggest that MEF2A occupies regulatory regions in the *Bex1* promoter *in vivo*, and that MEF2A has a higher preference for the distal site compared to the proximal site by 1.6-fold by comparing percent of immunoprecipitated input chromatin.

4.7 Discussion

This chapter describes experiments indicating that the mouse *Bex1* gene is a direct target gene of mouse MEF2A. We show through several *in vitro* and *in vivo* studies that MEF2A levels affect *Bex1* expression in cardiomyocytes. In MEF2A-deficient ventricles, we observe a downregulation of *Bex1* transcript levels. Conversely, we observe an

upregulation of *Bex1* expression in the ventricles of transgenic *Mef2a* overexpressing mice. These results clearly demonstrate that *Bex1* expression is sensitive to MEF2A levels in the heart. We also show through ChIP-qPCR studies that MEF2A occupies the promoter of the *Bex1* gene. We observe a 1.5-fold increase in chromatin binding of MEF2A on the distal MEF2 binding site compared to the proximal MEF2 binding site. Additionally, luciferase reporter experiments show that both the proximal and distal regions of the promoter harboring the predicted MEF2 sites are able to respond to MEF2A in *in vitro* reporter assays.

It is interesting to note that *Bex1* expression is not enriched in wild-type atrial nor ventricular tissues, but it is preferentially dysregulated in *Mef2a* KO hearts. These observations indicate that *Bex1* expression between atrial and ventricular chambers is differentially regulated, and that MEF2A may interact with transcriptional co-regulators to fine-tune the expression of *Bex1* in the adult mouse heart. Previous studies suggest that the BEX1 protein localizes to the cytosol due to its interaction with the intracellular domain of p75-NTR (Vilar *et al.* 2006). We are interested in characterizing the cellular localization pattern of the BEX1 protein in cardiomyocytes. Altogether, these studies point to a new role and function for MEF2A in the adult heart through its ability to upregulate *Bex1* transcription.

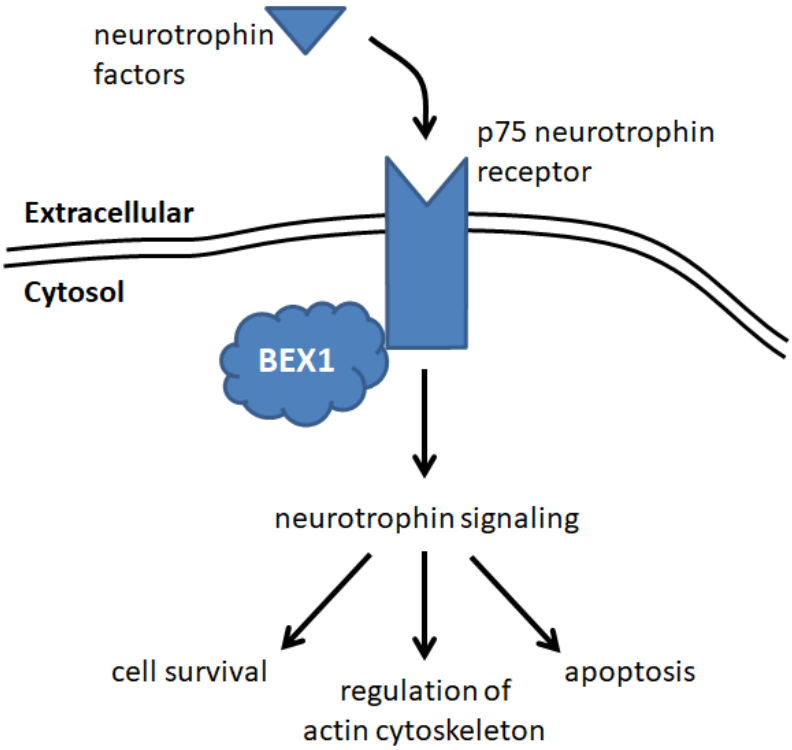

Figure 4.1 BEX1 in neurotrophin signaling. BEX1 has been shown to interact with the intracellular domain of the p75 neurotrophin receptor. Cell survival, regulation of the actin cytoskeleton, and apoptosis are all downstream cellular processes of neurotrophin signaling (Reichardt 2006).

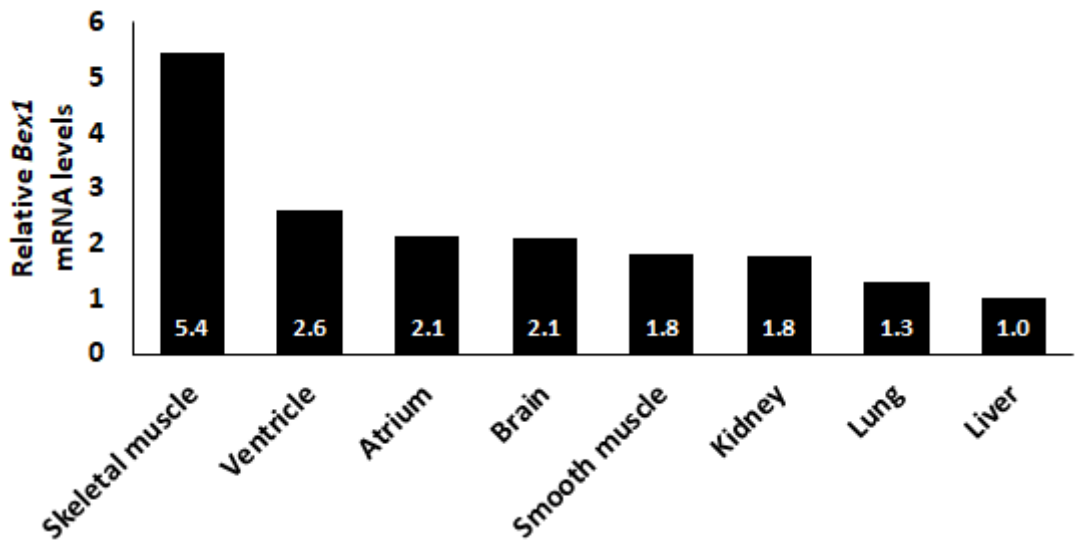

Figure 4.2 Expression of *Bex1* in mouse tissues. *Bex1* mRNA transcript levels normalized to *18S* ribosomal RNA were quantified across different tissues in mice. *Bex1* expression levels in all tissues were then normalized to liver expression levels. Skeletal muscle and cardiac ventricles show the highest expression levels of *Bex1*, while liver and lungs showed the lowest expression levels.

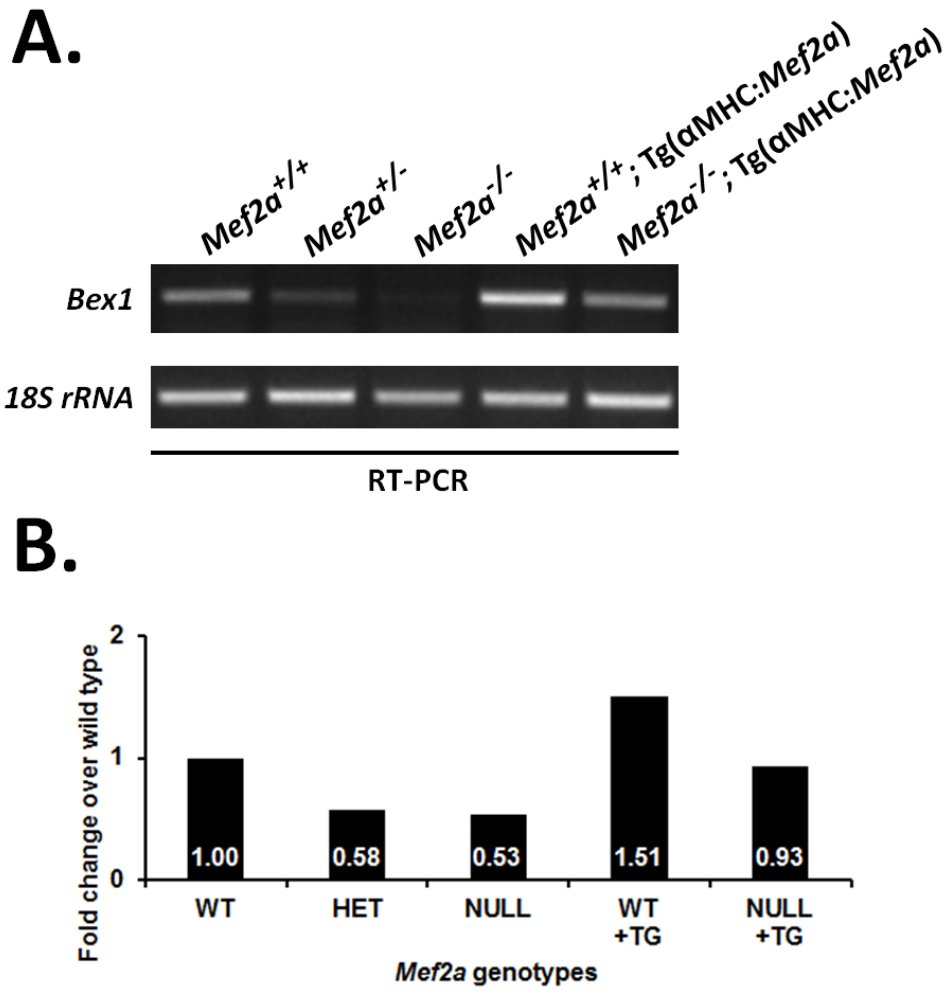

Figure 4.3 *Bex1* expression is sensitive to MEF2A levels *in vivo*. *A*, RT-PCR analysis of *Bex1* mRNA and *18S* ribosomal RNA levels in ventricles of different *Mef2a* genotypes in mice. *B*, Quantification of *Bex1* mRNA levels normalized to *18S* ribosomal RNA levels in ventricles of the indicated *Mef2a* genotypes.

Bex1 proximal MEF2 site

```
Human       --AGCAGCTGCGTGTAGAGTCTATATTTATATAATGACTTAACAGGACAG
Rat         GCAGCTGCTGCCTGTAGAGTCTATATTTATATAATGACTTAGCAGGAGAG
Mouse       GCAGCTGCTGCCTGTGGAGTCTATATTTATATAATGACTTAGCAGGAGAG
Rabbit      -------CTGCCTGTACAGTCTATATTTATATAATGACTTAACAGAAGAG
Cow         ------GCTGCCTGTAAAGTCTATATTTATATAACGACTTAGCAGAAGA-
Pig         ------GCTGCCTGTAGAGTCTATATTTATATAATGACTTGGCAG-----
Dog         ------GCTGCCTGTAGAGTCTATATTTATATAGTGACTTAGCAGAAGA-
Cat         ------GCTGGCTGTATAGTCTATATTTATGTAATGACTTAGAAG-----
                   ***  ***  ************ **  *****   **
```

Bex1 distal MEF2 site

```
Human*      ACAATATTTT-----GATA--TTTTTTC-AATAAATGCGTTTATATAACTGCTTAAGTA-
Rat         CAGACATTTA-----GATATTTTTTTTC-TGTAAATAGGAT-GTAAAAC--TTGAAGTAA
Mouse       CAGATATTTA-----GATAT--TTTTTC-TATAAATAGGAT-GTAAAAAAATTAAAGTA-
Rabbit*     CCTACACTTAGCAAAGAGT-------TC-AATAAATAGGATGAAAAAAAATGCTGACC--
Cow*        TTATAATAAC-----CTAA--TTTTTTC-TATTAAAAGGAT-GTAATATGATTTATTTA-
Pig*        TTTCTGTTTA-----GATA--TTTTTTCATAAAAATAGGAC--TAATATTCATAAACAGA
Dog*        -AAATATTTA-----GATA-TTCTTCTC-TATATACAGCAT-GTGTATT-ATGTAATGGA
Cat*        -GGCTATTTTA----GATA--ATTCTTC-TATAAATATCGGGATGCATATATCCCTTC--
                                        **      *
```

Figure 4.4 Sequence alignment of MEF2 sites. Mouse *Bex1* upstream regulatory sequences containing either the proximal MEF2 site (-995 bp) or the distal MEF2 site (-2,859 bp) were compared to human, rat, rabbit, cow, pig, dog, and cat *Bex1* upstream regulatory regions of respective species. The mouse *Bex1* proximal MEF2 site (*top alignment*) and the mouse *Bex1* distal MEF2 site (*bottom alignment*) are highlighted in yellow. In the *Bex1* distal MEF2 site alignment for human, rabbit, cow, pig, dog, and cat (*asterisk*), upstream regulatory sequences were not found within the -5,000 bp promoter region immediately upstream of the TSS. Instead, BLAST (NCBI) was performed to find the closest matching sequence on the X chromosome.

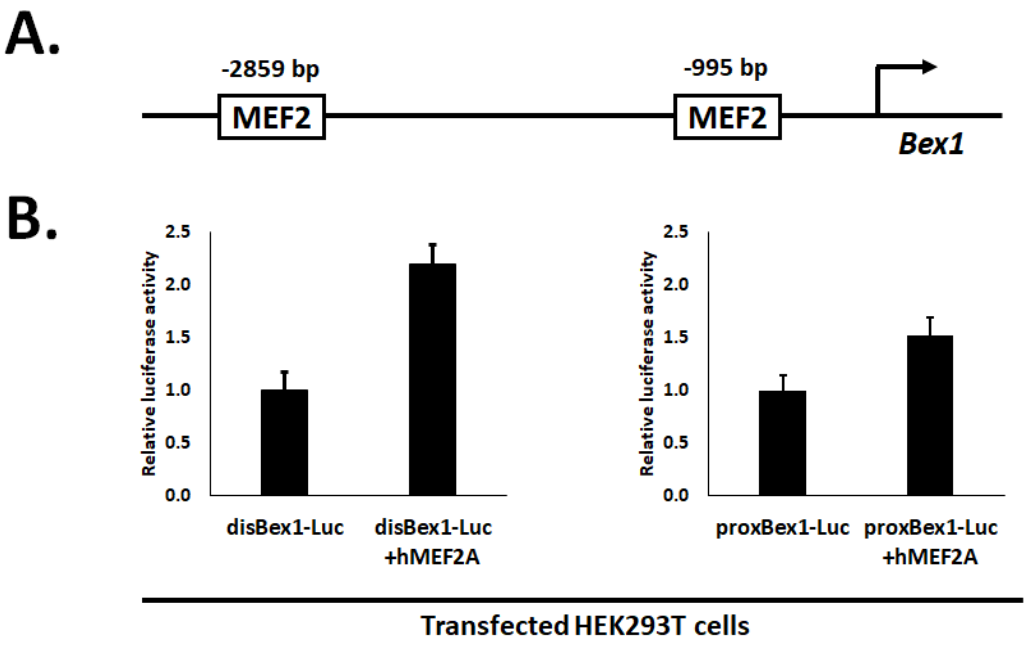

Figure 4.5 MEF2A activates *Bex1* gene expression *in vitro*. *A*, proximal (-995 bp) and distal (-2859 bp) candidate MEF2 binding sites were subcloned into pGL3-Basic and pGL3-Promoter, respectively. *B*, luciferase reporter assays of cloned predicted MEF2 sites display activation with transiently transfected human MEF2A in HEK293T cells. MEF2A transcriptional activation was tested using the distal MEF2 enhancer (pGL3Promoter-dis*Bex1*-Luciferase, *left graph*) and the proximal MEF2 enhancer (pGL3Basic-prox*Bex1*-Luciferase, *right graph*). Luciferase readings were normalized to an internal beta-galactosidase transfection control and normalized to reporter-alone.

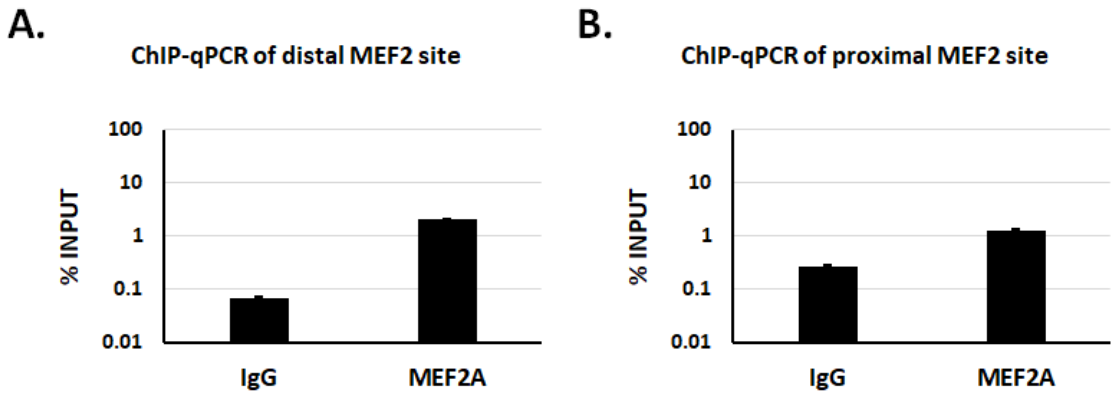

Figure 4.6 MEF2A binds to Bex1 upstream regulatory regions *in vivo*. ChIP analysis was performed with IgG as a negative control antibody, or a MEF2A-specific antibody (Santa Cruz sc-313). Immunoprecipitated chromatin was subjected to quantitative PCR with primers designed to amplify ~100 bp of upstream regulatory sequence containing the distal or proximal MEF2 site. MEF2A displays greater enrichment on the distal site by 1.5-fold (2.0% INPUT in distal MEF2 site over 1.3% INPUT in proximal MEF2 site).

RT-PCR primers	
Primer	***Sequence* (*5' → 3'*)**
Bex1 Fwd	TGAGCATCTCTAGAAAGAGG
Bex1 Rev	GGTCCCATCTATAGTGAGC
***Bex1* MEF2 enhancer sites**	
Primer	***Sequence* (*5' → 3'*)**
proxMEF2 Fwd	CCTTTTTCCAAGGTCCAAAAACAGC
proxMEF2 Rev	GTGCCACTTGCGTCAGAAGC
disMEF2 Fwd	ACTGCCCAGCTAGCCAAAGACATTC
disMEF2 Rev	CATGGTGGTGCACGCCTTTAATCC
ChIP-qPCR	
Primer	***Sequence* (*5' → 3'*)**
proxMEF2 Fwd	GCTGCCCTGTCCTTTTTCCAA
proxMEF2 Rev	CCAACCATCTGTCTCTCCTGCT
disMEF2 Fwd	ATGTGTTACAGGGAGACTGGAAA
disMEF2 Rev	GGCAAGCACTCTAACAACCG

Table 4.1 Primers used for *Bex1* expression and promoter analysis. Primers are listed 5' to '3'. Annealing temperatures for RT-PCR reactions and cloning PCR reactions using Q5 High-Fidelity Polymerase (New England Biolabs) were determined using NEB T_m calculator (https://tmcalculator.neb.com). ChIP-qPCR annealing temperature were 60 °C.

CHAPTER FIVE: Discussion

5.1 Discussion

MEF2A is a central regulator of gene programs in the adult heart. Studies have shown that MEF2A controls a spectrum of gene programs in cardiomyocytes including cell cycle pathways and a costamere gene program (Estrella *et al.* 2015, Ewen *et al.* 2011). While previous investigations have described the cellular defects in adult *Mef2a* knockout hearts (Naya *et al.* 2002), the molecular changes in adult MEF2A mutant hearts are poorly understood.

In Chapter Three I presented an analysis cardiac chamber-dependent transcriptional regulation of MEF2A-sensitive genes in the adult heart. These results suggest that MEF2A differentially regulates distinct pathways in the atrial and ventricular chambers of the heart. I validated a subset of preferentially dysregulated genes, supporting the dysregulation trends observed in the MEF2A-dependent transcriptome microarray. With this in mind, I sought to identify cellular pathways that were also affected in a chamber-dependent manner. Using a bioinformatics approach, I identified cell adhesion and the MSP-RON pathway as candidate dysregulated pathways in *Mef2a* KO atria and ventricles, respectively. By analyzing molecular components of these pathways, I found that phosphorylated FAK levels were downregulated in atrial chambers and TRAF6 protein levels were downregulated in ventricular chambers. These results imply that MEF2A also regulates signaling pathways in the heart in a chamber-dependent manner.

To understand the molecular mechanisms behind the chamber-dependent preferential dysregulation I analyzed the 5 kb proximal upstream regulatory region of the preferentially dysregulated genes in each separate chamber. I discovered a number of potential transcriptional co-regulators of MEF2A. Additionally, certain co-regulator candidates were shown to display chamber-specific expression patterns coinciding with their transcription factor module prediction. Namely, I discovered that estrogen receptor β, NKX2.5, and HAND factors can modulate the transcriptional activity of MEF2A. These observations suggest that interactions between MEF2A and distinct transcriptional co-regulators further modulate and fine-tune the expression of downstream cardiac gene programs and cellular processes in cardiac chambers.

In Chapter Four I describe the *Bex1* gene as a new target gene of MEF2A. BEX1 has been shown to be involved in the cell cycle and neurotrophin signaling through its interaction with the p75 neurotrophin receptor (p75-NTR). I show that *Bex1* transcript expression overlaps with *Mef2* expression patterns in cardiac and skeletal muscle as well as in the brain. I show that proximal and distal upstream regulatory sequences of the *Bex1* gene contain computationally predicted MEF2 binding sites. The proximal binding site is conserved across many mammalian species, while the non-conserved distal site in the mouse genome shows greater transcriptional activation in reporter assays. I demonstrate that MEF2A is able to activate transcription on reporter constructs *in vitro* using these two predicted MEF2 sites, and to occupy regions of chromatin harboring the aforementioned MEF2 enhancer sites *in vivo*.

5.2 Future Perspectives

5.2.1 Assembling the MEF2A-specfic cardiac transcriptome

Cardiac morphogenesis involves a precisely controlled network of transcriptional regulatory factors for proper chamber development. In addition to the considerable number of proteins in this network, genetic redundancy and interdependent interactions between many of these regulatory factors adds an extra layer of complexity when attempting to characterize functional roles for each transcription factor. My findings demonstrate that MEF2A in the adult heart cooperates with transcriptional co-regulators to modulate the expression of downstream genes and suggests that MEF2A has chamber-dependent roles in the adult heart. Since temporal and spatial expression patterns of regulatory factors change during and after cardiogenesis, these observations suggest that MEF2A also has chamber-dependent roles in the developing heart that are different from those in the adult heart. Recent advances in sequencing technologies have allowed researchers to collect global genomic and transcriptomic datasets. Therefore, we are interested in establishing a comprehensive data set of MEF2A target genes in the cardiac transcriptome. This data set would allow us to further study other uncharacterized cellular pathways that are defective in developing *Mef2a* KO hearts.

To assemble an exhaustive list of MEF2A target genes in the heart, we would compare MEF2A ChIP-seq data with *Mef2a* knockout RNA-seq data. One way to perform this study is by expressing both MEF2A-Flag and MEF2A-GFP proteins in adult mice. In this manner, MEF2A homodimers comprised of one MEF2A-Flag and one MEF2A-GFP protein would functionally bind to target genes. Prepared chromatin can

then be subjected to a series of immunoprecipitations to enrich for MEF2A-homodimer bound chromatin. By immunoprecipitating chromatin using a GFP-specific antibody, and then repeating the immunoprecipitation using a Flag epitope-specific antibody, chromatin bound by MEF2A-homodimers can be obtained and used for ChIP-seq studies. With this sample set, we can probe the genome for MEF2A-homodimer bound chromatin. In a parallel assay, we would use deep sequencing techniques in *Mef2a* KO mice to identify MEF2A-sensitive genes. By combining the results of these two separate studies, we can determine the complete MEF2A-homodimer target gene set. The results from these data sets will allow us to determine which genes are targets of MEF2A to further study uncharacterized defective gene programs cellular processes in developing MEF2A KO hearts. These results will allow us to gain insight into some of the developmental processes in cardiac morphogenesis and the molecular mechanisms behind congenital heart diseases.

5.2.2 Characterizing chamber-specific transcriptional co-regulators of MEF2A in the heart

The complexities of gene regulatory networks, and the interactions between transcriptional regulatory factors make it difficult to obtain a global picture of these molecular processes. Understanding the regulatory interactions that MEF2A participates in would provide greater insight into how other transcription factors might be regulated and a better understanding of the transcriptional regulatory network in the heart.

From our bioinformatics promoter screen in Chapter Three, we primarily focused our efforts on validating estrogen receptors, NKX2.5, HAND factors as co-regulators of MEF2A transcriptional activity. These three candidates were the most appealing in our initial efforts because of their established expression patterns in the heart. It is possible that other MEF2A transcriptional co-regulators exist aside from the aforementioned proteins. To search for other MEF2A transcriptional co-regulators, the dataset from the coupled ChIP-seq/RNA-seq study described in section 5.2.1 can be used to determine the direct targets of MEF2A and which MEF2 enhancer sites are bound by MEF2A. With this comprehensive gene list, an extensive bioinformatics analysis can be performed to search for other potential transcriptional co-regulators. The co-regulator study in Chapter Three was limited to the 5,000 bp proximal upstream regulatory region of preferentially dysregulated genes between atria and ventricles. By analyzing a coupled ChIP-seq/RNA-seq dataset, we can identify other co-regulators of MEF2A in order to gain insight into cardiac gene regulation. The co-regulator study in Chapter Three was also performed in combined atrial and combined ventricular chambers. It is known that the transcriptome between left and right tissues of atrial and ventricular chambers are not identical, and left/right chamber differences are present in their respective gene expression signatures (Tabibiazar *et al.* 2003). A refined study using ChIP-seq/RNA-seq coupled techniques would reveal interesting results if left and right chambers were analyzed separately in the atria and ventricles of the heart. From the studies presented in this dissertation, we demonstrate drastic spatial differences in global regulation patterns between different tissues of the same organ.

5.2.3 The cardiac specific and MEF2A related role of BEX1 in the adult heart

While our lab has gained considerable information regarding the transcriptional regulation of *Bex1* by MEF2A cardiomyocytes, much still remains to be characterized. Recently, neurotrophins and their receptors have been shown to be essential in heart development, and mice lacking p75-NTR display reduced cardiac parasympathetic innervation (Caporali & Emanueli 2009, Habecker *et al.* 2008). As a small adaptor protein of p75-NTR, it is important to understand the role *Bex1* has in cardiomyocytes. The BEX1 protein has been implicated in both neurotrophin signaling and the cell cycle (Vilar *et al.* 2006). These observations point to a role for MEF2A in neurotrophin signaling and the cell cycle in ventricular cardiomyocytes. It would be interesting to confirm a preferential dysregulation of downstream neurotrophin-dependent cellular processes and cell cycle components in ventricular chambers compared to atria.

Since little information is known about *Bex1* and its role in the heart, it would be interesting to characterize the MEF2A-related role of *Bex1* in the adult heart. *Bex1* KO mice appear to develop normally with skeletal muscle regeneration defects following intramuscular injection of cardiotoxin (Koo *et al.* 2007). These mice can be used to study the role of *Bex1* in cardiomyocytes, possibly following prolonged cardiac stress or acute injury to the heart. Another way to approach this study is to characterize global transcriptomic differences between MEF2A-knockdown NRVMs and MEF2A-knockdown NRVMs overexpressing BEX1. Knockdown of MEF2A in NRVMs would lead to *Bex1* downregulation and lead to dysregulation of downstream neurotrophin

signaling-related cellular processes. By overexpressing *Bex1* in MEF2A-deficient NRVMs, we would observe attenuation of pathways and processes dependent on MEF2A-BEX1 signaling. Additionally, it is interesting to note the lack of a conserved distal MEF2 enhancer in the upstream regulatory region of the human *Bex1* gene. Lack of this enhancer in the human *Bex1* upstream regulatory region would suggest that *Bex1* expression levels in humans compared to mice are controlled by different transcriptional regulatory mechanisms to maintain cellular processes downstream of BEX1 in the heart. By uncovering pathways and cellular processes attenuated by BEX1 overexpression, we can determine the role of BEX1 in the context of MEF2A.

5.2.4 Chamber-dependent regulation of *Bex1* spatial expression in the heart

It is interesting to note that *Bex1* mRNA levels are similar between atrial and ventricular chambers in wild-type mice, yet *Bex1* levels are not affected in KO atria and *Bex1* is one of the most dysregulated genes in KO ventricles, downregulated by 2.1-fold compared to WT levels. This observation reinforces that MEF2A interacts with transcriptional co-regulators to modulate the expression of target genes in different chambers of the heart. In Chapter Three, *Bex1* was part of the subset of genes that was preferentially dysregulated in *Mef2a* KO ventricles displaying no preferential enrichment in wild-type tissues. Through several *in silico* and *in vitro* analysis, we confirm that MEF2A and NKX2.5 cooperatively interact to regulate the transcription of target genes. However, NKX2.5 may not be the only transcriptional co-regulator interacting with MEF2A to fine-tune the expression of *Bex1* in the heart.

A detailed characterization of *Bex1* transcriptional regulatory elements responsive to transcription factors and co-regulators expressed in the heart would provide a better understanding of *Bex1* regulation in the heart. Additionally, by gaining knowledge of *Bex1* regulation, we can deepen our understanding of the mechanisms behind cardiac chamber differences.

5.3 Conclusion

The experiments proposed in this chapter will allow us to gain a greater understanding of global transcriptional regulatory differences between different chambers and cell types in the heart. Understanding the mechanisms behind uncharacterized defective pathways and cellular processes in various heart disease models will give greater insight into new avenues for treating various forms of cardiovascular disease. By doing so, we will be able to develop and advance existing therapies in treating congenital heart defects.

APPENDIX

A.1 Tables from microarray analysis

Complete microarray dataset in "log-base-2" format is available on NCBI (GEO accession GSE95364). Microarray gene expression comparisons in Table A.1.1, Table A.1.2, and Table A.1.3 have been converted to fold-change values (*i.e.*, upregulation is greater than 1.0, and downregulation is less than -1.0). Genes that were validated by qPCR in Section 3.3 are colored below: **red** for genes preferentially dysregulated in MEF2A KO atria, **blue** for genes preferentially dysregulated in MEF2A KO ventricles, and **purple** for genes dysregulated in MEF2A KO atria and ventricles.

A.1.1 Table of genes dysregulated in KO atria

A.1.1.1 Genes enriched in WT atrial chambers

Gene Number	Symbol	Description	KOA/ WTA Fold	KOV/ WTV Fold	KOA/ KOV Fold	WTA/ WTV Fold
381489	Rxfp1	relaxin/insulin-like family peptide receptor 1	-7.07	-1.15	1.10	6.75
57349	Ppbp	pro-platelet basic protein	-4.36	-1.03	1.35	5.73
19220	Ptgfr	prostaglandin F receptor	-4.05	-1.21	2.17	7.28
74513	Neto2	neuropilin (NRP) and tolloid (TLL)-like 2	-3.56	-1.35	-1.08	2.45
18166	Npy1r	neuropeptide Y receptor Y1	-3.34	-1.11	7.02	21.1
13106	Cyp2e1	cytochrome P450, family 2, subfamily e, polypeptide 1	-3.29	1.06	1.03	3.60
20360	Sema6c	sema domain, transmembrane domain (TM), and cytoplasmic domain, (semaphorin) 6C	-2.90	-1.13	1.51	3.88
64011	Nrgn	neurogranin	-2.46	1.09	-1.05	2.55
12797	Cnn1	calponin 1	-2.44	-1.01	2.30	5.55
64214	Rgs18	regulator of G-protein signaling 18	-2.40	-1.02	-1.08	2.17
19337	Rab33a	RAB33A, member of RAS oncogene family	-2.38	1.20	3.17	9.04
11484	Aspa	aspartoacylase	-2.24	-1.42	1.31	2.07
71703	Armcx3	armadillo repeat containing, X-linked 3	-2.11	-1.24	1.53	2.60
19088	Prkar2b	protein kinase, cAMP dependent regulatory, type II beta	-2.11	1.16	1.22	2.99

71724	Aox3	aldehyde oxidase 3	-2.11	-1.06	2.70	5.40
241263	Gpr158	G protein-coupled receptor 158	-2.03	1.20	1.70	4.15
235106	Ntm	neurotrimin	-2.00	-1.20	1.64	2.73
21743	Inmt	indolethylamine N-methyltransferase	-2.00	1.06	3.45	7.33
14658	Glrb	glycine receptor, beta subunit	-1.97	-1.03	1.77	3.39
246317	Neto1	neuropilin (NRP) and tolloid (TLL)-like 1	-1.95	-1.25	1.49	2.32
20249	Scd1	stearoyl-Coenzyme A desaturase 1	-1.90	-1.16	2.20	3.62
57262	Retnla	resistin like alpha	-1.89	-1.35	1.47	2.06
664883	Nova1	neuro-oncological ventral antigen 1	-1.88	-1.06	1.60	2.85
654812	Angptl7	angiopoietin-like 7	-1.85	1.11	1.23	2.52
50908	C1s	complement component 1, s subcomponent	-1.85	1.09	1.16	2.33
73748	Gadl1	glutamate decarboxylase-like 1	-1.79	-1.06	5.49	9.30
246104	Rhbdl3	rhomboid, veinlet-like 3 (Drosophila)	-1.78	-1.37	1.78	2.31
244198	Olfml1	olfactomedin-like 1	-1.76	-1.11	1.30	2.06
74071	Ifltd1	intermediate filament tail domain containing 1	-1.73	1.21	13.5	28.2
54612	Sfrp5	secreted frizzled-related sequence protein 5	-1.71	-1.04	1.75	2.87
16000	Igf1	insulin-like growth factor 1	-1.70	-1.14	1.40	2.09
73086	Rps6ka5	ribosomal protein S6 kinase, polypeptide 5	-1.69	-1.10	1.96	3.01
13008	Csrp2	cysteine and glycine-rich protein 2	-1.67	-1.26	2.72	3.62
76829	Dok5	docking protein 5	-1.66	-1.02	1.76	2.88
14579	Gem	GTP binding protein (gene overexpressed in skeletal muscle)	-1.64	1.11	1.31	2.39
23967	Osr1	odd-skipped related 1 (Drosophila)	-1.64	-1.27	4.38	5.64
54635	Pdgfc	platelet-derived growth factor, C polypeptide	-1.64	-1.26	3.70	4.80
18124	Nr4a3	nuclear receptor subfamily 4, group A, member 3	-1.63	1.09	2.00	3.54
20563	Slit2	slit homolog 2 (Drosophila)	-1.62	-1.16	1.54	2.14
13865	Nr2f1	nuclear receptor subfamily 2, group F, member 1	-1.61	-1.14	1.79	2.55
15370	Nr4a1	nuclear receptor subfamily 4, group A, member 1	-1.61	-1.05	1.79	2.74
21957	Tnnt3	troponin T3, skeletal, fast	-1.58	1.13	1.14	2.03
19888	Rp1	retinitis pigmentosa 1 (human)	-1.57	-1.34	4.49	5.27
56277	Tmem45a	transmembrane protein 45a	-1.56	-1.27	1.95	2.39
217430	Pqlc3	PQ loop repeat containing	-1.55	-1.12	1.51	2.08
19225	Ptgs2	prostaglandin-endoperoxide synthase 2	-1.55	-1.09	2.13	3.05
14396	Gabra3	gamma-aminobutyric acid (GABA) A receptor, subunit alpha 3	-1.55	1.09	2.32	3.90
18595	Pdgfra	platelet derived growth factor receptor, alpha polypeptide	-1.55	-1.16	1.52	2.02

76453	Prss23	protease, serine, 23	-1.54	1.02	1.55	2.44
56429	Dpt	dermatopontin	-1.54	-1.12	1.75	2.41
73732	Muc16	mucin 16	-1.53	-1.02	2.93	4.42
240058	Cpne5	copine V	-1.52	-1.12	7.95	10.8
13487	Slc26a3	solute carrier family 26, member 3	-1.52	-1.00	2.85	4.30
218294	Cdc14b	CDC14 cell division cycle 14 homolog B (S. cerevisiae)	-1.52	-1.07	1.48	2.10
17751	Mt3	metallothionein 3	1.54	1.31	2.47	2.10
240638	Slc16a12	solute carrier family 16 (monocarboxylic acid transporters), member 12	1.55	1.20	3.08	2.39
66438	Hamp2	hepcidin antimicrobial peptide 2	1.56	1.18	4.37	3.30
546161	Fbxw18	F-box and WD-40 domain protein 18	1.59	1.15	28.3	20.4
77836	Mlana	melan-A	1.60	1.14	24.2	17.2
71233	Enkur	enkurin, TRPC channel interacting protein	1.63	1.07	3.27	2.14
320981	Enpp6	ectonucleotide pyrophosphatase/phosphodiesterase 6	1.65	1.34	4.94	4.01
74438	Clvs1	clavesin 1	1.71	-1.12	4.51	2.36
382105	Fbxw15	F-box and WD-40 domain protein 15	1.71	-1.07	9.69	5.27
24050	40789	septin 3	1.82	1.06	5.64	3.27
170738	Kcnh7	potassium voltage-gated channel, subfamily H (eag-related), member 7	1.89	-1.07	9.24	4.58
12160	Bmp5	bone morphogenetic protein 5	2.03	1.20	9.03	5.35
56808	Cacna2d2	calcium channel, voltage-dependent, alpha 2/delta subunit 2	2.21	1.03	16.8	7.87
26950	Vsnl1	visinin-like 1	2.50	1.27	18.2	9.24

A.1.1.2 Genes enriched in WT ventricular chambers

Gene Number	Symbol	Description	KOA/ WTA Fold	KOV/ WTV Fold	KOA/ KOV Fold	WTA/ WTV Fold
68016	Murc	muscle-related coiled-coil protein	-3.57	-1.12	-9.13	-2.86
11607	Agtr1a	angiotensin II receptor, type 1a	-2.12	-1.05	-5.53	-2.75
78910	Asb15	ankyrin repeat and SOCS box-containing 15	-1.67	-1.03	-5.47	-3.39
76294	Asb5	ankyrin repeat and SOCs box-containing 5	-1.56	-1.16	-5.05	-3.75
68854	Asb11	ankyrin repeat and SOCS box-containing 11	-1.56	-1.21	-2.69	-2.09
71007	D7Ertd443e	DNA segment, Chr 7, ERATO Doi 443, expressed	1.51	1.34	-2.27	-2.55
16373	Irx3	Iroquois related homeobox 3 (Drosophila)	1.52	-1.25	-1.10	-2.11
11475	Acta2	actin, alpha 2, smooth muscle, aorta	1.53	1.29	-2.04	-2.42

72088	Ush1c	Usher syndrome 1C homolog (human)	1.53	1.03	-1.83	-2.73
353211	Prune2	prune homolog 2 (Drosophila)	1.57	1.10	-2.35	-3.36
213989	Tmem82	transmembrane protein 82	1.57	-1.15	-1.62	-2.92
17137	Magea1	melanoma antigen, family A, 1	1.57	-1.22	-1.17	-2.25
55987	Cpxm2	carboxypeptidase X 2 (M14 family)	1.58	1.07	-2.31	-3.40
258154	Olfr1029	olfactory receptor 1029	1.58	-1.09	-1.62	-2.80
17762	Mapt	microtubule-associated protein tau	1.63	1.09	-2.12	-3.17
16509	Kcne1	potassium voltage-gated channel, Isk-related subfamily, member 1	1.75	-1.03	-2.49	-4.46
67149	Nkain1	Na+/K+ transporting ATPase interacting 1	1.82	1.07	-2.12	-3.62
17329	Cxcl9	chemokine (C-X-C motif) ligand 9	1.96	1.46	-2.05	-2.75
380863	Tmem171	transmembrane protein 171	2.00	1.12	-1.47	-2.60
73010	Gpr22	G protein-coupled receptor 22	2.02	1.09	-2.96	-5.48
19215	Ptgds	prostaglandin D2 synthase (brain)	2.98	1.19	-1.47	-3.69
338417	Scgb1c1	secretoglobin, family 1C, member 1	3.18	-1.18	1.03	-3.62

A.1.1.3 No enrichment in either WT atria or ventricles

Gene Number	Symbol	Description	KOA/ WTA Fold	KOV/ WTV Fold	KOA/ KOV Fold	WTA/ WTV Fold
231086	Hadhb	hydroxyacyl-Coenzyme A dehydrogenase/3-ketoacyl-Coenzyme A thiolase/enoyl-Coenzyme A hydratase (trifunctional protein), beta subunit	-3.35	1.00	-6.32	-1.88
15951	Ifi204	interferon activated gene 204	-3.07	-1.31	-1.79	1.30
353208	Zfp931	zinc finger protein 931	-2.88	1.42	-6.28	-1.54
353374	Snord61	small nucleolar RNA, C/D box 61	-2.79	-1.28	-2.40	-1.10
20383	Srsf3	serine/arginine-rich splicing factor 3	-2.71	1.14	-2.09	1.48
18619	Penk	preproenkephalin	-2.53	-1.20	-1.56	1.35
72397	Rbm12b	RNA binding motif protein 12B	-2.51	1.08	-1.67	1.62
73710	Tubb2b	tubulin, beta 2B	-2.48	-1.06	-1.41	1.67
15289	Hmgb1	high mobility group box 1	-2.44	1.04	-2.45	1.03
12340	Capza1	capping protein (actin filament) muscle Z-line, alpha 1	-2.43	1.23	-2.77	1.08
27210	Snord34	small nucleolar RNA, C/D box 34	-2.42	-1.08	-1.31	1.72
621893	Hist2h2ab	histone cluster 2, H2ab	-2.41	1.09	-2.37	1.11
76022	Gon4l	gon-4-like (C.elegans)	-2.34	-1.20	-1.89	1.03
80828	Snord82	small nucleolar RNA, C/D box 82	-2.29	-1.14	-1.41	1.43
66167	Ccdc72	coiled-coil domain containing 72	-2.26	-1.01	-1.97	1.14
226695	Ifi205	interferon activated gene 205	-2.16	-1.13	-1.43	1.34
382245	Tmem29	transmembrane protein 29	-2.13	1.05	-1.62	1.38
57264	Retn	resistin	-2.10	-1.09	-1.08	1.79
69837	Pcgf1	polycomb group ring finger 1	-2.00	-1.10	-1.40	1.29

73738	Haus7	HAUS augmin-like complex, subunit 7	-1.98	-1.28	-1.94	-1.25
20259	Scin	scinderin	-1.97	-1.43	-1.60	-1.16
319636	Fsd1l	fibronectin type III and SPRY domain containing 1-like	-1.96	-1.04	-3.51	-1.87
68219	Nudt21	nudix (nucleoside diphosphate linked moiety X)-type motif 21	-1.93	1.43	-2.07	1.33
16404	**Itga7**	**integrin alpha 7**	**-1.92**	**-1.18**	**-2.68**	**-1.65**
225825	Cd226	CD226 antigen	-1.91	-1.13	-1.22	1.38
234736	Rfwd3	ring finger and WD repeat domain 3	-1.90	-1.43	-1.48	-1.11
26874	Abcd2	ATP-binding cassette, sub-family D (ALD), member 2	-1.89	-1.35	-1.63	-1.16
20091	Rps3a	ribosomal protein S3A	-1.89	-1.06	-1.44	1.24
494519	Abpd	androgen binding protein delta	-1.87	-1.31	1.01	1.44
223696	Tomm22	translocase of outer mitochondrial membrane 22 homolog (yeast)	-1.86	-1.08	-2.17	-1.26
667118	Zbed6	zinc finger, BED domain containing 6	-1.85	1.02	-1.45	1.30
545938	Zfp607	zinc finger proten 607	-1.84	1.06	-2.09	-1.07
170938	Zfp617	zinc finger protein 617	-1.84	-1.03	-2.02	-1.13
72560	Naalad2	N-acetylated alpha-linked acidic dipeptidase 2	-1.83	-1.08	-1.09	1.54
24001	Tiam2	T-cell lymphoma invasion and metastasis 2	-1.83	-1.08	-1.08	1.57
381067	Zfp229	zinc finger protein	-1.80	-1.13	-1.72	-1.08
17022	Lum	lumican	-1.79	-1.03	1.12	1.93
14455	Gas5	growth arrest specific 5	-1.79	-1.09	-1.27	1.28
20720	Serpine2	serine (or cysteine) peptidase inhibitor, clade E, member 2	-1.78	-1.13	1.22	1.92
21402	Skp1a	S-phase kinase-associated protein 1A	-1.75	1.06	-1.72	1.08
65103	Arl6ip6	ADP-ribosylation factor-like 6 interacting protein 6	-1.75	1.03	-1.70	1.06
27209	Snord32a	small nucleolar RNA, C/D box 32A	-1.74	-1.14	-1.19	1.28
244923	Klhl31	kelch-like 31 (Drosophila)	-1.73	-1.13	-2.57	-1.69
56077	Dgke	diacylglycerol kinase, epsilon	-1.72	-1.20	-1.56	-1.09
16518	Kcnj2	potassium inwardly-rectifying channel, subfamily J, member 2	-1.72	-1.23	-1.90	-1.36
214048	Larp1b	La ribonucleoprotein domain family, member 1B	-1.71	-1.02	-2.57	-1.53
16500	Kcnb1	potassium voltage gated channel, Shab-related subfamily, member 1	-1.71	-1.09	-2.63	-1.67
13136	Cd55	CD55 antigen	-1.70	-1.22	1.20	1.68
67771	Arpc5	actin related protein 2/3 complex, subunit 5	-1.70	1.06	-1.52	1.18
18263	Odc1	ornithine decarboxylase, structural 1	-1.70	1.09	-2.55	-1.38
234911	Mmp27	matrix metallopeptidase 27	-1.69	-1.39	1.30	1.58
75458	Cklf	chemokine-like factor	-1.69	-1.23	1.37	1.88

16948	Lox	lysyl oxidase	-1.69	-1.36	-1.07	1.16
407800	Ecm2	extracellular matrix protein 2, female organ and adipocyte specific	-1.69	-1.19	-1.01	1.41
66190	Acer3	alkaline ceramidase 3	-1.69	-1.18	-1.14	1.26
271005	Klhdc1	kelch domain containing 1	-1.69	-1.38	-2.11	-1.72
14727	Gp49a	glycoprotein 49 A	-1.69	-1.50	-1.47	-1.31
30926	Glrx3	glutaredoxin 3	-1.68	1.04	-2.57	-1.47
78506	Efha2	EF-hand domain family, member A2	-1.67	1.05	-1.79	-1.02
20229	Sat1	spermidine/spermine N1-acetyl transferase 1	-1.67	-1.05	-1.04	1.54
15129	Hbb-b1	hemoglobin, beta adult major chain	-1.67	-1.06	-2.64	-1.67
17420	Mnat1	menage a trois 1	-1.67	-1.03	-1.58	1.03
67148	Fam103a1	family with sequence similarity 103, member A1	-1.67	-1.16	-1.25	1.15
66222	Serpinb1a	serine (or cysteine) peptidase inhibitor, clade B, member 1a	-1.66	-1.26	-1.27	1.05
245902	Ccdc15	coiled-coil domain containing 15	-1.66	-1.10	-1.27	1.19
11450	Adipoq	adiponectin, C1Q and collagen domain containing	-1.66	-1.08	-1.11	1.38
21808	Tgfb2	transforming growth factor, beta 2	-1.66	1.06	-1.15	1.53
17181	Matn2	matrilin 2	-1.66	1.04	1.11	1.93
14299	Ncs1	neuronal calcium sensor 1	-1.65	-1.24	-1.32	1.00
209558	Enpp3	ectonucleotide pyrophosphatase/phosphodiesterase 3	-1.65	-1.23	1.42	1.91
628438	Hspe1-rs1	heat shock protein 1 (chaperonin 10), related sequence 1	-1.64	-1.11	-1.71	-1.16
67733	Itgb3bp	integrin beta 3 binding protein (beta3-endonexin)	-1.64	-1.01	-1.36	1.18
75316	Taf1d	TATA box binding protein (Tbp)-associated factor, RNA polymerase I, D	-1.64	-1.21	-1.34	1.00
79560	Ublcp1	ubiquitin-like domain containing CTD phosphatase 1	-1.63	-1.16	-1.62	-1.15
50720	Sacs	sacsin	-1.63	-1.11	-2.08	-1.41
12212	Chic1	cysteine-rich hydrophobic domain 1	-1.62	1.12	-1.11	1.64
12589	Ift81	intraflagellar transport 81 homolog (Chlamydomonas)	-1.62	-1.16	-1.66	-1.19
214804	Syde2	synapse defective 1, Rho GTPase, homolog 2 (C. elegans)	-1.62	-1.34	1.33	1.61
16420	Itgb6	integrin beta 6	-1.61	-1.42	-1.86	-1.64
18933	Prrx1	paired related homeobox 1	-1.61	-1.23	-2.18	-1.67
226548	Aph1a	anterior pharynx defective 1a homolog (C. elegans)	-1.61	1.24	-1.46	1.37
70676	Gulp1	GULP, engulfment adaptor PTB domain containing 1	-1.61	-1.17	-1.3	1.05

66488	Fam136a	family with sequence similarity 136, member A	-1.60	1.15	-2.98	-1.60
107476	Acaca	acetyl-Coenzyme A carboxylase alpha	-1.60	1.12	1.00	1.81
142687	Asb14	ankyrin repeat and SOCS box-containing 14	-1.60	-1.43	-2.15	-1.91
19258	Ptpn4	protein tyrosine phosphatase, non-receptor type 4	-1.60	-1.13	-1.80	-1.26
93761	Smarca1	SWI/SNF related, matrix associated, actin dependent regulator of chromatin, subfamily a, member 1	-1.60	-1.17	1.01	1.39
258571	Olfr1033	olfactory receptor 1033	-1.6	-1.28	-1.93	-1.54
242735	Lrrc38	leucine rich repeat containing 38	-1.59	-1.10	1.00	1.45
66573	Dzip1	DAZ interacting protein 1	-1.59	-1.07	1.10	1.64
234344	Naf1	nuclear assembly factor 1 homolog (S. cerevisiae)	-1.59	-1.09	-1.10	1.31
224585	Zfp160	zinc finger protein 160	-1.59	1.11	-1.22	1.44
383619	Aim2	absent in melanoma 2	-1.59	-1.26	-1.3	-1.03
18669	Abcb1b	ATP-binding cassette, sub-family B (MDR/TAP), member 1B	-1.59	-1.09	-1.15	1.26
26399	Map2k6	mitogen-activated protein kinase kinase 6	-1.59	-1.28	1.25	1.55
83964	Jam3	junction adhesion molecule 3	-1.58	-1.19	1.32	1.75
381236	Lipo1	lipase, member O1	-1.58	-1.11	-1.04	1.35
66789	Alg14	asparagine-linked glycosylation 14 homolog (yeast)	-1.58	-1.03	-1.17	1.31
64050	Yeats4	YEATS domain containing 4	-1.58	-1.09	-1.64	-1.14
67010	Rbm7	RNA binding motif protein 7	-1.57	-1.00	-1.43	1.1
245026	Col6a6	collagen, type VI, alpha 6	-1.57	-1.11	1.02	1.45
252966	Cables2	CDK5 and Abl enzyme substrate 2	-1.57	1.01	-1.82	-1.14
74600	Mrpl47	mitochondrial ribosomal protein L47	-1.56	-1.09	-2.35	-1.63
66799	Ube2w	ubiquitin-conjugating enzyme E2W (putative)	-1.56	1.06	-1.41	1.17
240067	Zfp952	zinc finger protein 952	-1.56	1.03	-1.56	1.03
67115	Rpl14	ribosomal protein L14	-1.56	-1.27	-1.34	-1.09
213056	Fam126b	family with sequence similarity 126, member B	-1.56	1.14	-1.99	-1.11
13684	Eif4e	eukaryotic translation initiation factor 4E	-1.56	1.02	-2.04	-1.27
109676	Ank2	ankyrin 2, brain	-1.56	-1.10	-1.91	-1.36
21898	Tlr4	toll-like receptor 4	-1.56	1.01	-2.60	-1.64
14677	Gnai1	guanine nucleotide binding protein (G protein), alpha inhibiting 1	-1.56	-1.06	1.20	1.76
75894	Adal	adenosine deaminase-like	-1.56	-1.10	-1.4	1.01
449630	Snord15a	small nucleolar RNA, C/D box 15A	-1.55	-1.20	-1.45	-1.12
66205	Cd302	CD302 antigen	-1.55	-1.19	1.17	1.54
227485	Cdh19	cadherin 19, type 2	-1.55	-1.38	1.02	1.15

66341	Eid3	EP300 interacting inhibitor of differentiation 3	-1.55	-1.03	-1.30	1.15
170823	Glmn	glomulin, FKBP associated protein	-1.55	-1.14	-1.27	1.06
74385	Mudeng	MU-2/AP1M2 domain containing, death-inducing	-1.55	-1.04	-1.33	1.10
27207	Rps11	ribosomal protein S11	-1.54	-1.06	-1.23	1.17
56334	Tmed2	transmembrane emp24 domain trafficking protein 2	-1.54	-1.13	-1.07	1.26
18148	Npm1	nucleophosmin 1	-1.54	-1.08	-1.32	1.07
16341	Eif3e	eukaryotic translation initiation factor 3, subunit E	-1.54	1.06	-1.62	1.01
258668	Olfr823	olfactory receptor 823	-1.54	1.46	-1.30	1.72
14173	Fgf2	fibroblast growth factor 2	-1.53	-1.06	1.06	1.53
213068	Tmem71	transmembrane protein 71	-1.53	-1.13	-1.94	-1.44
381831	Igkv4-58	immunoglobulin kappa variable 4-58	-1.53	1.44	-1.60	1.38
244713	Zfp317	zinc finger protein 317	-1.53	-1.08	-1.32	1.05
56050	Cyp39a1	cytochrome P450, family 39, subfamily a, polypeptide 1	-1.53	-1.22	-1.07	1.15
233276	Tubgcp5	tubulin, gamma complex associated protein 5	-1.53	-1.13	-1.16	1.14
408067	Zfp874b	zinc finger protein 874b	-1.52	-1.03	-1.37	1.07
14105	Srsf10	serine/arginine-rich splicing factor 10	-1.52	-1.17	-1.27	1.01
16329	Inpp1	inositol polyphosphate-1-phosphatase	-1.52	-1.17	-1.69	-1.30
93737	Pard6g	par-6 partitioning defective 6 homolog gamma (C. elegans)	-1.52	-1.10	1.10	1.52
76915	Mnd1	meiotic nuclear divisions 1 homolog (S. cerevisiae)	-1.52	1.26	-1.22	1.57
434423	Dppa5a	developmental pluripotency associated 5A	-1.52	1.04	-1.30	1.22
20230	Satb1	special AT-rich sequence binding protein 1	-1.52	-1.19	-1.40	-1.10
330323	Fam188b	family with sequence similarity 188, member B	-1.52	1.02	1.11	1.73
20688	Sp4	trans-acting transcription factor 4	-1.52	-1.11	-1.13	1.20
228003	Kbtbd10	kelch repeat and BTB (POZ) domain containing 10	-1.51	-1.40	1.00	1.08
21780	Tfam	transcription factor A, mitochondrial	-1.51	1.01	-2.13	-1.38
13823	Epb4.1l3	erythrocyte protein band 4.1-like 3	-1.51	-1.17	1.43	1.84
229780	Ccdc76	coiled-coil domain containing 76	-1.51	1.07	-1.45	1.11
241568	Lrrc4c	leucine rich repeat containing 4C	-1.51	-1.07	-1.06	1.32
66254	Dimt1	DIM1 dimethyladenosine transferase 1-like (S. cerevisiae)	-1.51	1.07	-1.43	1.13
66880	Rsrc1	arginine/serine-rich coiled-coil 1	-1.51	-1.08	-1.29	1.08
68526	Gpr155	G protein-coupled receptor 155	-1.50	-1.32	-1.14	-1.01
269132	Glt25d2	glycosyltransferase 25 domain containing 2	-1.50	-1.07	-1.57	-1.12

242050	Igsf10	immunoglobulin superfamily, member 10	-1.50	-1.14	1.16	1.53
15109	Hal	histidine ammonia lyase	-1.50	-1.27	1.03	1.21
17084	Ly86	lymphocyte antigen 86	-1.50	-1.04	-1.05	1.37
18491	Pappa	pregnancy-associated plasma protein A	-1.50	-1.24	1.49	1.80
140483	Hnmt	histamine N-methyltransferase	-1.50	-1.30	1.27	1.46
104943	Fam110c	family with sequence similarity 110, member C	-1.50	-1.08	1.14	1.58
436583	Snora74a	small nucleolar RNA, H/ACA box 74A	-1.50	-1.27	-1.23	-1.04
226182	Taf5	TAF5 RNA polymerase II, TATA box binding protein (TBP)-associated factor	-1.50	-1.17	-1.19	1.06
72504	Taf4b	TAF4B RNA polymerase II, TATA box binding protein (TBP)-associated factor	-1.50	-1.07	-1.76	-1.26
56078	Car5b	carbonic anhydrase 5b, mitochondrial	-1.50	1.18	-1.27	1.39
21953	Tnni2	troponin I, skeletal, fast 2	-1.50	-1.15	1.10	1.43
15426	Hoxc8	homeobox C8	1.50	1.07	1.17	-1.19
114889	Vsx1	visual system homeobox 1 homolog (zebrafish)	1.50	-1.04	1.40	-1.11
54651	Usp27x	ubiquitin specific peptidase 27, X chromosome	1.50	-1.07	1.57	-1.02
258377	Olfr654	olfactory receptor 654	1.50	-1.03	1.47	-1.05
14086	Fscn1	fascin homolog 1, actin bundling protein (Strongylocentrotus purpuratus)	1.50	1.18	-1.16	-1.47
68509	Ptx4	pentraxin 4	1.50	1.07	1.44	1.02
18588	Pde6g	phosphodiesterase 6G, cGMP-specific, rod, gamma	1.50	-1.23	1.60	-1.16
545817	Cyp2w1	cytochrome P450, family 2, subfamily w, polypeptide 1	1.50	-1.03	1.46	-1.06
56811	Dkk2	dickkopf homolog 2 (Xenopus laevis)	1.50	-1.08	1.34	-1.21
269356	Slc4a11	solute carrier family 4, sodium bicarbonate transporter-like, member 11	1.50	-1.09	1.27	-1.29
625823	Vmn1r1	vomeronasal 1 receptor 1	1.50	-1.08	1.50	-1.08
56365	Clcnkb	chloride channel Kb	1.50	1.10	1.18	-1.15
14773	Grk5	G protein-coupled receptor kinase 5	1.51	1.47	-1.03	-1.06
244550	Podnl1	podocan-like 1	1.51	1.17	1.37	1.06
259172	Mfrp	membrane-type frizzled-related protein	1.51	-1.01	1.63	1.06
15486	Hsd17b2	hydroxysteroid (17-beta) dehydrogenase 2	1.51	-1.09	2.05	1.23
170761	Pdzd3	PDZ domain containing 3	1.51	1.04	1.06	-1.35
69638	Enho	energy homeostasis associated	1.51	-1.17	1.71	-1.04
18261	Ocm	oncomodulin	1.51	1.28	1.10	-1.07

235582	Glyctk	glycerate kinase	1.51	1.06	1.43	1.01
16198	Il9	interleukin 9	1.51	-1.12	1.57	-1.08
108114	Slc22a7	solute carrier family 22 (organic anion transporter), member 7	1.51	1.01	1.66	1.11
18787	Serpine1	serine (or cysteine) peptidase inhibitor, clade E, member 1	1.51	1.43	-1.32	-1.40
12534	Cdk1	cyclin-dependent kinase 1	1.51	-1.04	1.06	-1.48
258833	Olfr1132	olfactory receptor 1132	1.51	-1.00	1.28	-1.17
243090	BC051076	cDNA sequence BC051076	1.51	-1.08	1.36	-1.20
22773	Zic3	zinc finger protein of the cerebellum 3	1.51	-1.19	1.39	-1.29
235628	Prss42	protease, serine, 42	1.51	-1.02	1.40	-1.09
66727	Hrasls5	HRAS-like suppressor family, member 5	1.51	-1.22	1.61	-1.14
70274	Ly6g6e	lymphocyte antigen 6 complex, locus G6E	1.51	1.04	1.33	-1.08
69655	Cd164l2	CD164 sialomucin-like 2	1.51	-1.21	1.60	-1.14
16668	Krt18	keratin 18	1.51	-1.08	2.34	1.41
14580	Gfap	glial fibrillary acidic protein	1.52	-1.09	1.36	-1.21
245865	Spag4	sperm associated antigen 4	1.52	1.05	1.30	-1.09
235044	BC018242	cDNA sequence BC018242	1.52	1.14	1.04	-1.27
626299	Vmn1r194	vomeronasal 1 receptor 194	1.52	1.22	1.15	-1.08
18292	Sebox	SEBOX homeobox	1.52	-1.24	1.41	-1.33
19094	Mapk11	mitogen-activated protein kinase 11	1.52	-1.01	-1.07	-1.66
57442	Kcne3	potassium voltage-gated channel, Isk-related subfamily, gene 3	1.52	1.00	1.24	-1.21
80986	Ckap2	cytoskeleton associated protein 2	1.53	-1.00	1.10	-1.39
11425	Apoc4	apolipoprotein C-IV	1.53	1.01	1.37	-1.09
667441	Trav3-1	T cell receptor alpha variable 3-1	1.53	1.15	1.68	1.27
70571	Tcerg1l	transcription elongation regulator 1-like	1.53	1.09	1.28	-1.08
18332	Olfr33	olfactory receptor 33	1.53	-1.02	1.30	-1.19
13446	Doc2a	double C2, alpha	1.53	1.03	1.46	-1.01
110785	Iglc1	immunoglobulin lambda constant 1	1.53	1.44	1.03	-1.03
12209	Brs3	bombesin-like receptor 3	1.53	-1.09	1.56	-1.07
20505	Slc34a1	solute carrier family 34 (sodium phosphate), member 1	1.53	-1.12	1.46	-1.18
20204	Prrx2	paired related homeobox 2	1.53	-1.15	2.88	1.62
20211	Saa4	serum amyloid A 4	1.53	1.11	1.22	-1.12
271424	Ip6k3	inositol hexaphosphate kinase 3	1.54	-1.23	-1.00	-1.90
73259	Cib4	calcium and integrin binding family member 4	1.54	-1.02	1.37	-1.14
21414	Tcf7	transcription factor 7, T-cell specific	1.54	1.10	1.53	1.10
277978	Exoc3l	exocyst complex component 3-like	1.54	1.13	1.26	-1.07
69564	Itgb1bp3	integrin beta 1 binding protein 3	1.54	1.12	2.54	1.85

11488	Adam11	a disintegrin and metallopeptidase domain 11	1.54	-1.11	2.32	1.34
72040	Cdhr5	cadherin-related family member 5	1.54	1.15	1.23	-1.08
21960	Tnr	tenascin R	1.54	1.21	1.30	1.02
212937	Tifab	TRAF-interacting protein with forkhead-associated domain, family member B	1.54	-1.02	1.14	-1.38
20871	Aurkc	aurora kinase C	1.54	1.08	1.20	-1.18
11989	Slc7a3	solute carrier family 7 (cationic amino acid transporter, y+ system), member 3	1.54	1.32	1.33	1.14
69219	Ddah1	dimethylarginine dimethylaminohydrolase 1	1.54	1.37	-1.53	-1.72
12563	Cdh6	cadherin 6	1.54	1.48	-1.20	-1.25
104080	Nxph4	neurexophilin 4	1.55	1.03	1.34	-1.11
16005	Igfals	insulin-like growth factor binding protein, acid labile subunit	1.55	1.26	-1.34	-1.65
280635	Emilin3	elastin microfibril interfacer 3	1.55	1.05	1.25	-1.16
12518	Cd79a	CD79A antigen (immunoglobulin-associated alpha)	1.55	1.06	1.21	-1.20
71664	Mettl7b	methyltransferase like 7B	1.55	-1.08	1.44	-1.16
654821	Gcnt7	glucosaminyl (N-acetyl) transferase family member 7	1.55	1.05	1.33	-1.10
224840	Treml4	triggering receptor expressed on myeloid cells-like 4	1.55	1.02	1.30	-1.16
234700	Nrn1l	neuritin 1-like	1.55	-1.06	1.59	-1.03
18329	Olfr30	olfactory receptor 30	1.55	-1.10	1.61	-1.05
258303	Olfr518	olfactory receptor 518	1.55	-1.00	1.41	-1.10
14562	Gdf3	growth differentiation factor 3	1.55	-1.10	1.51	-1.12
170828	Vgll1	vestigial like 1 homolog (Drosophila)	1.55	-1.14	1.51	-1.18
74673	Spdyb	speedy homolog B (Xenopus laevis)	1.55	-1.09	1.18	-1.44
21405	Hnf1a	HNF1 homeobox A	1.55	1.08	1.42	-1.00
18349	Olfr5	olfactory receptor 5	1.56	-1.00	1.42	-1.10
258423	Olfr1510	olfactory receptor 1510	1.56	-1.03	1.55	-1.03
11470	Actl7a	actin-like 7a	1.56	-1.08	1.53	-1.10
16560	Kif1a	kinesin family member 1A	1.56	1.00	2.48	1.60
259116	Olfr559	olfactory receptor 559	1.56	-1.23	1.32	-1.45
18781	Pla2g2c	phospholipase A2, group IIC	1.56	1.18	1.36	1.03
74488	Lrrc15	leucine rich repeat containing 15	1.56	1.16	-1.01	-1.36
69539	Trnp1	TMF1-regulated nuclear protein 1	1.57	1.11	1.62	1.15
19039	Lgals3bp	lectin, galactoside-binding, soluble, 3 binding protein	1.57	1.16	1.12	-1.20
20389	Sftpc	surfactant associated protein C	1.57	-1.25	1.60	-1.23
14766	Gpr56	G protein-coupled receptor 56	1.57	1.05	-1.13	-1.69
620235	Siglec15	sialic acid binding Ig-like lectin 15	1.57	-1.02	1.49	-1.07
78088	Ankrd56	ankyrin repeat domain 56	1.57	1.00	1.57	1.00
210673	Prrt3	proline-rich transmembrane protein 3	1.57	-1.16	1.25	-1.45
54419	Cldn6	claudin 6	1.57	1.02	1.43	-1.07

328699	Gabrr3	gamma-aminobutyric acid (GABA) receptor, rho 3	1.57	1.00	1.29	-1.21
12684	Cideb	cell death-inducing DNA fragmentation factor, alpha subunit-like effector B	1.58	1.34	1.43	1.21
330890	Piwil4	piwi-like homolog 4 (Drosophila)	1.58	1.29	1.48	1.21
11925	Neurog3	neurogenin 3	1.58	1.02	1.60	1.03
630294	H2-t9	MHC class Ib T9	1.58	1.44	1.67	1.52
11872	Art2b	ADP-ribosyltransferase 2b	1.58	1.00	1.35	-1.17
114712	Ferd3l	Fer3-like (Drosophila)	1.58	1.05	1.37	-1.09
21853	Timeless	timeless homolog (Drosophila)	1.58	1.14	1.06	-1.30
67874	Rprm	reprimo, TP53 dependent G2 arrest mediator candidate	1.58	1.08	1.40	-1.04
77531	Anks1b	ankyrin repeat and sterile alpha motif domain containing 1B	1.58	1.07	1.16	-1.26
259111	Olfr974	olfactory receptor 974	1.58	-1.05	1.34	-1.24
114640	Pth2	parathyroid hormone 2	1.59	1.06	1.60	1.07
76527	Il34	interleukin 34	1.59	-1.11	1.06	-1.67
94179	Krt23	keratin 23	1.59	1.11	1.36	-1.04
13088	Cyp2b10	cytochrome P450, family 2, subfamily b, polypeptide 10	1.59	-1.11	2.20	1.24
14990	H2-M2	histocompatibility 2, M region locus 2	1.59	1.00	1.71	1.07
13392	Dlx2	distal-less homeobox 2	1.59	1.01	1.33	-1.17
258309	Olfr657	olfactory receptor 657	1.59	-1.33	1.33	-1.60
17144	Magea8	melanoma antigen, family A, 8	1.59	-1.08	1.52	-1.14
257932	Olfr332	olfactory receptor 332	1.59	1.16	1.37	1.00
280621	BC089491	cDNA sequence BC089491	1.59	1.42	1.36	1.21
14068	F7	coagulation factor VII	1.59	-1.30	1.55	-1.34
625530	Dub3	deubiquitinating enzyme 3	1.60	-1.29	1.62	-1.27
72269	Cda	cytidine deaminase	1.60	1.15	1.53	1.11
23966	Odz4	odd Oz/ten-m homolog 4 (Drosophila)	1.60	1.05	1.19	-1.26
17386	Mmp13	matrix metallopeptidase 13	1.60	1.10	1.04	-1.39
546648	Klhdc7b	kelch domain containing 7B	1.60	-1.07	1.44	-1.19
106014	Fam19a5	family with sequence similarity 19, member A5	1.60	1.12	1.08	-1.32
104245	Slc6a5	solute carrier family 6 (neurotransmitter transporter, glycine), member 5	1.61	1.05	1.26	-1.20
56293	Amac1	acyl-malonyl condensing enzyme 1	1.61	1.19	1.28	-1.05
620105	Igkv1-35	immunoglobulin kappa chain variable 1-35	1.61	-1.13	1.54	-1.17
11838	Arc	activity regulated cytoskeletal-associated protein	1.61	1.43	1.25	1.11
73340	Nptxr	neuronal pentraxin receptor	1.61	1.01	1.25	-1.26
231821	Adap1	ArfGAP with dual PH domains 1	1.61	-1.02	1.92	1.15
319217	Vmn2r7	vomeronasal 2, receptor 7	1.61	1.10	1.30	-1.12

22784	Slc30a3	solute carrier family 30 (zinc transporter), member 3	1.62	-1.02	1.47	-1.12
271711	Tmem169	transmembrane protein 169	1.63	-1.24	1.66	-1.22
211027	Trav3-4	T cell receptor alpha variable 3-4	1.63	1.49	1.63	1.49
109332	Cdcp1	CUB domain containing protein 1	1.63	-1.43	3.34	1.43
140806	Il25	interleukin 25	1.63	1.21	1.10	-1.22
20344	Selp	selectin, platelet	1.63	1.33	1.40	1.14
11648	Akp3	alkaline phosphatase 3, intestine, not Mn requiring	1.63	1.22	1.18	-1.12
16517	Kcnj16	potassium inwardly-rectifying channel, subfamily J, member 16	1.63	-1.15	1.59	-1.19
230579	Fam151a	family with sequence simliarity 151, member A	1.63	1.07	1.30	-1.16
235416	Lman1l	lectin, mannose-binding 1 like	1.63	1.13	1.38	-1.04
15376	Foxa2	forkhead box A2	1.64	1.03	1.19	-1.33
213765	BC125332	cDNA sequence BC125332	1.65	-1.10	1.60	-1.14
12143	Blk	B lymphoid kinase	1.65	1.18	1.17	-1.19
226781	Slc30a10	solute carrier family 30, member 10	1.65	1.07	1.10	-1.39
225471	Ticam2	toll-like receptor adaptor molecule 2	1.65	1.08	1.31	-1.15
106407	Osta	organic solute transporter alpha	1.66	1.14	1.40	-1.03
272382	Spib	Spi-B transcription factor (Spi-1/PU.1 related)	1.66	1.08	1.40	-1.10
330863	Trim67	tripartite motif-containing 67	1.66	-1.09	2.57	1.41
71562	Afmid	arylformamidase	1.66	1.36	1.81	1.48
404316	Olfr403	olfactory receptor 403	1.66	1.13	1.18	-1.23
258087	Olfr963	olfactory receptor 963	1.67	-1.09	1.30	-1.40
667550	Igkv10-94	immunoglobulin kappa variable 10-94	1.67	1.23	1.47	1.09
226180	Ina	internexin neuronal intermediate filament protein, alpha	1.67	-1.07	1.57	-1.14
320631	Abca15	ATP-binding cassette, sub-family A (ABC1), member 15	1.67	1.15	1.39	-1.04
209176	Ido2	indoleamine 2,3-dioxygenase 2	1.68	1.00	1.30	-1.28
432576	Tmem95	transmembrane protein 95	1.68	1.11	1.38	-1.09
72185	Dbndd1	dysbindin (dystrobrevin binding protein 1) domain containing 1	1.68	-1.12	1.43	-1.31
17231	Mcpt8	mast cell protease 8	1.68	1.23	1.38	1.00
69902	Mrto4	MRT4, mRNA turnover 4, homolog (S. cerevisiae)	1.69	1.48	-1.43	-1.62
668257	Dgat2l6	diacylglycerol O-acyltransferase 2-like 6	1.69	-1.16	1.54	-1.26
231290	Slc10a4	solute carrier family 10 (sodium/bile acid cotransporter family), member 4	1.70	1.09	-1.02	-1.59
11658	Alcam	activated leukocyte cell adhesion molecule	1.70	1.12	2.62	1.73
21877	Tk1	thymidine kinase 1	1.70	-1.06	1.72	-1.05

243755	Slc13a4	solute carrier family 13 (sodium/sulfate symporters), member 4	1.70	1.09	2.01	1.28
16016	Ighg2b	immunoglobulin heavy constant gamma 2B	1.71	-1.16	2.14	1.07
19373	Rag1	recombination activating gene 1	1.71	-1.09	1.56	-1.19
17285	Meox1	mesenchyme homeobox 1	1.71	1.27	-1.02	-1.39
18125	Nos1	nitric oxide synthase 1, neuronal	1.71	1.08	1.45	-1.08
107993	Bfsp2	beaded filament structural protein 2, phakinin	1.72	-1.05	2.01	1.11
258985	Olfr1256	olfactory receptor 1256	1.72	1.21	1.22	-1.16
258383	Olfr1347	olfactory receptor 1347	1.72	-1.29	2.05	-1.08
18072	Nhlh2	nescient helix loop helix 2	1.72	1.05	1.13	-1.44
12709	Ckb	creatine kinase, brain	1.73	1.46	1.27	1.08
94215	Ugt2a1	UDP glucuronosyltransferase 2 family, polypeptide A1	1.73	-1.07	1.78	-1.04
193034	Trpv1	transient receptor potential cation channel, subfamily V, member 1	1.74	1.10	1.33	-1.18
83380	Prp2	proline rich protein 2	1.75	-1.04	1.60	-1.13
434484	Sp140	Sp140 nuclear body protein	1.75	-1.19	1.55	-1.34
258541	Olfr800	olfactory receptor 800	1.75	-1.18	1.90	-1.09
434017	Vmn1r20	vomeronasal 1 receptor 20	1.76	-1.09	-1.01	-1.96
404336	Olfr1380	olfactory receptor 1380	1.76	1.18	1.67	1.12
269019	Stk32a	serine/threonine kinase 32A	1.76	-1.11	2.45	1.24
20965	Syn2	synapsin II	1.77	-1.03	3.24	1.76
11688	Alox8	arachidonate 8-lipoxygenase	1.77	-1.07	2.33	1.22
14408	Gabrr1	gamma-aminobutyric acid (GABA) C receptor, subunit rho 1	1.78	-1.03	1.99	1.08
66120	Fkbp11	FK506 binding protein 11	1.78	1.20	2.17	1.45
380702	**Shisa6**	**shisa homolog 6 (Xenopus laevis)**	**1.79**	**-1.14**	**2.23**	**1.08**
54150	Rdh7	retinol dehydrogenase 7	1.80	-1.18	1.64	-1.30
229302	Tm4sf4	transmembrane 4 superfamily member 4	1.81	1.22	1.55	1.05
71970	Scand3	SCAN domain containing 3	1.82	-1.10	1.75	-1.15
330581	Vmn2r69	vomeronasal 2, receptor 69	1.83	-1.19	1.42	-1.53
15965	Ifna2	interferon alpha 2	1.83	1.25	1.18	-1.23
258525	Olfr1170	olfactory receptor 1170	1.84	1.17	1.07	-1.46
18346	Olfr47	olfactory receptor 47	1.84	-1.00	1.31	-1.41
233870	Tufm	Tu translation elongation factor, mitochondrial	1.84	1.10	2.14	1.28
387132	Ssxb2	synovial sarcoma, X member B, breakpoint 2	1.85	1.03	1.22	-1.45
17116	Mab21l1	mab-21-like 1 (C. elegans)	1.85	-1.11	1.65	-1.24
16017	Ighg1	immunoglobulin heavy constant gamma 1 (G1m marker)	1.85	1.09	1.77	1.04
232345	A2m	alpha-2-macroglobulin	1.86	1.09	2.60	1.52
14065	F2rl3	coagulation factor II (thrombin) receptor-like 3	1.86	-1.14	1.63	-1.29
20301	Ccl27a	chemokine (C-C motif) ligand 27A	1.86	-1.33	1.49	-1.67

74091	Npl	N-acetylneuraminate pyruvate lyase	1.87	-1.00	1.96	1.04
53610	Nono	non-POU-domain-containing, octamer binding protein	1.87	-1.16	1.38	-1.57
16007	Cyr61	cysteine rich protein 61	1.87	1.33	1.49	1.06
14407	Gabrg3	gamma-aminobutyric acid (GABA) A receptor, subunit gamma 3	1.87	1.31	1.18	-1.20
23882	Gadd45g	growth arrest and DNA-damage-inducible 45 gamma	1.87	1.31	1.98	1.39
59069	Tpm3	tropomyosin 3, gamma	1.88	1.01	1.26	-1.46
14816	Grm1	glutamate receptor, metabotropic 1	1.88	1.24	-1.26	-1.92
213649	**Arhgef19**	**Rho guanine nucleotide exchange factor (GEF) 19**	**1.90**	**1.39**	**1.16**	**-1.17**
258156	Olfr605	olfactory receptor 605	1.95	1.06	1.23	-1.48
71733	Susd2	sushi domain containing 2	1.96	1.08	3.45	1.90
58243	Nap1l5	nucleosome assembly protein 1-like 5	1.96	1.18	2.70	1.62
69121	**Chrdl2**	**chordin-like 2**	**1.99**	**1.04**	**2.34**	**1.22**
16616	Klk1b21	kallikrein 1-related peptidase b21	2.01	-1.32	1.68	-1.57
74267	Iqcf1	IQ motif containing F1	2.01	1.19	1.72	1.02
64293	Stk32b	serine/threonine kinase 32B	2.01	1.29	2.95	1.89
636752	Igkv4-62	immunoglobulin kappa variable 4-62	2.02	1.00	1.42	-1.41
625131	Vmn2r87	vomeronasal 2, receptor 87	2.02	-1.01	1.54	-1.33
66373	Lsm5	LSM5 homolog, U6 small nuclear RNA associated (S. cerevisiae)	2.02	-1.14	1.56	-1.48
15018	H2-Q7	histocompatibility 2, Q region locus 7	2.03	1.23	1.01	-1.62
16617	Klk1b24	kallikrein 1-related peptidase b24	2.09	1.07	1.36	-1.42
258315	Olfr767	olfactory receptor 767	2.14	1.17	2.13	1.17
636177	Rhox4f	reproductive homeobox 4F	2.20	-1.20	3.02	1.13
320452	P4ha3	procollagen-proline, 2-oxoglutarate 4-dioxygenase (proline 4-hydroxylase), alpha polypeptide III	2.22	-1.11	4.09	1.64
404737	Igl-J1	immunoglobulin lambda chain, joining region 1	2.26	1.17	1.14	-1.68
100038947	LOC100038947	signal-regulatory protein beta 1-like	2.26	-1.13	1.91	-1.34
237221	Gemin8	gem (nuclear organelle) associated protein 8	2.27	1.34	1.89	1.12
19131	Prh1	proline rich protein HaeIII subfamily 1	2.32	1.06	1.35	-1.62
268697	Ccnb1	cyclin B1	2.44	1.49	1.44	-1.13
258737	Olfr1316	olfactory receptor 1316	2.46	-1.07	1.34	-1.95
209195	**Clic6**	**chloride intracellular channel 6**	**2.83**	**1.14**	**3.60**	**1.46**
19051	Gsbs	G substrate	5.10	-1.24	9.25	1.45

A.1.2 Tables of genes dysregulated in KO ventricles

A.1.2.1 Enriched in WT atrial chambers

Gene Number	Symbol	Description	KOA/ WTA Fold	KOV/ WTV Fold	KOA/ KOV Fold	WTA/ WTV Fold
329502	Pla2g4e	phospholipase A2, group IVE	-1.43	-1.94	4.13	3.05
66402	Sln	sarcolipin	-1.03	-1.81	123.70	70.90
216616	Efemp1	epidermal growth factor-containing fibulin-like extracellular matrix protein 1	-1.23	-1.62	4.25	3.23
239618	Pdzrn4	PDZ domain containing RING finger 4	-1.37	-1.61	4.43	3.78
22228	Ucp2	uncoupling protein 2 (mitochondrial, proton carrier)	1.06	1.51	2.59	3.68
20250	Scd2	stearoyl-Coenzyme A desaturase 2	1.04	1.53	1.52	2.23
14190	Fgl2	fibrinogen-like protein 2	1.01	1.55	1.36	2.08
18162	Npr3	natriuretic peptide receptor 3	1.12	1.60	4.66	6.68
77674	Defb12	defensin beta 12	-1.11	1.62	1.15	2.06
23836	Cdh20	cadherin 20	1.37	1.66	2.39	2.89
245578	Pcdh11x	protocadherin 11 X-linked	-1.12	1.71	1.17	2.23
13024	Ctla2a	cytotoxic T lymphocyte-associated protein 2 alpha	-1.50	1.71	1.35	3.47
18260	Ocln	occludin	-1.03	1.77	1.82	3.33
14187	Akr1b8	aldo-keto reductase family 1, member B8	-1.10	1.77	1.33	2.60
72535	Aldh1b1	aldehyde dehydrogenase 1 family, member B1	-1.03	2.00	1.79	3.67
238447	Igh-2	immunoglobulin heavy chain 2 (serum IgA)	-1.07	2.01	1.36	2.95
18576	Pde3b	phosphodiesterase 3B, cGMP-inhibited	1.27	2.08	1.32	2.16
22004	Tpm2	tropomyosin 2, beta	-1.12	2.78	2.45	7.63
545725	Mterf	mitochondrial transcription termination factor	-1.07	2.84	-1.22	2.48

A.1.2.2 Enriched in WT ventricular chambers

Gene Number	Symbol	Description	KOA/ WTA Fold	KOV/ WTV Fold	KOA/ KOV Fold	WTA/ WTV Fold
56839	Lgi1	leucine-rich repeat LGI family, member 1	-1.41	-10.8	-2.07	-15.8
26878	B3galt2	UDP-Gal:betaGlcNAc beta 1,3-galactosyltransferase, polypeptide 2	-1.14	-5.54	-2.10	-10.20
11459	Acta1	actin, alpha 1, skeletal muscle	-1.49	-3.54	-2.39	-5.65
214531	Tmprss13	transmembrane protease, serine 13	-1.29	-3.01	-1.34	-3.14
106869	Tnfaip8	tumor necrosis factor, alpha-induced protein 8	-1.21	-2.74	-1.73	-3.93

12477	Ctla4	cytotoxic T-lymphocyte-associated protein 4	1.01	-2.56	-1.11	-2.88
76884	Cyfip2	cytoplasmic FMR1 interacting protein 2	1.39	-2.55	-1.68	-5.98
233199	Mybpc2	myosin binding protein C, fast-type	-1.16	-2.04	-1.86	-3.28
20750	Spp1	secreted phosphoprotein 1	1.01	-1.99	-2.12	-4.29
18639	Pfkfb1	6-phosphofructo-2-kinase/fructose-2,6-biphosphatase 1	-1.45	-1.95	-2.84	-3.81
60440	Iigp1	interferon inducible GTPase 1	-1.03	-1.90	-3.11	-5.75
105387	Akr1c14	aldo-keto reductase family 1, member C14	-1.50	-1.88	-1.88	-2.36
24117	Wif1	Wnt inhibitory factor 1	1.03	-1.84	-1.67	-3.17
56508	Rapgef4	Rap guanine nucleotide exchange factor (GEF) 4	-1.05	-1.75	-1.75	-2.89
330953	Hcn4	hyperpolarization-activated, cyclic nucleotide-gated K+ 4	-1.03	-1.74	-1.30	-2.21
667597	BC023105	cDNA sequence BC023105	-1.25	-1.63	-4.16	-5.42
110595	Timp4	tissue inhibitor of metalloproteinase 4	-1.44	-1.60	-2.49	-2.76
57816	Tesc	tescalcin	1.44	-1.59	-3.88	-8.90
208618	Etl4	enhancer trap locus 4	-1.20	-1.57	-1.55	-2.04
626578	Gbp10	guanylate-binding protein 10	1.12	-1.53	-1.31	-2.24
80903	**Fgf16**	**fibroblast growth factor 16**	**1.04**	**-1.50**	**-6.08**	**-9.45**
15166	Hcn2	hyperpolarization-activated, cyclic nucleotide-gated K+ 2	1.27	1.56	-3.34	-2.71
258554	Olfr873	olfactory receptor 873	-1.02	1.57	-3.85	-2.41
16647	Kpna2	karyopherin (importin) alpha 2	-1.02	1.57	-3.29	-2.05
109019	Obfc2a	oligonucleotide/oligosaccharide-binding fold containing 2A	1.20	1.66	-3.91	-2.83
71911	Bdh1	3-hydroxybutyrate dehydrogenase, type 1	1.37	1.78	-10.70	-8.29
71889	Epn3	epsin 3	1.44	1.93	-3.72	-2.78
140781	Myh7	myosin, heavy polypeptide 7, cardiac muscle, beta	1.01	1.99	-4.35	-2.22
13195	Ddc	dopa decarboxylase	1.00	2.41	-5.38	-2.24

A.1.2.3 No enrichment in either WT atria or ventricles

Gene Number	Symbol	Description	KOA/ WTA Fold	KOV/ WTV Fold	KOA/ KOV Fold	WTA/ WTV Fold
66212	Sec61b	Sec61 beta subunit	-1.25	-2.39	1.11	-1.73
320225	Catsperg1	cation channel, sperm-associated, gamma 1	1.24	-2.38	2.42	-1.22
625109	Vmn2r86	vomeronasal 2, receptor 86	-1.35	-2.32	1.56	-1.10
19716	**Bex1**	**brain expressed gene 1**	**-1.46**	**-2.14**	**-1.08**	**-1.59**
245446	**Slitrk4**	**SLIT and NTRK-like family, member 4**	**-1.11**	**-2.14**	**-1.01**	**-1.94**

258276	Olfr960	olfactory receptor 960	1.03	-2.02	1.34	-1.55
320027	Fstl4	follistatin-like 4	1.10	-2.02	2.20	-1.01
667277	C1rb	complement component 1, r subcomponent B	1.22	-1.92	2.16	-1.08
241494	Zfp385b	zinc finger protein 385B	-1.26	-1.92	2.67	1.75
20616	Snap91	synaptosomal-associated protein 91	-1.04	-1.92	2.82	1.53
218038	Amph	amphiphysin	1.17	-1.85	1.16	-1.88
100041449	Cyp3a59	cytochrome P450, subfamily 3A, polypeptide 59	1.49	-1.81	1.47	-1.83
52882	Rgs7bp	regulator of G-protein signalling 7 binding protein	-1.12	-1.78	-1.04	-1.66
16142	Iglv1	immunoglobulin lambda variable 1	1.15	-1.78	1.17	-1.74
320581	Idi2	isopentenyl-diphosphate delta isomerase 2	1.39	-1.76	1.62	-1.52
547329	Trav16d-dv11	T cell receptor alpha variable 16D-DV11	1.26	-1.75	1.52	-1.45
208076	**Pknox2**	**Pbx/knotted 1 homeobox 2**	**-1.30**	**-1.70**	**1.15**	**-1.14**
108956	Apol7c	apolipoprotein L 7c	-1.13	-1.69	1.05	-1.42
233813	Vwa3a	von Willebrand factor A domain containing 3A	-1.05	-1.66	-1.01	-1.60
258334	Olfr1396	olfactory receptor 1396	-1.21	-1.65	-1.39	-1.90
243574	Kbtbd8	kelch repeat and BTB (POZ) domain containing 8	1.06	-1.63	1.04	-1.67
258216	Olfr1034	olfactory receptor 1034	1.20	-1.63	-1.02	-2.00
212996	Wbscr17	Williams-Beuren syndrome chromosome region 17 homolog (human)	-1.33	-1.63	-1.27	-1.56
385138	BC061237	cDNA sequence BC061237	-1.00	-1.61	1.34	-1.20
56546	Sec1	secretory blood group 1	1.25	-1.61	1.87	-1.08
257881	Olfr205	olfactory receptor 205	1.17	-1.61	1.13	-1.68
258769	Olfr508	olfactory receptor 508	1.08	-1.59	1.08	-1.59
217721	Mfsd7c	major facilitator superfamily domain containing 7C	-1.27	-1.59	1.09	-1.14
258008	Olfr1513	olfactory receptor 1513	-1.16	-1.59	1.46	1.06
16979	Lrrn1	leucine rich repeat protein 1, neuronal	1.20	-1.59	1.34	-1.43
13032	Ctsc	cathepsin C	-1.39	-1.58	1.73	1.52
13190	Dct	dopachrome tautomerase	1.22	-1.58	1.22	-1.58
20112	Rps6ka2	ribosomal protein S6 kinase, polypeptide 2	1.17	-1.57	1.60	-1.16
14664	Slc6a9	solute carrier family 6 (neurotransmitter transporter, glycine), member 9	-1.26	-1.57	2.14	1.72
208943	Myo5c	myosin VC	-1.09	-1.57	-1.16	-1.67
209268	Igsf1	immunoglobulin superfamily, member 1	-1.30	-1.57	1.01	-1.19

18020	Nfatc2ip	nuclear factor of activated T-cells, cytoplasmic, calcineurin-dependent 2 interacting protein	-1.17	-1.56	1.22	-1.09
192216	Tmem47	transmembrane protein 47	-1.11	-1.55	1.37	-1.02
331524	Xkrx	X Kell blood group precursor related X linked	-1.11	-1.54	1.08	-1.29
66101	Ppih	peptidyl prolyl isomerase H	1.27	-1.54	1.25	-1.57
76808	Rpl18a	ribosomal protein L18A	1.10	-1.54	1.72	1.01
93695	Gpnmb	glycoprotein (transmembrane) nmb	-1.46	-1.53	-1.29	-1.36
231238	Sel1l3	sel-1 suppressor of lin-12-like 3 (C. elegans)	1.01	-1.53	1.10	-1.40
14776	Gpx2	glutathione peroxidase 2	1.46	-1.53	1.71	-1.31
233274	Siglech	sialic acid binding Ig-like lectin H	-1.15	-1.53	1.15	-1.15
100040268	Olfr157	olfactory receptor 157	-1.09	-1.53	1.33	-1.05
234779	Plcg2	phospholipase C, gamma 2	-1.02	-1.52	-1.01	-1.50
217615	Ctage5	CTAGE family, member 5	-1.46	-1.52	-1.38	-1.44
21788	Tfpi	tissue factor pathway inhibitor	1.06	-1.52	2.20	1.36
22146	Tuba1c	tubulin, alpha 1C	-1.01	-1.51	1.23	-1.23
53945	Slc40a1	solute carrier family 40 (iron-regulated transporter), member 1	-1.04	-1.51	1.70	1.17
381777	Igkv1-110	immunoglobulin kappa chain variable 1-110	1.46	-1.51	1.15	-1.92
245670	Rragb	Ras-related GTP binding B	-1.12	-1.51	1.14	-1.19
17171	Mas1	MAS1 oncogene	1.10	-1.50	1.09	-1.51
218763	Lrrc3b	leucine rich repeat containing 3B	-1.24	-1.50	1.74	1.44
15382	Hnrnpa1	heterogeneous nuclear ribonucleoprotein A1	-1.22	-1.50	-1.21	-1.50
79201	Tnfrsf23	tumor necrosis factor receptor superfamily, member 23	1.06	1.51	-1.61	-1.13
258242	Olfr955	olfactory receptor 955	1.10	1.51	-1.27	1.09
56441	Nat6	N-acetyltransferase 6	1.01	1.52	-1.55	-1.03
547109	Trim43a	tripartite motif-containing 43A	-1.10	1.52	-1.27	1.32
17844	Mup5	major urinary protein 5	1.12	1.52	-1.38	-1.02
668923	Zfp442	zinc finger protein 442	1.09	1.52	-2.14	-1.53
230903	**Fbxo44**	**F-box protein 44**	**1.27**	**1.52**	**1.00**	**1.20**
17110	Lyz1	lysozyme 1	1.12	1.52	1.11	1.52
637898	Vmn2r60	vomeronasal 2, receptor 60	1.01	1.53	-1.20	1.26
16592	Fabp5	fatty acid binding protein 5, epidermal	1.21	1.53	1.47	1.86
12683	Cidea	cell death-inducing DNA fragmentation factor, alpha subunit-like effector A	1.22	1.53	-2.14	-1.70
240899	Lrrc52	leucine rich repeat containing 52	1.31	1.53	-2.16	-1.85
72599	Pdia5	protein disulfide isomerase associated 5	1.36	1.54	1.35	1.53
11520	Plin2	perilipin 2	1.13	1.55	-2.28	-1.66
192657	Ell2	elongation factor RNA polymerase II 2	-1.04	1.56	-1.93	-1.18

75829	Prame	preferentially expressed antigen in melanoma	1.34	1.56	-1.04	1.11
14645	Glul	glutamate-ammonia ligase (glutamine synthetase)	1.38	1.56	-1.83	-1.61
259032	Olfr1134	olfactory receptor 1134	1.18	1.57	-1.49	-1.12
272428	Acsm5	acyl-CoA synthetase medium-chain family member 5	1.29	1.58	-2.03	-1.66
258902	Olfr1220	olfactory receptor 1220	1.02	1.59	-1.43	1.08
83672	Sytl3	synaptotagmin-like 3	1.46	1.60	1.10	1.21
245526	Pgr15l	G protein-coupled receptor 15-like	1.11	1.60	-1.24	1.16
20471	Six1	sine oculis-related homeobox 1 homolog (Drosophila)	1.14	1.61	-1.58	-1.12
258201	Olfr538	olfactory receptor 538	1.01	1.61	-1.88	-1.18
215061	Trim50	tripartite motif-containing 50	1.42	1.61	-1.24	-1.09
434903	Mageb4	melanoma antigen, family B, 4	-1.05	1.61	-1.80	-1.06
100042921	Vmn2r51	vomeronasal 2, receptor 51	1.11	1.62	-1.39	1.04
620631	Ttc30a2	tetratricopeptide repeat domain 30A2	1.40	1.63	-1.56	-1.35
20425	Shmt1	serine hydroxymethyltransferase 1 (soluble)	1.25	1.63	-1.91	-1.46
23960	Oas1g	2'-5' oligoadenylate synthetase 1G	-1.06	1.64	-1.96	-1.12
320705	Bend6	BEN domain containing 6	1.26	1.64	1.23	1.59
13646	Klk1b22	kallikrein 1-related peptidase b22	1.40	1.65	1.00	1.18
18367	Olfr66	olfactory receptor 66	-1.07	1.67	-1.26	1.42
382427	Best3	bestrophin 3	-1.16	1.69	-2.94	-1.49
17153	Mal	myelin and lymphocyte protein, T-cell differentiation protein	1.07	1.71	-1.50	1.05
11898	Ass1	argininosuccinate synthetase 1	1.28	1.73	-1.00	1.33
258550	Olfr869	olfactory receptor 869	-1.35	1.82	-4.64	-1.86
665255	Vmn2r28	vomeronasal 2, receptor 28	1.11	1.84	-1.67	-1.01
11833	Aqp8	aquaporin 8	1.16	1.85	-2.34	-1.47
554292	AB099516	cDNA sequence AB099516	-1.05	1.92	-1.80	1.12
235283	Gramd1b	GRAM domain containing 1B	-1.05	1.96	-3.58	-1.73
667666	Zfp600	zinc finger protein 600	1.06	1.98	-2.01	-1.08
626674	Olfr471	olfactory receptor 471	-1.23	2.03	-1.82	1.37
18775	Prl3d1	prolactin family 3, subfamily d, member 1	1.21	2.06	1.11	1.89
13587	Ear2	eosinophil-associated, ribonuclease A family, member 2	-1.18	2.07	-1.41	1.73
15586	Hyal1	hyaluronoglucosaminidase 1	1.03	2.09	-2.35	-1.15
620297	Trav6n-6	T cell receptor alpha variable 6N-6	1.34	2.14	-1.29	1.23
13180	Pcbd1	pterin 4 alpha carbinolamine dehydratase/dimerization cofactor of hepatocyte nuclear factor 1 alpha (TCF1) 1	1.29	2.45	-1.16	1.63
258602	Olfr150	olfactory receptor 150	-1.06	2.54	-2.04	1.32
228413	Prrg4	proline rich Gla (G-carboxyglutamic acid) 4 (transmembrane)	-1.12	3.11	-2.43	1.44

65969	Cubn	cubilin (intrinsic factor-cobalamin receptor)	1.11	3.41	-4.13	-1.34

A.1.3 Table of genes dysregulated in both chambers

A.1.3.1 Enriched in WT atria

Gene Number	Symbol	Description	KOA/ WTA Fold	KOV/ WTV Fold	KOA/ KOV Fold	WTA/ WTV Fold
17901	Myl1	myosin, light polypeptide 1	-13.60	-12.3	2.29	2.53
12350	Car3	carbonic anhydrase 3	-4.26	1.67	-1.98	3.58
51788	H2afz	H2A histone family, member Z	-4.01	-1.85	1.21	2.62
76376	Slc24a2	solute carrier family 24 (sodium/potassium/calcium exchanger), member 2	-3.02	-2.28	1.92	2.54
664608	Rhox4g	reproductive homeobox 4G	-2.14	1.61	-1.47	2.34
14169	**Fgf14**	**fibroblast growth factor 14**	**-2.00**	**-1.99**	**2.28**	**2.29**
24012	Rgs7	regulator of G protein signaling 7	-1.73	-1.88	7.41	6.82
216188	Aldh1l2	aldehyde dehydrogenase 1 family, member L2	-1.67	-1.55	2.38	2.57
67547	Slc39a8	solute carrier family 39 (metal ion transporter), member 8	1.54	1.51	8.04	7.87
14219	Ctgf	connective tissue growth factor	1.82	1.62	2.99	2.67

A.1.3.2 Enriched in WT ventricles

Gene Number	Symbol	Description	KOA/ WTA Fold	KOV/ WTV Fold	KOA/ KOV Fold	WTA/ WTV Fold
80978	Mrgprh	MAS-related GPR, member H	-4.29	-2.73	-3.17	-2.02
12372	Casq1	calsequestrin 1	-3.75	-6.78	-1.62	-2.93
18670	Abcb4	ATP-binding cassette, sub-family B (MDR/TAP), member 4	-2.10	-2.78	-1.81	-2.41
76886	Fam81a	family with sequence similarity 81, member A	-1.87	-4.37	-1.77	-4.14
620240	Igkv8-26	immunoglobulin kappa chain variable 8-26	-1.83	-3.69	-1.22	-2.47
20315	Cxcl12	chemokine (C-X-C motif) ligand 12	-1.57	-1.79	-1.82	-2.09
50874	Tmod4	tropomodulin 4	-1.53	-2.36	-1.30	-2.00
21835	Thrsp	thyroid hormone responsive SPOT14 homolog (Rattus)	1.50	3.56	-5.12	-2.16

A.1.3.3 No enrichment in either WT atria or ventricles

Gene Number	Symbol	Description	KOA/ WTA Fold	KOV/ WTV Fold	KOA/ KOV Fold	WTA/ WTV Fold
22187	Ubb	ubiquitin B	-4.74	1.58	-3.75	1.99

241431	Xirp2	xin actin-binding repeat containing 2	-4.73	-2.09	-4.45	-1.97
244867	**Arhgap20**	**Rho GTPase activating protein 20**	**-3.65**	**-3.23**	**-1.69**	**-1.49**
234854	Cdk10	cyclin-dependent kinase 10	-2.66	-1.70	-1.13	1.39
65255	**Asb4**	**ankyrin repeat and SOCS box-containing 4**	**-2.47**	**-2.03**	**-1.38**	**-1.13**
21665	Tdg	thymine DNA glycosylase	-2.28	1.51	-2.11	1.63
11431	Acp1	acid phosphatase 1, soluble	-2.18	-1.56	-1.31	1.07
353169	Slc2a12	solute carrier family 2 (facilitated glucose transporter), member 12	-2.01	-1.81	-1.10	1.01
232413	Clec12a	C-type lectin domain family 12, member a	-1.90	-1.78	-1.15	-1.07
60532	Wtap	Wilms' tumour 1-associating protein	-1.83	-1.61	-1.07	1.07
18583	**Pde7a**	**phosphodiesterase 7A**	**-1.78**	**-2.49**	**1.23**	**-1.14**
380614	Intu	inturned planar cell polarity effector homolog (Drosophila)	-1.73	-1.73	-1.48	-1.48
330812	Rnf150	ring finger protein 150	-1.70	-1.63	-1.11	-1.06
71738	Mamdc2	MAM domain containing 2	-1.68	-1.64	1.93	1.98
17996	Neb	nebulin	-1.53	-2.85	2.52	1.35
12116	Bhmt	betaine-homocysteine methyltransferase	1.51	-1.51	1.63	-1.41
74127	Krt80	keratin 80	1.52	1.70	-1.18	-1.06
11304	Abca4	ATP-binding cassette, sub-family A (ABC1), member 4	1.57	2.73	-2.77	-1.59
75668	Rasl10a	RAS-like, family 10, member A	1.58	1.66	-1.18	-1.12
105243	Slc9a3	solute carrier family 9 (sodium/hydrogen exchanger), member 3	1.62	3.00	-2.74	-1.48
14695	Gnb3	guanine nucleotide binding protein (G protein), beta 3	1.64	2.04	-2.23	-1.79
53622	Krt85	keratin 85	1.72	-1.52	1.92	-1.36
627132	Vmn2r93	vomeronasal 2, receptor 93	1.84	1.73	-1.22	-1.30
258329	Olfr135	olfactory receptor 135	1.92	2.34	-1.74	-1.43
17750	Mt2	metallothionein 2	1.96	2.36	1.13	1.35
20289	Scx	scleraxis	1.98	1.76	-1.70	-1.91
71310	Tbc1d9	TBC1 domain family, member 9	2.79	1.96	2.06	1.45
11829	**Aqp4**	**aquaporin 4**	**2.81**	**2.06**	**-1.41**	**-1.92**
72373	Psca	prostate stem cell antigen	8.41	2.72	4.65	1.50

A.2 Python script for gene info accession

“ExtractGeneInfo.py”

```
#Importation of tools
from xlrd import open_workbook
from tempfile import TemporaryFile
from xlwt import Workbook
import time
```

```
from Bio import Entrez

Entrez.email = "medrano@bu.edu"

#Open the workbook named FIMO.xls and summon first sheet
book = open_workbook('FIMOfile.xls')
sheet = book.sheet_by_index(0)

#Prime the new worksheet
newbook = Workbook()
newsheet1 = newbook.add_sheet('Sheet 1')

#To perform on all rows in FIMO.xls sheet
for i in range(sheet.nrows):

    Entrez.email = "medrano@bu.edu"

    #Assign variables
    genenum = int(sheet.cell_value(i,0))

    #Fetch genes from Entrez
    handle = Entrez.efetch(db="gene", id=genenum, rettype="gb", retmode="text")

    #Extract out information
    print(handle.read())

    #Begin to save variables into new worksheet
    handle = Entrez.efetch(db="gene", id=genenum, rettype="gb", retmode="text")
    newsheet1.write(i,0,genenum)
    newsheet1.write(i,1,handle.read())

    #Will repeat until done with all the rows of data
    time.sleep(1)
#Save the file
newbook.save('OUTPUTfile.xls')
newbook.save(TemporaryFile())
```

LIST OF JOURNAL ABBREVIATIONS

Acta Physiol	Acta Physiologica
Am J Physiol Hear Circ Physiol	American Journal of Physiology-Heart and Circulatory Physiology
Am J Physiol Physiol	American Journal of Physiology-Cell Physiology
Ann Anat	Annals of Anatomy
Ann N Y Acad Sci	Annals of the New York Academy of Sciences
Annu Rev Cell Dev Biol	Annual Review of Cell and Developmental Biology
Annu Rev Pathol Mech Dis	Annual Review of Pathology: Mechanisms of Disease
Auton Neurosci	Autonomic Neuroscience
Basic Res Cardiol	Basic Research in Cardiology
Biochem Biophys Res Commun	Biochemical and Biophysical Research Communications
Biochem Cell Biol	Biochemistry and cell biology
Can J Cardiol	Canadian Journal of Cardiology
Cardiovasc Res	Cardiovascular Research
Cell	Cell
Cell Stem Cell	Cell Stem Cell
Cell Mol Life Sci	Cellular and Molecular Life Sciences
Cell Physiol Biochem	Cellular Physiology and Biochemistry
Circ J	Circulation Journal

Circ Res	Circulation Research
Circulation	Circulation
Cold Spring Harb Perspect Biol	Cold Spring Harbor perspectives in biology
Curr Opin Cell Biol	Current Opinion in Cell Biology
Curr Probl Pediatr	Current Problems in Pediatrics
Curr Protoc Mol Biol	Current Protocols in Molecular Biology
Cytokine Growth Factor Rev	Cytokine and Growth Factor Reviews
Dev Biol	Developmental Biology
Dev Cell	Developmental Cell
Dev Dyn	Developmental Dynamics
Development	Development
EMBO J	EMBO Journal
Eur Heart J	European Heart Journal
Eur J Biochem	European Journal of Biochemistry
FASEB J	FASEB Journal
FEBS Lett	FEBS Letters
Gene	Gene
Genes Dev	Genes and Development
Genesis	Genesis
Genome Biol	Genome Biology
Int J Dev Biol	The International Journal of Developmental Biology

J Biol Chem	Journal of Biological Chemistry
J Cell Biol	Journal of Cell Biology
J Cell Sci	Journal of Cell Science
J Cell Biochem	Journal of Cellular Biochemistry
J Clin Invest	Journal of Clinical Investigation
J Mol Cell Cardiol	Journal of Molecular and Cellular Cardiology
J Mol Endocrinol	Journal of Molecular Endocrinology
J Neurosci	The Journal of Neuroscience
Mech Dev	Mechanisms of Development
Mol Brain Res	Molecular Brain Research
Mol Cell Biol	Molecular and Cellular Biology
Mol Cell Endocrinol	Molecular and Cellular Endocrinology
Nat Cell Biol	Nature Cell Biology
Nat Commun	Nature Communications
Nat Genet	Nature Genetics
Nat Protoc	Nature Protocols
Nat Rev Genet	Nature Reviews Genetics
Nature	Nature
Neurosci Lett	Neuroscience Letters
Oncogene	Oncogene
Oncol Rep	Oncology Reports
Pediatr Cardiol	Pediatric Cardiology

Pflugers Arch Eur J Physiol	Pflugers Archiv European Journal of Physiology
Pharmacol Ther	Pharmacology and Therapeutics
Philos Trans R Soc B Biol Sci	Philosophical Transactions of the Royal Society B: Biological Sciences
Physiol Genomics	Physiological Genomics
Physiol Rev	Physiological Reviews
PLoS Genet	PLoS Genetics
PLoS One	PLoS ONE
Proc Natl Acad Sci U S A	Proceedings of the National Academy of Sciences of the United States of America
Science	Science
Semin Cell Dev Biol	Seminars in Cell and Developmental Biology
Semin Fetal Neonatal Med	Seminars in Fetal and Neonatal Medicine
Stem Cells	Stem Cells
Trends Biochem Sci	Trends in Biochemical Sciences
Trends Cardiovasc Med	Trends in Cardiovascular Medicine
Trends Genet	Trends in Genetics

REFERENCES

Akazawa, H. & Komuro, I. (2005). Cardiac transcription factor Csx/Nkx2-5: Its role in cardiac development and diseases. *Pharmacol. Ther.* **107**(2): 252–68.

Alvarez, E., Zhou, W., Witta, S.E., & Freed, C.R. (2005). Characterization of the Bex gene family in humans, mice, and rats. *Gene* **357**(1): 18–28.

Angelelli, C., Magli, A., Ferrari, D., Ganassi, M., Matafora, V., Parise, F., Razzini, G., Bachi, A., Ferrari, S., & Molinari, S. (2008). Differentiation-dependent lysine 4 acetylation enhances MEF2C binding to DNA in skeletal muscle cells. *Nucleic Acids Res.* **36**(3): 915–28.

Barnes, R.M. & Firulli, A.B. (2009). A twist of insight - the role of Twist-family bHLH factors in development. *Int. J. Dev. Biol.* **53**(7): 909–24.

Barnes, R.M., Harris, I.S., Jaehnig, E.J., Sauls, K., Sinha, T., Rojas, A., Schachterle, W., McCulley, D.J., Norris, R.A., & Black, B.L. (2016). MEF2C regulates outflow tract alignment and transcriptional control of Tdgf1. *Development* **143**(5): 774–9.

Barth, A.S., Merk, S., Arnoldi, E., Zwermann, L., Kloos, P., Gebauer, M., Steinmeyer, K., Bleich, M., Kääb, S., Pfeufer, A., Überfuhr, P., Dugas, M., Steinbeck, G., & Nabauer, M. (2005). Functional profiling of human atrial and ventricular gene expression. *Pflugers Arch. Eur. J. Physiol.* **450**(4): 201–8.

Bartlett, H., Veenstra, G.J.C., & Weeks, D.L. (2010). Examining the cardiac NK-2 genes in early heart development. *Pediatr. Cardiol.* **31**(3): 335–41.

Bassel-Duby, R., Hernandez, M.D., Gonzalez, M.A., Krueger, J.K., & Williams, R.S. (1992). A 40-kilodalton protein binds specifically to an upstream sequence element essential for muscle-specific transcription of the human myoglobin promoter. *Mol. Cell. Biol.* **12**(11): 5024–32.

Belaguli, N.S., Schildmeyer, L.A., & Schwartz, R.J. (1997). Organization and myogenic restricted expression of the murine serum response factor gene. A role for autoregulation. *J. Biol. Chem.* **272**(29): 18222–31.

Bertos, N.R., Wang, A.H., & Yang, X.J. (2001). Class II histone deacetylases: structure, function, and regulation. *Biochem. Cell Biol.* **79**(3): 243–52.

Black, B.L., Ligon, K.L., Zhang, Y., & Olson, E.N. (1996). Cooperative transcriptional activation by the neurogenic basic helix- loop-helix protein MASH1 and members of the myocyte enhancer factor-2 (MEF2) family. *J. Biol. Chem.* **271**(43): 26659–63.

Black, B.L., Lu, J., & Olson, E.N. (1997). The MEF2A 3' untranslated region functions

as a cis-acting translational repressor. *Mol. Cell. Biol.* **17**(5): 2756–63.

Black, B.L., Martin, J.F., & Olson, E.N. (1995). The mouse MRF4 promoter is trans-activated directly and indirectly by muscle-specific transcription factors. *J. Biol. Chem.* **270**(7): 2889–92.

Black, B.L. & Olson, E.N. (1998). Transcriptional Control of Muscle Development By Myocyte Enhancer Factor-2 (Mef2) Proteins. *Annu. Rev. Cell Dev. Biol.* **14**:167-96.

Bruneau, B.G., Bao, Z.Z., Fatkin, D., Xavier-Neto, J., Georgakopoulos, D., Maguire, C.T., Berul, C.I., Kass, D. a, Kuroski-de Bold, M.L., de Bold, A.J., Conner, D. a, Rosenthal, N., Cepko, C.L., Seidman, C.E., & Seidman, J.G. (2001). Cardiomyopathy in Irx4-deficient mice is preceded by abnormal ventricular gene expression. *Mol. Cell. Biol.* **21**(5): 1730–6.

Bruneau, B.G., Nemer, G., Schmitt, J.P., Charron, F., Robitaille, L., Caron, S., Conner, D.A., Gessler, M., Nemer, M., Seidman, C.E., & Seidman, J.G. (2001). A murine model of Holt-Oram syndrome defines roles of the T-Box transcription factor Tbx5 in cardiogenesis and disease. *Cell* **106**(6): 709–21.

Buckingham, M., Meilhac, S., & Zaffran, S. (2005). Building the mammalian heart from two sources of myocardial cells. *Nat. Rev. Genet.* **6**(November): 826–35.

Cao, Q., Dong, P., Wang, Y., Zhang, J., Shi, X., & Wang, Y. (2015). MiR-218 suppresses cardiac myxoma proliferation by targeting myocyte enhancer factor 2D. *Oncol. Rep.* **33**(5): 2606–12.

Caporali, A. & Emanueli, C. (2009). Cardiovascular actions of neurotrophins. *Physiol. Rev.* **89**(1): 279–308.

Chang, S., Young, B.D., Li, S., Qi, X., Richardson, J.A., & Olson, E.N. (2006). Histone deacetylase 7 maintains vascular integrity by repressing matrix metalloproteinase 10. *Cell* **126**(2): 321–34.

Cheng, T.C., Wallace, M.C., Merlie, J.P., & Olson, E.N. (1993). Separable regulatory elements governing myogenin transcription in mouse embryogenesis. *Science* **261**(5118): 215–8.

Christoffels, V.M., Burch, J.B.E., & Moorman, A.F.M. (2004). Architectural plan for the heart: Early patterning and delineation of the chambers and the nodes. *Trends Cardiovasc. Med.* **14**(8): 301–7.

Clark, A.L. & Naya, F.J. (2015). MicroRNAs in the myocyte enhancer factor 2 (MEF2)-regulated Gtl2-Dio3 noncoding RNA locus promote cardiomyocyte proliferation by targeting the transcriptional coactivator Cited2. *J. Biol. Chem.* **290**(38): 23162–72.

Conway, S.J., Firulli, B., & Firulli, A.B. (2010). A bHLH code for cardiac morphogenesis. *Pediatr. Cardiol.* **31**(3): 318–24.

Cox, D.M., Du, M., Marback, M., Yang, E.C.C., Chan, J., Siu, K.W.M., & McDermott, J.C. (2003). Phosphorylation motifs regulating the stability and function of myocyte enhancer factor 2A. *J. Biol. Chem.* **278**(17): 15297–303.

Dechesne, C. a, Wei, Q., Eldridge, J., Gannoun-Zaki, L., Millasseau, P., Bougueleret, L., Caterina, D., & Paterson, B.M. (1994). E-box- and MEF-2-independent muscle-specific expression, positive autoregulation, and cross-activation of the chicken MyoD (CMD1) promoter reveal an indirect regulatory pathway. *Mol. Cell. Biol.* **14**(8): 5474–86.

DeLaughter, D.M., Bick, A.G., Wakimoto, H., McKean, D., Gorham, J.M., Kathiriya, I.S., Hinson, J.T., Homsy, J., Gray, J., Pu, W., Bruneau, B.G., Seidman, J.G., & Seidman, C.E. (2016). Single-cell resolution of temporal gene expression during heart development. *Dev. Cell* **39**(4): 480–90.

Desjardins, C.A. & Naya, F.J. (2017). Antagonistic regulation of cell-cycle and differentiation gene programs in neonatal cardiomyocytes by homologous MEF2 transcription factors. *J. Biol. Chem.* **292**(25): 10613–29.

Desjardins, C.A. & Naya, F.J. (2016). The function of the MEF2 family of transcription factors in cardiac development, cardiogenomics, and direct reprogramming. *J. Cardiovasc. Dev. Dis.* **3**(3): 1–23.

Dodou, E. & Treisman, R. (1997). The *Saccharomyces cerevisiae* MADS-box transcription factor Rlm1 is a target for the Mpk1 mitogen-activated protein kinase pathway. *Mol. Cell. Biol.* **17**(4): 1848–59.

Dodou, E., Verzi, M.P., Anderson, J.P., Xu, S.-M., & Black, B.L. (2004). Mef2c is a direct transcriptional target of ISL1 and GATA factors in the anterior heart field during mouse embryonic development. *Development* **131**(16): 3931–42.

Dodou, E., Xu, S.M., & Black, B.L. (2003). MEF2C is activated directly by myogenic basic Helix-Loop-Helix proteins during skeletal muscle development *in vivo*. *Mech. Dev.* **120**(9): 1021–32.

Dupays, L. & Mohun, T. (2016). Spatiotemporal regulation of enhancers during cardiogenesis. *Cell. Mol. Life Sci.* **74**(2): 1–9.

Durham, J.T., Brand, O.M., Arnold, M., Reynolds, J.G., Muthukumar, L., Weiler, H., Richardson, J.A., & Naya, F.J. (2006). Myospryn is a direct transcriptional target for MEF2A that encodes a striated muscle, α-actinin-interacting, costamere-localized protein. *J. Biol. Chem.* **281**(10): 6841–9.

Edmondson, D.G., Lyons, G.E., Martin, J.F., & Olson, E.N. (1994). Mef2 gene expression marks the cardiac and skeletal muscle lineages during mouse embryogenesis. *Development* **120**(5): 1251–63.

Estrella, N.L., Clark, A.L., Desjardins, C.A., Nocco, S.E., & Naya, F.J. (2015). MEF2D deficiency in neonatal cardiomyocytes triggers cell cycle re-entry and programmed cell death in vitro. *J. Biol. Chem.* **290**(40): 24367–80.

Estrella, N.L., Desjardins, C.A., Nocco, S.E., Clark, A.L., Maksimenko, Y., & Naya, F.J. (2015). MEF2 transcription factors regulate distinct gene programs in mammalian skeletal muscle differentiation. *J. Biol. Chem.* **290**(2): 1256–68.

Evans, S.M., Yelon, D., Conlon, F.L., & Kirby, M.L. (2010). Myocardial lineage development. *Circ. Res.* **107**(12): 1428–44.

Ewen, E.P., Snyder, C.M., Wilson, M., Desjardins, D., & Naya, F.J. (2011). The Mef2A transcription factor coordinately regulates a costamere gene program in cardiac muscle. *J. Biol. Chem.* **286**(34): 29644–53.

Feng, Y., Desjardins, C.A., Cooper, O., Kontor, A., Nocco, S.E., & Naya, F.J. (2015). EGR1 functions as a potent repressor of MEF2 transcriptional activity. *PLoS One* **10**(5): 1–14.

Firulli, A.B. (2003). A HANDful of questions: The molecular biology of the heart and neural crest derivatives (HAND)-subclass of basic helix-loop-helix transcription factors. *Gene* **312**(1–2): 27–40.

Firulli, A.B., McFadden, D.G., Lin, Q., Srivastava, D., & Olson, E.N. (1998). Heart and extra-embryonic mesodermal defects in mouse embryos lacking the bHLH transcription factor Hand1. *Nat. Genet.* **18**(3): 266–70.

Firulli, B.A., Hadzic, D.B., McDaid, J.R., & Firulli, A.B. (2000). The basic helix-loop-helix transcription factors dHAND and eHAND exhibit dimerization characteristics that suggest complex regulation of function*. *J. Biol. Chem.* **275**(43): 33567–73.

Firulli, B.A., McConville, D.P., Byers, J.S., Vincentz, J.W., Barnes, R.M., & Firulli, A.B. (2010). Analysis of a Hand1 hypomorphic allele reveals a critical threshold for embryonic viability. *Dev. Dyn.* **239**(10): 2748–60.

Franchini, K.G. (2012). Focal adhesion kinase - The basis of local hypertrophic signaling domains. *J. Mol. Cell. Cardiol.* **52**(2): 485–92.

Gage, P.J., Suh, H., & Camper, S.A. (1999). Dosage requirement of Pitx2 for development of multiple organs. *Development* **126**(20): 4643–51.

Gaspera, B. della, Armand, A.S., Sequeira, I., Lecolle, S., Gallien, C.L., Charbonnier, F., & Chanoine, C. (2009). The Xenopus MEF2 gene family: Evidence of a role for XMEF2C in larval tendon development. *Dev. Biol.* **328**(2): 392–402.

Gossett, L. a, Kelvin, D.J., Sternberg, E. a, & Olson, E.N. (1989). A new myocyte-specific enhancer-binding factor that recognizes a conserved element associated with multiple muscle-specific genes. *Mol. Cell. Biol.* **9**(11): 5022–33.

Grohé, C., Kahlert, S., Löbbert, K., Stimpel, M., Karas, R.H., Vetter, H., & Neyses, L. (1997). Cardiac myocytes and fibroblasts contain functional estrogen receptors. *FEBS Lett.* **416**(1): 107–12.

Habecker, B.A., Bilimoria, P., Linick, C., Gritman, K., Lorentz, C.U., Woodward, W., & Birren, S.J. (2008). Regulation of cardiac innervation and function via the p75 neurotrophin receptor. *Auton. Neurosci.* **140**(1–2): 40–8.

Habets, P.E.M.H., Moorman, A.F.M., Clout, D.E.W., Van Roon, M.A., Lingbeek, M., Van Lohuizen, M., Campione, M., & Christoffels, V.M. (2002). Cooperative action of Tbx2 and Nkx2.5 inhibits ANF expression in the atrioventricular canal: Implications for cardiac chamber formation. *Genes Dev.* **16**(10): 1234–46.

Han, J. & Molkentin, J.D. (2000). Regulation of MEF2 by p38 MAPK and its implication in cardiomyocyte biology. *Trends Cardiovasc. Med.* **10**(1): 19–22.

Harvey, R.P. (1996). NK-2 homeobox genes and heart development. *Dev. Biol.* **178**(2): 203–16.

Hasin, T., Elhanani, O., Abassi, Z., Hai, T., & Aronheim, A. (2011). Angiotensin II signaling up-regulates the immediate early transcription factor ATF3 in the left but not the right atrium. *Basic Res. Cardiol.* **106**(2): 175–87.

Hidaka, K., Yamamoto, I., Arai, Y., & Mukai, T. (1993). The MEF-3 motif is required for MEF-2-mediated skeletal muscle-specific induction of the rat aldolase A gene. *Mol. Cell. Biol.* **13**(10): 6469–78.

Hinits, Y., Pan, L., Walker, C., Dowd, J., Moens, C.B., & Hughes, S.M. (2012). Zebrafish Mef2ca and Mef2cb are essential for both first and second heart field cardiomyocyte differentiation. *Dev. Biol.* **369**(2): 199–210.

Huang, H., Brand, O.M., Mathew, M., Ignatiou, C., Ewen, E.P., McCalmon, S.A., & Naya, F.J. (2006). Myomaxin is a novel transcriptional target of MEF2A that encodes a Xin-related alpha-actinin-interacting protein. *J. Biol. Chem.* **281**(51): 39370–9.

Ikeda, S., He, A., Kong, S.W., Lu, J., Bejar, R., Bodyak, N., Lee, K.-H., Ma, Q., Kang, P.M., Golub, T.R., & Pu, W.T. (2009). MicroRNA-1 negatively regulates expression of

the hypertrophy-associated calmodulin and Mef2a genes. *Mol. Cell. Biol.* **29**(8): 2193–204.

Jankowski, M., Rachelska, G., Donghao, W., McCann, S.M., & Gutkowska, J. (2001). Estrogen receptors activate atrial natriuretic peptide in the rat heart. *Proc. Natl. Acad. Sci. U. S. A.* **98**(20): 11765–70.

Jiang, C., Wang, J.H., Yue, F., & Kuang, S. (2016). The brain expressed x-linked gene 1 (Bex1) regulates myoblast fusion. *Dev. Biol.* **409**(1): 16–25.

Kim, Y., Phan, D., Van Rooij, E., Wang, D.Z., McAnally, J., Qi, X., Richardson, J.A., Hill, J.A., Bassel-Duby, R., & Olson, E.N. (2008). The MEF2D transcription factor mediates stress-dependent cardiac remodeling in mice. *J. Clin. Invest.* **118**(1): 124–32.

Knowlton, A.A. & Lee, A.R. (2012). Estrogen and the cardiovascular system. *Pharmacol. Ther.* **135**(1): 54–70.

Koo, J.H., Smiley, M.A., Lovering, R.M., & Margolis, F.L. (2007). Bex1 knock out mice show altered skeletal muscle regeneration. *Biochem. Biophys. Res. Commun.* **363**(2): 405–10.

Kuisk, I.R., Li, H., Tran, D., & Capetanaki, Y. (1996). A single MEF2 site governs desmin transcription in both heart and skeletal muscle during mouse embryogenesis. *Dev. Biol.* **174**(1): 1–13.

Kuo, C.T., Morrisey, E.E., Anandappa, R., Sigrist, K., Lu, M.M., Parmacek, M.S., Soudais, C., & Leiden, J.M. (1997). Transcription factor GATA4 is required for heart tube formation and ventral morphogenesis. *Circulation* **96**(8): 1686.

Li, J., Chanda, D., Shiri-Sverdlov, R., & Neumann, D. (2015). MSP: An emerging player in metabolic syndrome. *Cytokine Growth Factor Rev.* **26**(1): 75–82.

Lien, C.L., Wu, C., Mercer, B., Webb, R., Richardson, J. a, & Olson, E.N. (1999). Control of early cardiac-specific transcription of Nkx2-5 by a GATA-dependent enhancer. *Development* **126**75–84.

Lilly, B., Galewsky, S., Firulli, A.B., Schulz, R.A., & Olson, E.N. (1994). D-MEF2: a MADS box transcription factor expressed in differentiating mesoderm and muscle cell lineages during Drosophila embryogenesis. *Proc. Natl. Acad. Sci. U. S. A.* **91**(12): 5662–6.

Lin, Q., Schwarz, J., Bucana, C., & Olson, E.N. (1997). Control of mouse cardiac morphogenesis and myogenesis by transcription factor MEF2C. *Science* **276**(5317): 1404–7.

Liu, C., Liu, W., Lu, M.F., Brown, N.A., & Martin, J.F. (2001). Regulation of left-right asymmetry by thresholds of Pitx2c activity. *Development* **128**(11): 2039–48.

Liu, M.L., Olson, A.L., Edgington, N.P., Moye-Rowley, W.S., & Pessin, J.E. (1994). Myocyte enhancer factor 2 (MEF2) binding site is essential for C2C12 myotube-specific expression of the rat GLUT4/muscle-adipose facilitative glucose transporter gene. *J. Biol. Chem.* **269**(45): 28514–21.

Livak, K.J. & Schmittgen, T.D. (2001). Analysis of relative gene expression data using real-time quantitative PCR and the 2(-Delta Delta C(T)) Method. *Methods* **25**(4): 402–8.

Lizotte, E., Grandy, S.A., Tremblay, A., Allen, B.G., & Fiset, C. (2009). Expression, distribution and regulation of sex steroid hormone receptors in mouse heart. *Cell. Physiol. Biochem.* **23**(1–3): 75–86.

Luo, T. & Kim, J.K. (2016). The role of estrogen and estrogen receptors on cardiomyocytes: an overview. *Can. J. Cardiol.* **32**(8): 1017–25.

Lyons, I., Parsons, L.M., Hartley, L., Li, R., Andrews, J.E., Robb, L., & Harvey, R.P. (1995). Myogenic and morphogenetic defects in the heart tubes of murine embryos lacking the homeo box gene Nkx2-5. *Genes Dev.* **9**(13): 1654–66.

Ma, K., Chan, J.K.L., Zhu, G., & Wu, Z. (2005). Myocyte enhancer factor 2 acetylation by p300 enhances its DNA binding activity, transcriptional activity, and myogenic differentiation. *Mol. Cell. Biol.* **25**(9): 3575–82.

Mahmoodzadeh, S., Eder, S., Nordmeyer, J., Ehler, E., Huber, O., Martus, P., Weiske, J., Pregla, R., Hetzer, R., & Regitz-Zagrosek, V. (2006). Estrogen receptor alpha up-regulation and redistribution in human heart failure. *FASEB J.* **20**(7): 926–34.

McKinsey, T.A. & Olson, E.N. (2005). Toward transcriptional therapies for the failing heart: Chemical screens to modulate genes. *J. Clin. Invest.* **115**(3): 538–46.

McKinsey, T.A., Zhang, C.L., & Olson, E.N. (2002). MEF2: A calcium-dependent regulator of cell division, differentiation and death. *Trends Biochem. Sci.* **27**(1): 40–7.

Medrano, J.L. & Naya, F.J. (2017). The transcription factor MEF2A fine-tunes gene expression in the atrial and ventricular chambers of the adult heart. *J. Biol. Chem.* jbc.M117.806422.

Miano, J.M. (2003). Serum response factor: Toggling between disparate programs of gene expression. *J. Mol. Cell. Cardiol.* **35**(6): 577–93.

Mitra, S.K. & Schlaepfer, D.D. (2006). Integrin-regulated FAK-Src signaling in normal and cancer cells. *Curr. Opin. Cell Biol.* **18**(5): 516–23.

Molkentin, J.D., Black, B.L., Martin, J.F., & Olson, E.N. (1996). Mutational analysis of the DNA binding, dimerization, and transcriptional activation domains of MEF2C. *Mol. Cell. Biol.* **16**(6): 2627–36.

Molkentin, J.D., Lin, Q., Duncan, S.A., & Olson, E.N. (1997). Requirement of the transcription factor GATA4 for heart tube formation and ventral morphogenesis. *Genes Dev.* **11**(8): 1061–72.

Moorman, A.F.M. & Christoffels, V.M. (2003). Cardiac chamber formation: development, genes, and evolution. *Physiol. Rev.* **83**(4): 1223–67.

Morin, S., Charron, F., Robitaille, L., & Nemer, M. (2000). GATA-dependent recruitment of MEF2 proteins to target promoters. *EMBO J.* **19**(9): 2046–55.

Morin, S., Pozzulo, G., Robitaille, L., Cross, J., & Nemer, M. (2005). MEF2-dependent recruitment of the HAND1 transcription factor results in synergistic activation of target promoters. *J. Biol. Chem.* **280**(37): 32272–8.

Morisaki, T., Sermsuvitayawong, K., Byun, S.H., Matsuda, Y., Hidaka, K., Morisaki, H., & Mukai, T. (1997). Mouse Mef2b gene: unique member of MEF2 gene family. *J. Biochem.* **122**(5): 939–46.

Naya, F.J., Black, B.L., Wu, H., Bassel-Duby, R., Richardson, J.A., Hill, J.A., & Olson, E.N. (2002). Mitochondrial deficiency and cardiac sudden death in mice lacking the MEF2A transcription factor. *Nat. Med.* **8**(11): 1303–9.

Naya, F.J., Wu, C., Richardson, J.A., Overbeek, P., & Olson, E.N. (1999). Transcriptional activity of MEF2 during mouse embryogenesis monitored with a MEF2-dependent transgene. *Development* **126**(10): 2045–52.

Ng, S.Y., Wong, C.K., & Tsang, S.Y. (2010). Differential gene expressions in atrial and ventricular myocytes: insights into the road of applying embryonic stem cell-derived cardiomyocytes for future therapies. *Am. J. Physiol. Physiol.* **299**(6): C1234–C1249.

Nguyen, H.T., Bodmer, R., Abmayr, S.M., McDermott, J.C., & Spoerel, N.A. (1994). D-mef2: a Drosophila mesoderm-specific MADS box-containing gene with a biphasic expression profile during embryogenesis. *Proc. Natl. Acad. Sci. U. S. A.* **91**(16): 7520–4.

Paige, S.L., Plonowska, K., Xu, A., & Wu, S.M. (2015). Molecular regulation of cardiomyocyte differentiation. *Circ. Res.* **116**(2): 341–53.

Pereira, F.A., Yuhong, Q., Zhou, G., Tsai, M.J., & Tsai, S.Y. (1999). The orphan nuclear receptor COUP-TFII is required for angiogenesis and heart development. *Genes Dev.* **13**(8): 1037–49.

Phan, D., Rasmussen, T.L., Nakagawa, O., McAnally, J., Gottlieb, P.D., Tucker, P.W., Richardson, J. a, Bassel-Duby, R., & Olson, E.N. (2005). BOP, a regulator of right ventricular heart development, is a direct transcriptional target of MEF2C in the developing heart. *Development* **132**(11): 2669–78.

Potthoff, M.J. & Olson, E.N. (2007). MEF2: a central regulator of diverse developmental programs. **134**(23): 4131–40.

Ramachandran, B., Yu, G., Li, S., Zhu, B., & Gulick, T. (2008). Myocyte enhancer factor 2A is transcriptionally autoregulated. *J. Biol. Chem.* **283**(16): 10318–29.

Rana, M.S., Christoffels, V.M., & Moorman, A.F.M. (2013). A molecular and genetic outline of cardiac morphogenesis. *Acta Physiol.* **207**(4): 588–615.

Reecy, J.M., Li, X., Yamada, M., DeMayo, F.J., Newman, C.S., Harvey, R.P., & Schwartz, R.J. (1999). Identification of upstream regulatory regions in the heart-expressed homeobox gene Nkx2-5. *Development* **126**(4): 839–49.

Reichardt, L.F. (2006). Neurotrophin-regulated signalling pathways. *Philos. Trans. R. Soc. B Biol. Sci.* **361**(1473): 1545–64.

Reiter, J.F., Alexander, J., Rodaway, A., Yelon, D., Patient, R., Holder, N., & Stainier, D.Y.R. (1999). Gata5 is required for the development of the heart and endoderm in zebrafish. *Genes Dev.* **13**(22): 2983–95.

Riley, P., Anaon-Cartwight, L., & Cross, J.C. (1998). The Hand1 bHLH transcription factor is essential for placentation and cardiac morphogenesis. *Nat. Genet.* **18**(3): 271–5.

Riquelme, C., Barthel, K.K.B., & Liu, X. (2006). SUMO-1 modification of MEF2A regulates its transcriptional activity. *J. Cell. Mol. Med.* **10**(1): 132–44.

Van Rooij, E., Fielitz, J., Sutherland, L.B., Thijssen, V.L., Crijns, H.J., Dimaio, M.J., Shelton, J., De Windt, L.J., Hill, J.A., & Olson, E.N. (2010). Myocyte enhancer factor 2 and class ii histone deacetylases control a gender-specific pathway of cardioprotection mediated by the estrogen receptor. *Circ. Res.* **106**(1): 155–65.

Ross, R.S., Navankasattusas, S., Harvey, R.P., & Chien, K.R. (1996). An HF-1a/HF-1b/MEF-2 combinatorial element confers cardiac ventricular specificity and established an anterior-posterior gradient of expression. *Development* **122**(6): 1799–809.

Schagat, T., Paguio, A., & Kopish, K. (2007). Normalizing genetic reporter assays: approaches and considerations for increasing consistency and statistical significance [PDF file]. *Cell Notes* (17): 9–12. https://www.promega.com/-/media/files/resources/cell-notes/cn017/normalizing-genetic-reporter-assays.pdf?la=en

Schultheiss, T.M., Xydas, S., & Lassar, A.B. (1995). Induction of avian cardiac myogenesis by anterior endoderm. *Development* **121**(12): 4203–14.

Searcy, R.D., Vincent, E.B., Liberatore, C.M., & Yutzey, K.E. (1998). A GATA-dependent nkx-2.5 regulatory element activates early cardiac gene expression in transgenic mice. *Development* **125**(22): 4461–70.

Seok, H.Y., Tatsuguchi, M., Callis, T.E., He, A., Pu, W.T., & Wang, D.Z. (2011). miR-155 inhibits expression of the MEF2A protein to repress skeletal muscle differentiation. *J. Biol. Chem.* **286**(41): 35339–46.

Shore, P. & Sharrocks, A. (1995). The MADS-box family of transcription factors. *Eur. J. Biochem.* **229**(1): 1–13.

Singh, M.K., Christoffels, V.M., Dias, J.M., Trowe, M.-O., Petry, M., Schuster-Gossler, K., Bürger, A., Ericson, J., & Kispert, A. (2005). Tbx20 is essential for cardiac chamber differentiation and repression of Tbx2. *Development* **132**(12): 2697–707.

Small, E.M. & Krieg, P.A. (2004). Molecular regulation of cardiac chamber-specific gene expression. *Trends Cardiovasc. Med.* **14**(1): 13–8.

Snyder, C.M., Rice, A.L., Estrella, N.L., Held, A., Kandarian, S.C., & Naya, F.J. (2013). MEF2A regulates the Gtl2-Dio3 microRNA mega-cluster to modulate WNT signaling in skeletal muscle regeneration. *Development* **140**(1): 31–42.

Später, D., Hansson, E.M., Zangi, L., & Chien, K.R. (2014). How to make a cardiomyocyte. *Development* **141**(23): 4418–31.

Srivastava, D. & Olson, E.N. (2000). A genetic blueprint for cardiac development. *Nature* **407**(September): 221–6.

Srivastava, D., Thomas, T., Lin, Q., Kirby, M.L., Brown, D., & Olson, E.N. (1997). Regulation of cardiac mesodermal and neural crest development by the bHLH transcription factor, dHAND. *Nat. Genet.* **16**(2): 154–60.

Tabibiazar, R., Wagner, R.A., Liao, A., & Quertermous, T. (2003). Transcriptional profiling of the heart reveals chamber-specific gene expression patterns. *Circ. Res.* **93**(12): 1193–201.

Tanaka, M., Chen, Z., Bartunkova, S., Yamasaki, N., & Izumo, S. (1999). The cardiac homeobox gene Csx/Nkx2.5 lies genetically upstream of multiple genes essential for heart development. *Development* **126**(6): 1269–80.

Tanaka, M., Wechsler, S.B., Lee, I.W., Yamasaki, N., Lawitts, J. a, & Izumo, S. (1999). Complex modular cis-acting elements regulate expression of the cardiac specifying

homeobox gene Csx/Nkx2.5. *Development* **126**(7): 1439–50.

Taylor, M. V., Beatty, K.E., Hunter, H.K., & Baylies, M.K. (1995). Drosophila MEF2 is regulated by twist and is expressed in both the primordia and differentiated cells of the embryonic somatic, visceral and heart musculature. *Mech. Dev.* **50**(1): 29–41.

Tessari, A., Pietrobon, M., Notte, A., Cifelli, G., Gage, P.J., Schneider, M.D., Lembo, G., & Campione, M. (2008). Myocardial Pitx2 differentially regulates the left atrial identity and ventricular asymmetric remodeling programs. *Circ. Res.* **102**(7): 813–22.

Thattaliyath, B.D., Livi, C.B., Steinhelper, M.E., Toney, G.M., & Firulli, A.B. (2002). HAND1 and HAND2 are expressed in the adult-rodent heart and are modulated during cardiac hypertrophy. *Biochem. Biophys. Res. Commun.* **297**(4): 870–5.

Toro, R., Saadi, I., Kuburas, A., Nemer, M., & Russo, A.F. (2004). Cell-specific activation of the atrial natriuretic factor promoter by PITX2 and MEF2A. *J. Biol. Chem.* **279**(50): 52087–94.

Vedantham, V., Evangelista, M., Huang, Y., & Srivastava, D. (2013). Spatiotemporal regulation of an Hcn4 enhancer defines a role for Mef2c and HDACs in cardiac electrical patterning. *Dev. Biol.* **373**(1): 149–62.

Vilar, M., Murillo-Carretero, M., Mira, H., Magnusson, K., Besset, V., & Ibáñez, C.F. (2006). Bex1, a novel interactor of the p75 neurotrophin receptor, links neurotrophin signaling to the cell cycle. *EMBO J.* **25**(6): 1219–30.

Vincentz, J.W., Barnes, R.M., & Firulli, A.B. (2011). Hand factors as regulators of cardiac morphogenesis and implications for congenital heart defects. *Birth Defects Res. Part A - Clin. Mol. Teratol.* **91**(6): 485–94.

Vincentz, J.W., Barnes, R.M., Firulli, B.A., Conway, S.J., & Firulli, A.B. (2008). Cooperative interaction of Nkx2.5 and Mef2c transcription factors during heart development. *Dev. Dyn.* **237**(12): 3809–19.

Vong, L.H., Ragusa, M.J., & Schwarz, J.J. (2005). Generation of conditional Mef2cloxP/loxP mice for temporal- and tissue-specific analyses. *Genesis* **43**(1): 43–8.

Wales, S., Hashemi, S., Blais, A., & McDermott, J.C. (2014). Global MEF2 target gene analysis in cardiac and skeletal muscle reveals novel regulation of DUSP6 by p38MAPK-MEF2 signaling. *Nucleic Acids Res.* **42**(18): 11349–62.

Wang, J., Klysik, E., Sood, S., Johnson, R.L., Wehrens, X.H.T., & Martin, J.F. (2010). Pitx2 prevents susceptibility to atrial arrhythmias by inhibiting left-sided pacemaker specification. *Proc. Natl. Acad. Sci. U. S. A.* **107**(21): 9753–8.

Wu, S., Cheng, C.-M., Lanz, R.B., Wang, T., Respress, J.L., Ather, S., Chen, W., Tsai, S.-J., Wehrens, X.H.T., Tsai, M.-J., & Tsai, S.Y. (2013). Atrial identity is determined by a COUP-TFII regulatory network. *Dev. Cell* **25**(4): 417–26.

Xin, M., Small, E.M., van Rooij, E., Qi, X., Richardson, J.A., Srivastava, D., Nakagawa, O., & Olson, E.N. (2007). Essential roles of the bHLH transcription factor Hrt2 in repression of atrial gene expression and maintenance of postnatal cardiac function. *Proc. Natl. Acad. Sci. U. S. A.* **104**(19): 7975–80.

Yamagishi, H., Olson, E.N., & Srivastava, D. (2000). The basic helix-loop-helix transcription factor, dHAND, is required for vascular development. *J. Clin. Invest.* **105**(3): 261–70.

Yao, H.-P., Zhou, Y.-Q., Zhang, R., & Wang, M.-H. (2013). MSP–RON signalling in cancer: pathogenesis and therapeutic potential. *Nat. Rev. Cancer* **13**(7): 466–81.

Yu, Y.T., Breitbart, R.E., Smoot, L.B., Lee, Y., Mahdavi, V., & Nadal-Ginard, B. (1992). Human myocyte-specific enhancer factor 2 comprises a group of tissue-restricted MADS box transcription factors. *Genes Dev.* **6**(9): 1783–98.

Zang, M.X., Li, Y., Xue, L.X., Jia, H.T., & Jing, H. (2004). Cooperative activation of atrial naturetic peptide promoter by dHAND and MEF2C. *J. Cell. Biochem.* **93**(6): 1255–66.

Zhang, C.L., McKinsey, T.A., Chang, S., Antos, C.L., Hill, J.A., & Olson, E.N. (2002). Class II histone deacetylases act as signal-responsive repressors of cardiac hypertrophy. *Cell* **110**(4): 479–88.

Zhao, X.-S., Gallardo, T.D., Lin, L., Schageman, J.J., & Shohet, R. V (2002). Transcriptional mapping and genomic analysis of the cardiac atria and ventricles. *Physiol. Genomics* **12**(1): 53–60.

CURRICULUM VITAE